International Conference on Recent Trends in Geoscience Research and Applications 2023

October 23–27, 2023, Belgrade, Serbia & virtual

BOOK OF ABSTRACTS AND CONTRIBUTED PAPERS

GeosciRA23

Edited by Aleksandra Nina, Snežana Dragović, and Dejan Doljak

Belgrade
2023

Scientific Committee

Aleksandra Nina, Serbia, chair
Snežana Dragović, Serbia, co-chair
Ivan Lizaga, Belgium, co-chair
Oleg Odalović, Serbia, co-chair

Pier Francesco Biagi, Italy
Jozsef Bor, Hungary
Ranko Dragović, Serbia
Slobodan Đorđević, UK
Hans Eichelberger, Austria
Emil Fulajtar, Austria
Boško Gajić, Serbia
Maria Gritsevich, Finland
Pavlos Kassomenos, Greece
Konstantinos Kourtidis, Greece
Slavica Malinović-Milićević, Serbia
Ana Milanović Pešić, Serbia
Boško Milovanović, Serbia
Irina Mironova, Russia
Giovanni Nico, Italy
Antonije Onjia, Serbia
Marko D. Petrović, Serbia
Luka Č. Popović, Serbia
Sergey Pulinets, Russia
Milan Radovanović, Serbia
Ivana Smičiklas, Serbia
Vladimir Srećković, Serbia
Mirela Voiculescu, Romania
Desmond Walling, UK

Local Organizing Committee

Aleksandra Nina, Serbia, chair
Ana Milanović Pešić, Serbia, co-chair

Filip Arnaut, Serbia
Jovana Brankov, Serbia
Stefan Denda, Serbia
Dejan Doljak, Serbia
Milan Đorđević, Serbia
Sanja Grekulović, Serbia
Dejana Jakovljević, Serbia
Aleksandra Kolarski, Serbia
Maja Kuzmanoska, Serbia
Suzana Lović Obradović, Serbia
Dušan Petković, Serbia
Miljana Todorović Drakul, Serbia
Đorđe Trajković, Serbia

Scientific Rationale

Geoscience research and applications are of crucial interest in science and many areas of modern life. For this reason, exchanging knowledge in various relevant areas is essential for development in scientific, engineering and programming activities. The conference aims to highlight the importance of joint research of experts in these fields and provide a platform for knowledge exchange.

Venue: Institute of Physics Belgrade, Belgrade, Serbia & virtual

Organizers: Faculty of Civil Engineering, University of Belgrade and Institute of Physics Belgrade, University of Belgrade

Published by: Faculty of Civil Engineering, University of Belgrade; Institute of Physics Belgrade, University of Belgrade; and Geographical Institute "Jovan Cvijić" SASA

The publication of this issue is financially supported by the Ministry for Education, Science and Technological Development of Serbia

Picture on the first cover: Dejan Doljak

ISBN 978-86-7518-239-9

eISBN 978-86-7518-240-5

Printed by: Curent Print, Tvrtka Velikog 14, Beograd

Number of copies: 50

CONTENTS

Invited Lectures

Invited Progress Reports

Progress Reports

Posters

INVITED LECTURES

Abstract

COMPARATIVE PLANETOLOGY—WHAT DO WE LEARN ABOUT THE EARTH BY STUDYING OTHER PLANETS?

Nigel John Mason [1,2]*

[1]University of Kent, School of Physics and Astronomy, Canterbury, United Kingdom; e-mail: n.j.mason@kent.ac.uk
[2]Europlanet Research Infrastructure; e-mail: europlanet2024ri@kent.ac.uk

What can we learn about the Earth from studying other planets? *The answer is quite a lot!* Studies of Venus can provide a guide to what the Earth may become if we do not address the causes of global warming whilst Mars gives clues as to how Earth may have looked when life first began. Why did the Earth (with its moon) sustain its oceans and atmosphere when Mars did not? What can we learn about interior dynamics and plate tectonics from other planets and the role they play in habitability? What does Saturn's moon, Titan, tell us about the emergence of a life supporting atmosphere? Titan being a case study of the famous Urey-Miller experiment which provides clues as to formation of prebiotic molecules necessary for emergence of life. Only by studying other planets and their moons can we understand the myriad of exoplanets that we are detecting around other stars and thence seek those that may support life.

These studies are known as "comparative planetology", a term first coined by George Gamow, who reasoned that to fully understand our own planet, we must study others. Its goal is to develop a comprehensive theory of the origin and evolution of our planetary system and by this understand exoplanetary systems and the conditions necessary for support of life (at least as we know it). In this talk I will discuss the concept and why (and how) planetary scientists and geoscientists need to work together to unravel the history and future of both the Earth and other planets.

Acknowledgements
The author recognizes that Europlanet 2024 RI has received funding from the European Union's Horizon 2020 research and innovation programme under grant agreement No 871149

*Corresponding author, e-mail: n.j.mason@kent.ac.uk

Abstract

LITHOSPHERE GEODYNAMICS INFERRED FROM STUDY OF MANTLE XENOLITHS: THE EXAMPLE FROM SERBIA

Vladica Cvetković [1]*

[1]University of Belgrade, Faculty of Mining and Geology, Belgrade, Serbia; e-mail: vladica.cvetkovic@gf.bg.ac.rs

Given that deep drillings reach only first 5% of the lithosphere thickness, peridotite xenoliths found in basalts and kimberlites remain the only rocks of the subcontinental lithosphere available for direct observations. From studying these xenoliths, we know that the lithospheric mantle is composed of olivine, orthopyroxene, clinopyroxene and, depending on depth, spinel or garnet. Moreover, we are able to characterize the physico-chemical state of the mantle portion "sampled" by xenoliths and interpret its geodynamic evolution. One of the most relevant information is the extent of depletion that tells us how much of basaltic magma was extracted from mantle peridotite in the geological past. This is estimated by the content of modal clinopyroxene, Al_2O_3 concentrations in bulk xenoliths and in minerals, the values of Mg# [100×MgO/(MgO + FeO) mol] in silicates and Cr#[Cr_2O_3/(Cr_2O_3+Al_2O_3)mol] in spinels as well as by the concentrations of trace elements including rare earths (REE). The information about depletion degree is important because it differs in mantle sections from various geodynamic environments.

In Serbia, mantle xenoliths are found only in Palaeogene basalts near Sokobanja and Bela Palanka (SE Serbia). Our xenolith studies suggest that the uppermost mantle beneath the present-day SE Serbia is predominantly composed of highly depleted peridotites (≤ 5 vol. % of clinopyroxene) characterized by high Mg# in silicates (> 91) and Cr# in spinels (0.5–0.7) and low Al_2O_3 contents in orthopyroxene (1–2 wt. %). Modelling of REE concentrations in orthopyroxene from these xenoliths implies the amount of extraction of basaltic melts of 22–30%, which makes the SE Serbian mantle significantly more depleted than typical non-cratonic sub-continental lithosphere worldwide. Because of that, we hypothesized that the SE Serbian subcontinental mantle consists of pieces of the oceanic lithosphere of the Mesozoic Ocean Tethys, which were tectonically emplaced beneath the ancient European margin. This half-speculative scenario is corroborated by the fact that the same basalts host a sub-set of orthopyroxene-rich xenoliths which are similar to present day boninites known to occur exclusively in intraoceanic subduction zones.

Acknowledgements

This contribution is supported by the Serbian Academy of Sciences and Arts (F9, F17), the Ministry of Science, Technological Development and Innovations ("Contract on realization and financing of scientific research of SRI in 2023", No. 451-03-47/2023-01/200126) and the Science Fund of the Republic of Serbia (No. 7744807).

*Corresponding author, e-mail: vladica.cvetkovic@gf.bg.ac.rs

Abstract

ENERGY TRANSFORMATION, RELEASE AND DISSIPATION DURING EARTHQUAKE PREPARATION PERIOD AS THE MANIFESTATION OF GEOSPHERE'S INTERACTION

Sergey Pulinets[1]*

[1]Russian Academy of Sciences, Space Research Institute, Moscow, Russia; e-mail: pulse@cosmos.ru

The final stage of earthquake preparation can be described as a non-linear process in the open system with energy dissipation. It happens in the energy-saturated media concentrated within the area called the earthquake preparation zone (Dobrovolsky et al., 1979). Kadomtsev and Ryazanov (1983) claim that energy dissipation has irreversible character and can be transformed into other kinds of energy (oscillation of thermal atom's movements, or electromagnetic emissions). Together with energy exchange, a mass exchange may take place. At the same time, it is difficult to find estimations on the relationship between the energy released by the initial event and consequent events after the energy transformation processes. We will report on the examples of exceeding secondary energy release as it happens in comparison of the mechanical energy released by an earthquake and thermal energy released as a precursory phenomenon (Pulinets et al., 2022) or explosive energy release due to autocatalytic reaction in the atmosphere as a result of air ionization (Pulinets et al., 2023). All these effects are considered within the framework of the intergeospheres interaction concept proposed by Sir John Murray (1913) and developed by academician Vladimir Vernadsky (2013). Now these ideas started to be implemented in just founded international program "International Magnetic Circle Program" where the studies of geospheres interaction put as a main scientific problem of the project.

References

Dobrovolsky, I. R., Zubkov, S. I., & Myachkin, V. I. (1979). Estimation of the size of earthquake preparation zones. *Pageoph*, *117*, 1025–1044. https://link.springer.com/article/10.1007/BF00876083

Kadomtsev, B. B., & Ryazanov, A. I. (1983). What the synergetics is? *Priroda*, *8,* 2–11. https://ui.adsabs.harvard.edu/abs/1983Prir.....2K/abstract

Murray, Sir John. (1913). *The ocean: A general account of the science of the sea*. Williams and Norgate.

Pulinets, S., Ouzounov, D., Karelin, A., & Boyarchuk, K. (2022). *Earthquake Precursors in the Atmosphere and Ionosphere. New Concepts*. Springer Nature. https://link.springer.com/book/10.1007/978-94-024-2172-9

Pulinets, S., Budnikov, P., Karelin, A., & Žalohar J. (2023). Thermodynamic instability of the atmospheric boundary layer stimulated by tectonic and seismic activity. *Journal of Atmospheric and Solar-Terrestrial Physics, 246,* Article 106050, https://doi.org/10.1016/j.jastp.2023.106050.

Vernadsky V. I. (2013). *Khimicheskoe stroenie biosfery Zemli i eyo okruzheniya* [The chemical structure of the Earth's biosphere and its environment]. Nauka.

*Corresponding author, e-mail: pulse@cosmos.ru

Abstract

A 50 YEARS RESEARCH ON EARTHQUAKE PRECURSORS: A PERSONAL EXPERIENCE

Pier Francesco Biagi[1]*

[1]University of Bari, Department of Physics, Bari, Italy; e-mail: pf.biagi@gmail.com

The author started his research activity on earthquake precursors in 1973. At a site located near the epicenter of the Friuli earthquake (M_w = 6.5, 1976) an anomalous tilt variation appeared, during the three years preceding the earthquake. Then, a network of tilt-meters was put into operation in central Italy and several results were obtained. Furthermore, the author carried out research works related to groundwater Radon content (anomalies were detected before the Irpinia earthquake, M_w = 6.8, 1980), and other results were obtained in central Italy when performing systematic resistivity earth measurements. In addition, cooperation with Georgia and Kamchatka (Russia) researchers began; in this phase, anomalies in the Helium content in thermal waters (Georgia) had been revealed before the destructive Spitak (M_w = 6.9, 1988) earthquake and anomalies in ions and gases content in water of deep wells (Kamchatka) appeared before the largest (M_w = 6.6–7.1) earthquakes here occurred. In addition, since 1987, the author has put into operation instrumentation for detecting electric, magnetic, and seismic-acoustic signals inside natural caves located in the central Apennines obtaining several results. Then, the intensity of LF (150–300 kHz) and VLF (20–80 kHz) radio signals have been monitored and pre-seismic anomalies were revealed. Finally, in 2009, eight radio receivers for sampling VLF-LF radio signals were put into operation in different European countries and the INFREP cooperation started. Several results were obtained and new ones are expected as well.

*Corresponding author, e-mail: pf.biagi@gmail.com

Abstract

MODELLING WAVE STRUCTURES IN THE EARTH-ATMOSPHERE-IONOSPHERE AND RADIODIAGNOSTICS OF IONOSPHERIC SPACE WEATHER (ISW)

Yuriy Rapoport[1], Volodymyr Grimalsky[2], Sergei Petrishevskii[3], Asen Grytsai[3], Oleksandr Liashchuk[4], Andrzej Krankowski[1]*

[1]University of Warmia and Mazury in Olsztyn, Olsztyn, Poland; e-mails: yuriy.rapoport@gmail.com; kand@uwm.edu.pl
[2]University Autonomous University of State Morelos (UAEM), Cuernavaca, Mexico; e-mail: v_grim@hotmail.com
[3]Taras Shevchenko National University of Kyiv, Physical Faculty, Kyiv, Ukraine; e-mail: msergiyp@gmail.com; a.grytsai@gmail.com
[4]Main Center of Special Monitoring, National Space Facility Control and Tests Center, State Space Agency of Ukraine, Kyiv, Ukraine; e-mail: alex.liashchukk@gmail.com

New models of Ultra Low, Extremely Low, and Very Low Frequency (ULF, ELF, VLF, respectively) disturbances excited by given (current) sources placed inside Lithosphere (Earth)-Atmosphere-Ionosphere-Magnetosphere (LEAIM) system (Grimalsky et al., 2022; Rapoport et al., 2020, 2022; Rapoport and Grimalsky, 2022; Yutsis et al., 2021), are developing. Such disturbances include both waves passing through LEAIM system and VLF excitations of Waveguide Earth-Ionosphere (WGEI), ELF disturbances of coupled Schumann and Ionospheric Alfven resonator (SR-IAR), effective ULF geomagnetic Alfven waveguide connecting magnetically conjugated regions. Disturbance sources can be located above the ionosphere (solar wind disturbances and strong magnetic storms) and within and below the ionosphere (electro-discharges, earthquakes, volcanoes, and tropical cyclones). Influences of these sources on LEAIM system form ISW, i.e., ionospheric modification by Hunga-Tonga eruption (D'Arcangelo et al., 2022). Relevant naturally occurring ionospheric wave structures include, i.e., Traveling Ionospheric Disturbances (TIDs) associated with ionospheric nonlinearities and magneto-acoustic-gravity waves; nonlinear structures, such as plasma bubbles, etc., caused by impact on the ionosphere "from below" (Kuo et al., 2011); plasma structures at middle latitudes, based on (combined) *Es* (sporadic layer)-Perkins instabilities (Yokoyama et al., 2009); nonlinear plasma structures, for example, during magnetic storms, are generated at high and low latitudes, penetrating into middle latitudes, during period of maximum solar activity 2024–2026. Results of simulation of (1) waves passing through the LEAIM system, which are important for ISW radiodiagnostics; (2) (VLF) excitation of WGEI; (3) (ELF) perturbations of coupled Schumann and SR-IAR, and (4) scattering of Very High Frequency EMW on ionospheric plasma structures, are presented.

*Corresponding author, e-mail: kand@uwm.edu.pl

References

D'Arcangelo, S., Bonforte, A., De Santis, A., Maugeri, S. R., Perrone, L., Soldani, M., Arena, G., Brogi, F., Calcara, M., Campuzano, S. A., et al. (2022). A Multi-Parametric and Multi-Layer Study to Investigate the Largest 2022 Hunga Tonga–Hunga Ha'apai Eruptions. *Remote Sensing, 14*(15), Article 3649. https://doi.org/10.3390/rs14153649

Grimalsky, V., Rapoport, Y., Tecpoyotl-Torres, M., Ivantyshyn, O., & Nesterenko, A. (2022). Nonlinear frequency down-conversion of acoustic wave beams in the atmosphere and ionosphere under different types of modulation. *Journal of Atmospheric and Solar-Terrestrial Physics, 227*, Article 105774. https://doi.org/10.1016/j.jastp.2021.105774

Kuo, C. L., Huba, J. D., Joyce, G., & Lee, L. C. (2011). Ionosphere plasma bubbles and density variations induced by pre-earthquake rock currents and associated surface charges. *Journal of Geophysical Research: Space Physics, 116*, Article 10317. https://doi.org/10.1029/2011JA016628

Rapoport, Yu. G., Grimalsky, V. V., Krankowski, A., Pulinets, S, & Fedorenko, A. K. (2020). Algorithm for modeling electromagnetic channel of seismo-ionospheric coupling (SIC) and the variations in the electron concentration. *Acta Geophysica, 68, 253–278*. https://doi.org/10.1007/s11600-019-00385-0

Rapoport, Yu., Grimalsky, V., Fedun, F., Agapitov, O., Bonnell, J., Grytsai, A., Milinevsky, G., Liashchuk, A., Rozhnoi, A., Solovieva, M., & Gulin, A. (2020). Model of the propagation of very low-frequency beams in the Earth–ionosphere waveguide: principles of the tensor impedance method in multi-layered gyrotropic waveguides. *Annales Geophysicae, 38*(1), 207–230. https://doi.org/10.5194/angeo-38-207-2020

Rapoport, Yu., Reshetnyk, V., Grytsai, A., Grimalsky, V., Liashchuk, O., Fedorenko, A., Hayakawa, M., Krankowski, A., Błaszkiewicz, L., & Flisek, P. (2022). Spectral Analysis and Information Entropy Approaches to Data of VLF Disturbances in the Waveguide Earth-Ionosphere. *Sensors, 22*(21), Article 8191. https://doi.org/10.3390/s22218191

Rapoport, Yu. G., & Grimalsky, V. V. (2022). *Waves in Nonlinear Layered Metamaterials, Gyrotropic and Plasma Media*. https://iopscience.iop.org/book/mono/978-0-7503-2336-9

Yokoyama, T., Hysell, D. L., Otsuka, Y., & Yamamoto, M. (2009). Three-dimensional simulation of the coupled Perkins and Es-layer instabilities in the nighttime midlatitude ionosphere. *Journal of Geophysical Research: Space Physics, 114*, Article c03308. https://doi.org/10.1029/2008JA013789

Yutsis, V., Rapoport, Yu., Grimalsky, V., Grytsai, A., Ivchenko, V., Petrishchevskii, S., Fedorenko, A., & Krivodubskij, V. (2021). ULF Activity in the Earth Environment: Penetration of Electric Field from the Near-Ground Source to the Ionosphere under Different Configurations of the Geomagnetic Field. *Atmosphere, 12*(7), Article 801. https://doi.org/10.3390/atmos12070801

INVITED PROGRESS REPORTS

Abstract

INVESTIGATING THE ALTITUDE PROFILE OF D-REGION IONOSPHERIC RESPONSE TIME DURING SOLAR FLARES

Tamal Basak[1], Sayak Chakraborty[1]*

[1]Indian Centre for Space Physics, 466 Barakhola, Netai Nagar, Kolkata, India; e-mails: tamalbasak@gmail.com, sayak.kolkata@gmail.com

In this work, the response of the D-region to the solar flares, as well as, its effective response time delay was studied. The 'electron continuity equation' is used to investigate the D-region at mid-latitude. D-region response time delay is defined (Δt) as the time difference between the peaks of electron density ($N_e(t)$) profile and solar X-ray flux ($\phi\ (t)$). In this work, we report that Δt has a strong altitude (h) dependency and the nature of dependency is different for different classes of flares. Furthermore, the latitudinal and seasonal dependencies of Δt-h profiles were also studied. The C and M classes flares do hold minimum Δt during the middle of the year in the northern hemisphere and during the ending and beginning of a year in the southern hemisphere. Finally, we explain such altitude dependence of Δt with possible explanations from physical mechanisms going on there.

Acknowledgements

Authors thank SWPC-NOAA for GOES solar X-ray data.

*Corresponding author, e-mail: tamalbasak@gmail.com

GeosciRA23
Book of Abstracts and Contributed Papers
International Conference on Recent Trends in Geoscience Research and Applications 2023
Belgrade, Serbia & Virtual, October 23–27, 2023
Editors: Aleksandra Nina, Snežana Dragović, and Dejan Doljak

Contributed paper

MODELING LOWER IONOSPHERIC RESPONSE TO LIGHTNING-INDUCED ELECTRON PRECIPITATION USING VLF RADIO SIGNAL RECORDINGS

Aleksandra Kolarski[1]*

[1]Institute of Physics Belgrade, Belgrade, Serbia; e-mail: aleksandra.kolarski@ipb.ac.rs

Abstract: The Lightning-induced Electron Precipitation (LEP) events are well-known phenomena, with effects that are easily recognized on Very Low Frequency (VLF) radio signal night-time recordings, as VLF signal's amplitude and phase delay deviations of characteristic footprint compared to signal's regular nocturnal behavior. Since highly susceptible to causative agent of this type, nocturnal subionospheric VLF propagation is a suitable tool for indirect probing of transient lower ionospheric disturbances related to localized areas of short-lived electron density increases in the D-region altitude range, referred as Localized Ionization Enhancements (LIEs). An analysis of the lower ionospheric response to lightning-induced electron precipitation events during the last quarter of the year 2004 was carried out, for cases of two VLF signals transmitting from USA (NAA/24 kHz) and UK (GQD/22.1 kHz) towards Belgrade (Serbia). Based on amount of LEP driven VLF perturbations recorded in Belgrade, subionospheric VLF signal propagation parameters were modeled and through conducted numerical simulations ionospheric parameters were obtained. Main results are presented in this work.

Keywords: lower ionosphere; VLF radio signal; perturbations; modeling

1. Introduction

Incident radiation and energetic processes localised within Earth's ionosphere in a great deal affect its physical and chemical properties (e.g., Kelley, 2009; Rycroft, 2006). Energetic events of terrestrial or extraterrestrial origins can pose as a source of induced disturbances within ionosphere and consequently influence all ongoing processes within this region (e.g., Goodman, 2005). Atmospheric discharges are source of radio waves that propagate along geomagnetic field lines into the plasmasphere and there interact with energetic electrons (30–300 keV). Through such interaction, some of electrons enter energy loss processes and consequently precipitate into ionosphere (e.g., Strangeways, 1993), producing within D-region altitude range localised areas of increased electron densities, i.e. Localised Ionization Enhancements (LIEs; e.g., Nunn, 1997). Lower Ionospheric disturbances caused through the Lightning-induced Electron Precipitation (LEP) processes and corresponding ionospheric plasma irregularities cause amplitude and phase perturbations of man-made Very Low Frequency (VLF) signals transmited subionosphericaly (e.g., Silber & Price, 2017 and references therein) within Earth-ionosphere waveguide, where Earth's surface is the lower boundary and lower ionopsheric edge is the upper boundary of this waveguide.

*Corresponding author, e-mail: aleksandra.kolarski@ipb.ac.rs

Perturbations of VLF radio signals, related to such short-lived electron density increases due to LEP events, in period covering the last quarter of the year 2004 were monitored on data recorded by Belgrade VLF receiving system. VLF signals on frequencies 24 kHz and 22.1 kHz, arriving in Belgrade from USA (transmitter located in Maine) and UK (transmitter located in Skelton) were chosen for detailed analysis. Based on measured VLF data, numerical simulations were carried out in order to obtain simulated propagation parameters and ultimately, electron density changes produced by these sudden events.

2. Observations and Data

Instrumental set-up used in this research consisted of Belgrade (BEL) VLF receiving system Absolute Phase and Amplitude Logger (AbsPAL), operating in narrow-band operational mode and located at the Institute of physics Belgrade (44.85°N; 20.38°E), Serbia. Observations were simultaneously conducted for all VLF signals recorded by BEL system within inspected period, with VLF signals transmitting from USA (NAA/24.0 kHz) and UK (GQD/22.1 kHz) were analyzed in detailed (Table 1). Map with NAA and GQD signals' Great Circle Paths (GCPs), as registered in Belgrade, is given in Figure 1.

VLF signal perturbations recorded by BEL station on monitored VLF signals, for a case of one typical LEP event, are presented in Figure 2. Recorded VLF signal perturbations appear as characteristic amplitude decrease and phase increase mirroring each other, with maximal perturbation corresponding to the occurrence of the LEP event. Maximal perturbation and unperturbed nocturnal signal related to LEP event from 16 November 2004, which effects are presented in this paper, are indicated by red and black arrows, respectively. Amplitude and phase perturbations induced by this LEP event are of common features, regarding absolute amount of amplitude (up to 5 dB) and phase (up to a few tens of degrees) changes and of maximal duration (of up to 2 minutes) as well, as other typical LEP driven perturbations recorded in Belgrade in inspected period.

Table 1. VLF signals' transmitter characteristics

VLF signal (kHz)	Transmitter location (latitude; longitude)	Emitted power (kW)	GCP distance* (km)
NAA/24.0	Maine, USA (44.63°N; 67.28°W)	1000	6547
GQD/22.1	Skelton, UK (54.72°N; 2.88°W)	500	1982

Note. *Distance between transmitter and BEL receiver along GCP

Figure 1. Map with analysed VLF signals' GCPs (black lines) emitted towards BEL receiver site (blue circle) from USA (NAA/24.0 kHz) and UK (GQD/22.1 kHz) (red circle).

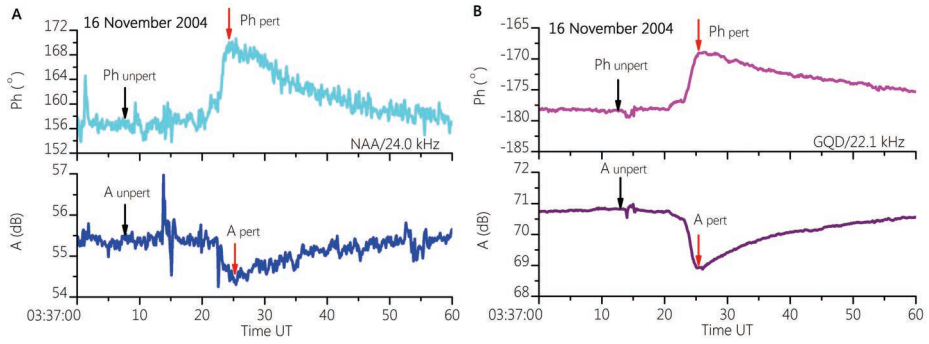

Figure 2. Amplitude and phase (dark and light solid lines, respectively) perturbations induced by LEP event occurred on 16 November 2004 recorded on monitored VLF signal traces: NAA/24.0 kHz (A) and GQD/22.1 kHz (B).

3. Results and Discussion

Changes in amplitude Δ*A* (dB) and phase Δ*Ph* (°) were obtained as differences between the measured maximum values of the perturbed signal compared to the regular nocturnal signal values before the perturbation onset. Based on values measured from the signal, modelling procedure was designed employing Long Wavelength Propagation Capability (LWPC) software (Ferguson, 1998) to obtain modelled values for both unperturbed and perturbed conditions, as best fitting to real measured data. In order to get simulated ionospheric conditions within waveguides to match as close as possible to real ones, pairs of propagation parameters sharpness β (km^{-1}) and reflection height *H*′ (km) were modelled within selected sections of the waveguides through REXP subroutine and estimated as best fitting, so that obtained and measured values of the signals' phase and amplitude at the place of the Belgrade receiver reach a good agreement. Measured and simulated data values are given in Table 2.

Table 2. Measured and modelled amplitude and phase for monitored VLF signals related to maximal perturbation induced by the LEP event from 16 November 2004

VLF signal (kHz)	Measured Δ*A* (dB)	Measured Δ*Ph* (°)	Simulated Δ*A* (dB)	Simulated Δ*Ph* (°)
NAA/24.0	−1.05	12.95	−1.01	21.84
GQD/22.1	−1.74	9	−1.75	5.66

Numerically simulated propagation parameters β (km^{-1}) and *H*′ (km) along GCPs of analysed VLF signals, related to maximal perturbation due to the LEP event occurred on 16 November 2004, are given in Figure 3, in blue and green for parameter *H*′ (block diagram on left) and olive and orange for parameter β (block diagram on right) in cases of NAA and GQD signals, respectively. Path varying unperturbed values for both signals are given in light and dark gray for NAA and GQD signal, respectively. For the sake of visibility, comparison between NAA and GQD signals' parameters is given only for the region covering slightly wider area corresponding to the GQD signal GCP. Place of GQD transmitter is indicated by black star, direction towards NAA transmitter by black arrow and BEL receiver location by red circle.

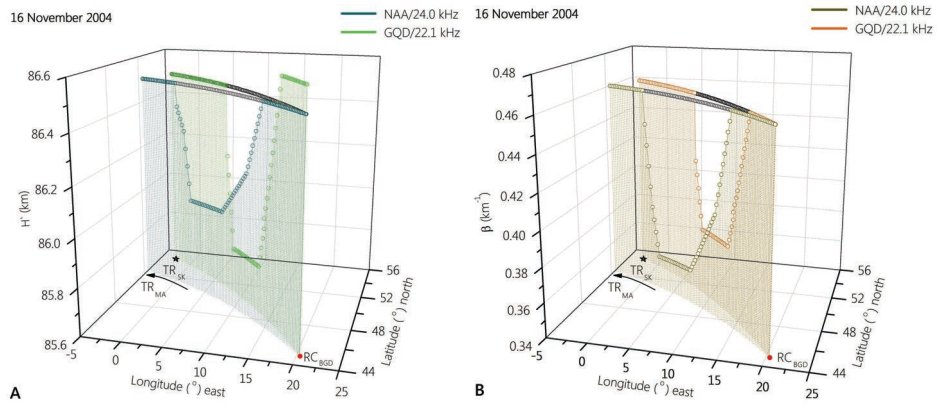

Figure 3. Propagation parameters' changes related to analysed LEP event influence along NAA and GQD signal GCPs towards Belgrade.

Note. Panel A: Parameter β (km^{-1}). Panel B: Parameter *H*′ (km). For perturbed state NAA is in blue and olive and GQD in green and orange, while for unperturbed state in light and dark gray, respectively; RC is for BEL receiver, TR is for transmitter).

As expected, due to the influence of analysed LEP event, propagation parameters changed in a great deal, compared to their unperturbed nocturnal values. Although propagating close to each other, especially near BEL receiver, conditions within waveguides of monitored VLF signals considerably differ indicating that these signals undergo divergent perturbations in spite that were induced by the same LEP event. In maximal intensity of the perturbation, in case of GQD signal reflection height is more lowered, while in case of NAA signal sharpness became more reduced, as compared with each other. After the LEP event's impact, in case of parameter β both waveguides recovered entirely and went back to their regular values at the place of BEL receiver, while in case of parameter *H*′, waveguide of GQD signal remained slightly perturbed.

Based on modeled propagation conditions, relying on Wait's theory application (e.g., Wait & Spies, 1964; Wait, 1970), electron density height profiles $N_e(z)$ (m^{-3}), for given parameters β (km^{-1}) and *H*′ (km), were calculated using the Equation 1 for the nocturnal ionospheric conditions given by (Nunn, 1997):

$$N_e(z, H', \beta) = 1.86 \cdot 10^{11} \cdot e^{-0.15 \cdot z} \cdot 78.57 \cdot e^{\beta(z - H')}, \quad (m^{-3}) \tag{1}$$

Electron density height profiles throughout lower ionospheric altitude range (50–90 km) were calculated for cases of analysed VLF signals, both for perturbed and unperturbed ionospheric conditions. Due to present ionospheric irregularity, propagation parameters deviated from regular values causing corresponding increase in electron densities within waveguides. Comparison between perturbed states within waveguides of NAA and GQD signals along their GCPs, at their reflection heights, corresponding to maximal perturbation due to the influence of the LEP event on 16 November 2004, is given in Figure 4. Electron densities along analysed VLF

signals' GCPs, related to unperturbed and perturbed ionospheric conditions for NAA and GQD signals are given in light and dark gray and blue and pink, respectively. Ionisation increased by this LEP event for both analysed VLF signals stayed within the same order of magnitude, compared to unperturbed ionospheric conditions.

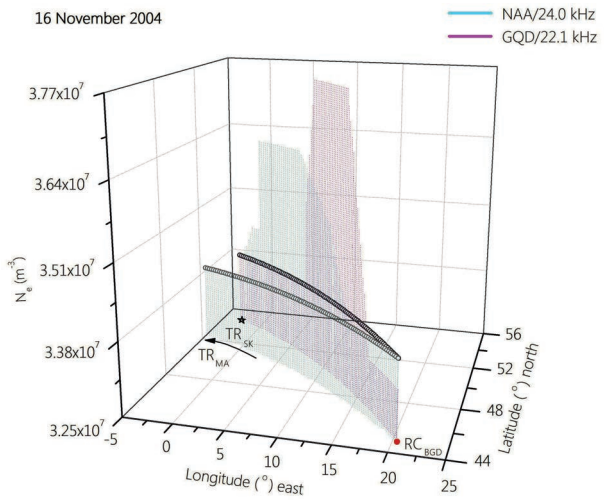

Figure 4. Electron density height profiles along NAA and GQD signal GCPs towards Belgrade, for unperturbed (light and dark gray, respectively) and perturbed (blue and pink, respectively) ionospheric states related to analysed LEP event (RC is for BEL receiver, TR is for transmitter).

4. Conclusions

During the influence of LEP event on 16 November 2004, perturbations in amplitude and phase of similar amount and with features characteristic for this type of driving agent were observed on both monitored VLF signals at the place of BEL receiver. Decrease in amplitude in both analysed VLF signals is less than 2 dB, while increase in phase is roughly around 10°, with more pronounced change of amplitude in GQD signal and of phase in NAA signal. However, although in general with some similar characteristics, these two signals undergo different perturbations even though arising from the same inducing agent. Modelled amplitude and phase values of NAA and GQD signals, as well as their relative changes compared to unperturbed state, obtained trough conducted numerical simulations are both in good agreement with data measured at the BEL receiver site. Lowering of the VLF signal reflection height with reducing of reflection edge sharpness took place in case of both analysed VLF signals, as the effect of occurred LEP event. During maximal perturbation, in case of NAA signal reflection height was lowered for 0.5 km and reflection edge sharpness decreased for 0.10 km^{-1} compared to unperturbed state, while in case of GQD signal reflection height descended for 0.7 km and reflection edge sharpness decreased for 0.08 km^{-1}. Parameter of sharpness in both perturbed VLF signals reached values that are characteristic for daytime ionospheric conditions. After the perturbation, both waveguides went back to recovered states of regular nocturnal ionospheric conditions. Obtained

maximum electron density change at the signal's reflection height reached approximately 10.9% for GQD signal, which is notably higher than in case of NAA signal where it reached approximately 7.7%, as compared to their unperturbed states. Obtained results are in line with other studies (Clilverd et al., 2002; Kerrache et al., 2021; Silber & Price, 2017; Šulić, Nina, et al., 2010; Šulić, Žigman, et al., 2010).

Acknowledgements

This work was funded by the Institute of Physics Belgrade, University of Belgrade, through a grant by the Ministry of Science, Technological Development and Innovations of the Republic of Serbia. Author thanks D. Šulić for instrumental set-up.

References

Clilverd, M. A., Nunn, D., Lev-Tov, S. J., Inan, U. S., Dowden, R. L., Rodger, C. J. & Smith, A. J. (2002). Determining the size of lightning-induced electron precipitation patches. *Journal of Geophysical Research: Space Physics*, *107*(A8), Article 1168. https://doi.org/10.1029/2001JA000301

Ferguson, J. (1998). *Computer Programs for Assessment of Long-Wavelength Radio Communications, Version 2.0: User's Guide and Source Files* (Technical Document 3030). Space and Naval Warfare Systems Center.

Goodman, J. M. (2005). *Space Weather & Telecommunications* (2005th ed.). Springer.

Kelley, M. C. (2009). *The Earth's Ionosphere: Plasma Physics and Electrodynamics* (2nd ed.). Academic Press.

Kerrache, F., Nait Amor, S., & Kumar, S. (2021). Ionospheric D region disturbances due to FAC and LEP associated with three severe Geomagnetic Storms as observed by VLF Signals. *Journal of Geophysical Research: Space Physics*, *126*(2), Article e2020JA027838. https://doi.org/10.1029/2020JA027838

Nunn, D. (1997). On the numerical modelling of the VLF Trimpi effect. *Journal of Atmospheric and Solar-Terrestrial Physics*, *59*(5), 537–560. https://doi.org/10.1016/S1364-6826(96)00048-X

Rycroft, M. J. (2006). Electrical processes coupling the atmosphere and ionosphere: An overview. *Journal of Atmospheric and Solar-Terrestrial Physics*, *68*(3–5), 445–456. https://doi.org/10.1016/j.jastp.2005.04.009

Silber, I. & Price, C. (2017). On the Use of VLF Narrowband Measurements to Study the Lower Ionosphere and the Mesosphere–Lower Thermosphere. *Surveys in Geophysics*, *38*, 407–441. https://doi.org/10.1007/s10712-016-9396-9

Strangeways, H. (1993). *Lightning, Trimpis and Sprites*. Oxford University Press.

Šulić, D., Nina, A. & Srećković, V. (2010). Numerical Simulations of the Effect of Localised Ionospheric Perturbations on Subionospheric VLF Propagation. *Publications of the Astronomical Observatory of Belgrade*, *89*, 391–395. https://publications.aob.rs/89/pdf/391-395.pdf

Šulić, D., Žigman, V. & Nina, A. (2010, September 13–17). *Study of the observed amplitude and phase perturbations on VLF signals from lighting induced electron precipitation and reconstruction of D-region electron density height profile* [Abstract]. 4th VERSIM Workshop 2010, Prague, Czech Republic. https://physics.mff.cuni.cz/kfpp/versim10/program.pdf

Wait, J. R. (1970). *Electromagnetic Waves in Stratified Media* (2nd ed.). Pergamon Press

Wait, J. R., & Spies, K. P. (1964). *Characteristics of the Earth-Ionosphere Waveguide for VLF Radio Waves* (Technical Note No. 300). U. S. Department of Commerce, National Bureau of Standards.

PROGRESS REPORTS

Abstract

INVESTIGATION OF VLF TRANSMITTER AMPLITUDE VARIABILITIES BEFORE THE M_W7.8 TURKEY SYRIA EARTHQUAKES OF FEBRUARY 6, 2023

Mohamed Y. Boudjada[1], Pier Francesco Biagi[2], Hans Ulrich Eichelberger[1], Giovanni Nico[3], Patrick H. M. Galopeau[4], Maria Solovieva[5], Helmut Lammer[1], Bruno P. Besser[1], Manfred Stachel[1], Franz Giner[1]*

[1]Space Research Institute, Graz, Austria; e-mails: mohammed.boudjada@oeaw.ac.at; hans.ulrich.eichelberger@oeaw.ac.at; helmut.lammer@oeaw.ac.at; bruno.besser@oeaw.ac.at; manfred.stachel@oeaw.ac.at; franz.giner@oeaw.ac.at
[2]Department of Physics, University of Bari, Bari, Italy; e-mail: pf.biagi@gmail.com
[3]Institute of Applied Mathematics (IAC), National Research Council of Italy (CNR), Bari, Italy; e-mail: g.nico@ba.iac.cnr.it
[4]LATMOS-CNRS, UVSQ Université Paris-Saclay, Guyancourt, France; e-mail: patrick.galopeaug@latmos.ipsl.fr
[5]Institute of the Earth Physics, Russian Academy of Sciences, Moscow, Russia; e-mail: solovieva@ifz.ru

We report on the recent earthquakes (EQs) that occurred with the main shock on February 6, 2023 principally in the central southern part of Turkey and northwestern Syria. This region is predisposed to earthquakes because of the tectonic plate movements between Anatolian, Arabian and African plates. The seismic epicenter was localized at 37.08°E and 37.17°N with depth in the order of 10 km and magnitude M_W7.8. We use VLF Graz facility (Biagi et al., 2019; Schwingenschuh et al., 2011) to investigate the amplitude variation of TBB transmitter (Bafa, Turkey; 27.31°E, 37.40°N) radiating at frequency of 26.7 kHz. TBB signal is daily detected by Graz facility with an appropriate signal to noise ratio predominantly during night observations. We study in this analysis the variations of TBB amplitude signals, as detected by Graz facility (15.43°E, 47.06°N) eight weeks before and after the earthquakes occurrence. It is essential to note that the geographical latitude of the epicenter and the TBB transmitter is about 37°N, and the distance is in the order of 850 km. This distance is found smaller than the radius of the earthquake preparation zone, as derived from Dobrovolsky et al. (1979), taking into consideration the magnitude of the seismic event, i.e. M_W7.8. We discuss potential fluctuations of TBB transmitter amplitude probably due to the ionospheric disturbances generated by the EQs preparation area. Those fluctuations are compared to previous TBB observations recorded from 2019 to 2022, and to the M_W6.8 EQ that occurred on January 24, 2020, in the Anatolian region.

References

Biagi, P. F., Colella, R., Schiavulli, L., Ermini, A., Boudjada, M., Eichelberger, H., Schwingenschuh, K., Katzis, K., Contadakis, M. E., Skeberis, C., Moldovan, I. A., & Bezzeghoud, M. (2019). The INFREP network: Present situation and recent results. *Open Journal of Earthquake Research, 8*(2), 101–115. https://doi.org/10.4236/ojer.2019.82007

*Corresponding author, e-mail: mohammed.boudjada@oeaw.ac.at

Dobrovolsky, I. R., Zubkov, S. I., & Myachkin, V. I. (1979). Estimation of the size of earthquake preparation zones. *Pure and Applied Geophysics, 117,* 1025–1044. https://doi.org/10.1007/BF00876083

Schwingenschuh, K., Prattes, G., Besser, B. P., Močnik, K., Stachel, M., Aydogar, Ö., Jernej, I., Boudjada, M. Y., Stangl, G., Rozhnoi, A., Solovieva, M., Biagi, P. F., Hayakawa, M., & Eichelberger, H. U. (2011). The Graz seismo-electromagnetic VLF facility. Natural Hazards and Earth System Sciences, 11(4), 1121–1127. https://doi.org/10.5194/nhess-11-1121-2011

Abstract

ANALYSES OF MAGNITUDE $M_W \geq 5.5$ EARTHQUAKES WITH SUB-IONOSPHERIC VLF/LF ELECTRIC FIELD MEASUREMENTS IN EUROPE

Hans U. Eichelberger[1], Mohammed Y. Boudjada[1], Konrad Schwingenschuh[1], Pier F. Biagi[2], Patrick H. M. Galopeau[3], Maria Solovieva[4], Christoph Schirninger[5], Bruno P. Besser[1], Manfred Stachel[1], Werner Magnes[1]*

[1]Austrian Academy of Sciences, Space Research Institute, Graz, Austria; e-mail: hue@oeaw.ac.at, mohammed.boudjada@oeaw.ac.at, konrad.schwingenschuh@oeaw.ac.at, bruno.besser@oeaw.ac.at, manfred.stachel@oeaw.ac.at, werner.magnes@oeaw.ac.at
[2]Università di Bari, Physics Department, Bari, Italy; e-mail: pf.biagi@gmail.com
[3]LATMOS-CNRS, UVSQ Université Paris-Saclay, Guyancourt, France; e-mail: patrick.galopeau@latmos.ipsl.fr
[4] Russian Academy of Sciences, Institute of the Earth Physics, Moscow, Russia; e-mail: MCSolovieva@gmail.com
[5]University of Graz, Institute for Physics, Graz, Austria; e-mail: christoph.schirninger@uni-graz.at

Long-term investigations of strong (impending) earthquakes (EQs) could have a key role in the mitigation of socioeconomic outcomes related to these events, but powerful explanations about important processes and open research questions remain. In this study we investigate magnitude $M_w \geq 5.5$ EQs in Europe since 2018 adapted from the United States Geological Survey data base (2023) with sub-ionospheric VLF/LF radio paths. The receiver systems in Graz, Austria, which are part of the spatially distributed INFREP network stations, permanently measure electric fields between transmitters and receivers and have the potential to characterize the seismic (nucleation) phases and couplings in the VLF/LF waveguide from the lithosphere up the lower ionosphere (Biagi et al., 2019, Schwingenschuh et al., 2011). Affected links are mainly from the transmitters TBB (26.70 kHz, Bafa, Turkey), ITS (45.90 kHz, Niscemi, Sicily, Italy), and ICV (20.27 kHz, Tavolara, Sardinia, Italy), i.e., path crossings in EQ prone areas within the radius of the effective precursor manifestation zone (Dobrovolsky et al., 1979) around the EQ epicenter. The findings suggest that the intricate patterns of VLF/LF electric field variations based on the nighttime amplitude method (Hayakawa et al., 2010) could be related to $M_w \geq 5.5$ (threshold) EQs, the assumed significance level is 5%. In combination with complementary observations more robust results and extensions to lower magnitude thresholds could possibly be achieved.

Acknowledgement

We kindly acknowledge the long-term administrative support and network services from the IWF/ÖAW (Space Research Institute, Austrian Academy of Sciences) teams related to the VLF/LF facility.

*Corresponding author, e-mail: hue@oeaw.ac.at

References

Biagi, P. F., Colella, R., Schiavulli, L., Ermini, A., Boudjada, M., Eichelberger, H., Schwingenschuh, K., Katzis, K., Contadakis, M. E., Skeberis, C., Moldovan, I. A., & Bezzeghoud, M. (2019). The INFREP Network: Present Situation and Recent Results. *OJER*, *8*(2), 101–115. https://doi.org/10.4236/ojer.2019.82007

Dobrovolsky, I. P., Zubkov, S. I., & Miachkin, V. I. (1979). Estimation of the size of earthquake preparation zones. *Pageoph*, 117, 1025–1044. https://doi.org/10.1007/BF00876083

Hayakawa, M., Kasahara, Y., Nakamura, T., Muto, F., Horie, T., Maekawa, S., Hobara, Y., Rozhnoi, A. A., Solovieva, M., & Molchanov, O. A. (2010). A statistical study on the correlation between lower ionospheric perturbations as seen by subionospheric VLF/LF propagation and earthquakes. *Journal of Geophysical Research: Space Physics*, *115*(A9), Article 09305, https://doi.org/10.1029/2009JA015143

Schwingenschuh, K., Prattes, G., Besser, B. P., Mocnik, K., Stachel, M., Aydogar, Ö., Jernej, I., Boudjada, M. Y., Stangl, G., Rozhnoi, A., Solovieva, M., Biagi, P. F., Hayakawa, M., & Eichelberger H. U. (2011). The Graz seismo-electromagnetic VLF facility. *Natural Hazards and Earth System Sciences* 11, 1121–1127. https://doi.org/10.5194/nhess-11-1121-2011

United States Geological Survey. (2023). *Earthquake catalog* [Data base]. https://earthquake.usgs.gov/

Abstract

NEW POTENTIAL EARTHQUAKE PRECURSOR: REDUCTION OF THE VLF SIGNAL NOISE

Aleksandra Nina[1]*, *Pier Francesco Biagi*[2], *Sergey Pulinets*[3], *Srđan Mitrović*[4], *Giovanni Nico*[5], *Luka Č. Popović*[6,7]

[1]Institute of Physics Belgrade, University of Belgrade, Belgrade, Serbia; e-mail: sandrast@ipb.ac.rs
[2]Università di Bari, Physics Department, Bari, Italy; e-mail: pf.biagi@gmail.com
[3]Russian Academy of Sciences, Space Research Institute, Moscow, Russia; e-mail: pulse1549@gmail.com
[4]Novelic, Belgrade, Serbia; e-mail: mitar027@beotel.net
[5]Istituto per le Applicazioni del Calcolo (IAC), Consiglio Nazionale delle Ricerche (CNR), Bari, Italy; e-mail: giovanni.nico@gmail.com
[6]Astronomical Observatory, Belgrade, Serbia; e-mail: lpopovic@aob.ac.rs
[7]University of Belgrade, Faculty of Mathematics, Department of Astronomy, Belgrade, Serbia; e-mail: lpopovic@matf.bg.ac.rs.

In this study we present a possible new earthquake precursor which is manifested as the reduction of very low frequency (VLF) signal noise several minutes or tents of minutes before an event. We analyse changes in the signal amplitude and phase in both the time and frequency domains. The observed events are divided in the two groups related to the seismic activity in a localised area during a short time period. Namely, the results show that the intensive seismic activity can induce long-term reduction of the signal noise which includes more earthquakes with magnitude larger than four. We analyse the VLF signal emitted in Italy and received in Belgrade by the Absolute Phase and Amplitude Logger (AbsPAL) receiver located at the Institute of Physics Belgrade. In the first group of the earthquakes occurred when intensive seismic activity were not recorded, we analyse periods around the four events with magnitudes larger than four which occurred near Kraljevo (November 3 and 4, 2010), in the Tyrrhenian Sea (November 3, 2010), and in the Western Mediterranean Sea (November 9, 2010). In the second group, we present a study of the signal noise reduction during the period of intense seismic activity when almost 1,000 earthquakes occurred in Central Italy from October 25 to November 3, 2016.

Acknowledgements

The authors acknowledge funding provided by the Institute of Physics Belgrade and the Astronomical Observatory (the contract 451-03-47/2023-01/200002) through the grants by the Ministry of Science, Technological Development and Innovation of the Republic of Serbia.

*Corresponding author, e-mail: sandrast@ipb.ac.rs

Book of Abstracts and Contributed Papers
International Conference on Recent Trends in Geoscience Research and Applications 2023
Belgrade, Serbia & Virtual, October 23–27, 2023
Editors: Aleksandra Nina, Snežana Dragović, and Dejan Doljak

Abstract

ON THE DETECTION OF ANOMALIES IN TIME SERIES OF VLF SIGNALS RELATED TO SEISMIC ACTIVITY

Giovanni Nico[1], Manilo Monaco[2], Pier Francesco Biagi[3], Anita Ermini[4], Aleksandra Nina[5]*

[1]Institute of Applied Mathematics, Italy's National Research Council, Bari, Italy; e-mail: giovanni.nico@cnr.it
[2]Italian Space Agency, Matera, Italy; e-mail: manilo.monaco@asi.it
[3]University of Bari, Department of Physics, Bari, Italy; e-mail: pf.biagi@gmail.com
[4]University of Tor Vergata, Department of Industrial Engineering, Rome, Italy; e-mail: ermini@uniroma2.it
[5]University of Belgrade, Institute of Physics Belgrade, Belgrade, Serbia; e-mail: sandrast@ipb.ac.rs

In this work we present an application of the Perceptually Important Points (PIP) technique for the analysis of time series of VLF signals collected during some earthquakes (Mw = 5.0–6.0) occurred in the European area. The aim of the analysis is to detect "anomalies" of VLF signals with respect to the normal variations of the data trends; these anomalies could reveal possible radio precursors of the earthquakes. Since 2009, several radio receivers have been installed throughout Europe in order to realize the INFREP European radio network for studying the VLF (10–60 kHz) and LF (150–300 kHz) radio precursors of earthquakes (Biagi et al., 2011), (Righetti et al., 2012). The analysis has been applied to earthquakes with M ≥ 5.0 located inside the 5th Fresnel zone defined by each receiver and transmitter or inside a circle with a 300km radius around each receiver or transmitter. The time series which have been analyzed are referring to earthquakes that occurred on 2009-09-06 (Mw = 5.6), 2010-02-06 (Mw = 5.0), 2010-03-08 (Mw = 6.0), and 2020-01-30 (Mw = 5.6).

References

Biagi, P. F., Maggipinto, T., Righetti, F., Loiacono, D., Schiavulli, L., Ligonzo, T., Ermini, A., Moldovan, I. A., Moldovan, A. S., Buyuksarac, A., Silva, H. G., Bezzeghoud, M., and Contadakis, M. E. (2011). The European VLF/LF radio network to search for earthquake precursors: setting up and natural/man-made disturbances. *Natural Hazards and Earth System Sciences, 11*(2), 333–341. https://doi.org/10.5194/nhess-11-333-2011

Righetti, F., Biagi, P. F., Maggipinto, T., Schiavulli, L., Ligonzo, T., Ermini, A., Moldovan, I. A., Moldovan, A. S., Buyuksarac, A., Silva, H. G., Bezzeghoud, M., Contadakis, M. E., Arabelos, D. N., & Xenos, T. D. (2012). Wavelet analysis of the LF radio signals collected by the European VLF/LF network from July 2009 to April 2011. *Annals of Geophysics, 55*, 171–180. https://ui.adsabs.harvard.edu/abs/2012AnGp...55..171R/abstract

*Corresponding author, e-mail: giovanni.nico@cnr.it

GeosciRA23
Book of Abstracts and Contributed Papers
International Conference on Recent Trends in Geoscience Research and Applications 2023
Belgrade, Serbia & Virtual, October 23–27, 2023
Editors: Aleksandra Nina, Snežana Dragović, and Dejan Doljak

Abstract

AEROSOL VERTICAL PROFILES AND ABL HEIGHTS CORRESPONDING TO DIFFERENT PM_{10} POLLUTION LEVELS IN BELGRADE, SERBIA

Maja Kuzmanoski[1]*, *Zorica Podraščanin*[2], *Ana Ćirišan*[3], *Zoran Mijić*[1]

[1]Institute of Physics Belgrade, University of Belgrade, Belgrade, Serbia; e-mails: maja.kuzmanoski@ipb.ac.rs, zoran.mijic@ipb.ac.rs
[2]Department of Physics, Faculty of Sciences, University of Novi Sad, Novi Sad, Serbia; e-mail: zorica.podrascanin@df.uns.ac.rs
[3]Faculty of Ecology and Environmental Protection, Union-Nikola Tesla University, Belgrade, Serbia; e-mail: acirisan@unionnikolatesla.edu.rs

Western Balkans is among the regions with the highest level of air pollution in Europe (European Environmental Agency, 2022). Particulate matter (PM) has been recognized as one of the most harmful air pollutants, posing threat to human health. To design efficient pollution control measures, better understanding of conditions that contribute to elevated PM concentrations is necessary. The information on aerosol vertical profile, along with vertical profile of meteorological parameters, is important to understand dispersion of PM, the development of air pollution and the contribution of the long-range transport to surface PM concentrations.

In this study, the lidar measurements at 355 nm, performed in Belgrade, Serbia, are used to analyze the atmospheric boundary layer height (ABLH) and vertical profiles of aerosol backscatter coefficient. The ABLH is estimated with 1-min temporal resolution using the gradient method (Ilić et al., 2018), while the aerosol backscatter coefficient is derived from lidar signals averaged over 30-min intervals using Klett-Fernald retrieval method (Fernald, 1984; Klett, 1981). PM_{10} concentrations in Belgrade, used in this study, are obtained from the Serbian Environmental Protection Agency automatic monitoring stations.

Focusing on the 2018–2020 period, excluding data collected in presence of low- or mid-altitude clouds, we analyze the aerosol vertical structure and ABLH for periods of different levels of PM_{10} pollution in Belgrade, as well as the periods of different temporal changes of PM_{10} concentration. Additionally, the thermodynamic stability of the ABL in the analyzed cases is discussed, based on radiosounding measurements in Belgrade.

Acknowledgements

MK and ZM acknowledge funding provided by the Institute of Physics Belgrade, through the grant by the Ministry of Education, Science and Technological Development of the Republic of Serbia. EU COST Action CA18235 "Profiling the atmospheric boundary layer at European scale" is acknowledged.

*Corresponding author, e-mail: maja.kuzmanoski@ipb.ac.rs

References

European Environmental Agency. (2022). *Air quality in Europe 2022 (*Report No. 05/2022). https://doi.org/10.2800/488115

Fernald, F. G. (1984). Analysis of atmospheric lidar observations: some comments. *Applied Optics, 23*(5), 652–653. https://doi.org/10.1364/AO.23.000652

Ilić, L., Kuzmanoski, M., Kolarž, P., Nina, A., Srećković, V., Mijić, Z., Bajčetić, J., & Andrić, M. (2018). Changes of atmospheric properties over Belgrade, observed using remote sensing and in situ methods during the partial solar eclipse of 20 March 2015. *Journal of Atmospheric and Solar-Terrestrial Physics, 171*, 250–259. https://doi.org/10.1016/j.jastp.2017.10.001

Klett, J. D. (1981). Stable analytical inversion solution for processing lidar returns. *Applied Optics, 20*(2), 211–220. https://doi.org/10.1364/AO.20.000211

Abstract

STUDY OF POLAR OZONE ANNUAL CYCLE WITH CCM SOCOL-3

Andrey Mironov [1], Vladimir Zubov [1,2], Eugene Rozanov [1]*

[1]St. Petersburg State University, St. Petersburg, Russia; e-mails: st095857@student.spbu.ru; e.rozanov@spbu.ru
[2]Voeikov Main Geophysical Observatory, St. Petersburg, Russia; e-mails: v_zubov@rambler.ru

Comparison of the chemistry climate model (CCM) SOCOL-3 basic numerical experiment (without changing any parameters) with the Infrared Atmospheric Sounder Interferometer (IASI) satellite instrument shows that the greatest difference in total ozone content is observed in the polar region of the southern hemisphere.

To resolve this problem and to assess the role of the main physical and photochemical processes that affect the annual cycle of polar ozone in the southern hemisphere, we considered changes in the following processes in the model: (1) the rate of ozone photodissociation for large zenith angles of the Sun; (2) rates of stratospheric heterogeneous reactions under polar night conditions; and (3) intensity of the meridional mixing on the model sub-grid scales in the polar southern hemisphere.

A comparison of the model results with the corresponding IASI measurement data showed that photolysis and horizontal mixing are the most important features for improving ozone modeling. A reasonable adjustment of these factors has made it possible to significantly improve the model representation of the annual ozone cycle over the polar region in the southern hemisphere.

Acknowledgements

The work was carried out at the St. Petersburg State University "Ozone Layer and Upper Atmosphere Research laboratory" with the support of the Government of the Russian Federation (Grant No. 075-15-2021-583).

References

Ball, W. T., Alsing, J., Mortlock, D. J., Staehelin, J., Haigh, J. D., Peter, T., Tummon, F., Stübi, R., Stenke, A., Anderson, J., Bourassa, A., Davis, S. M., Degenstein, D., Frith, S., Froidevaux, L., Roth, C., Sofieva, V., Wang, R., Wild, J., . . . Rozanov, E. V. (2018). Evidence for a continuous decline in lower stratospheric ozone offsetting ozone layer recovery. *Atmospheric Chemistry and Physics, 18*(2), 1379–1394. https://doi.org/10.5194/acp-18-1379-2018

Dhomse, S. S., Kinnison, D., Chipperfield, M. P., Salawitch, R. J., Cionni, I., Hegglin, M. I., Abraham, N. L., Akiyoshi, H., Archibald, A. T., Bednarz, E. M., Bekki, S., Braesicke, P., Butchart, N., Dameris, M., Deushi, M., Frith, S., Hardiman, S. C., Hassler, B., Horowitz, L. W., . . . Zeng, G. (2018). Estimates of ozone return dates from Chemistry-Climate Model Initiative simulations. *Atmospheric Chemistry and Physics, 18*(11), 8409–8438. https://doi.org/10.5194/acp-18-8409-2018

*Corresponding author, e-mail: st095857@student.spbu.ru

Abstract

REXDAN—A NEW RESEARCH INFRASTRUCTURE WHOSE VESSEL WILL SOON SAIL ON DANUBE

Mirela Voiculescu[1], Cătălina Iticescu[1], Constantin Apetrei[1], Maxim Arseni[1], Mădălina Călmuc[1], Valentina Călmuc[1], Daniel Constantin[1], Adrian Roșu[1], Mihaela Timofti[1], Cătălina Țopa[1], Lucian P. Georgescu[1]*

[1]University Dunărea de Jos, Galați, Faculty of Sciences and Envirnoment, Galați, Romania, e-mails: Mirela.Voiculescu@ugal.ro; Catalina.ITicescu@ugal.ro; Constantin.Apetrei@ugal.ro; Maxim.Arseni@ugal.ro; Madalina.Calmuc@ugal.ro; Valentina.Calmuc@ugal.ro; Daniel.Constantin@ugal.ro; Mihaela.Timofti@ugal.ro; Catalina.Topa@ugal.ro; Lucian.Georgescu@ugal.ro

During the last three years, a new research infrastructure (REXDAN) was built, consisting of a research vessel and an on-land research center (REXDAN, n.d.). The research vessel will undertake research activities in: chemistry, biology, physics, environmental science, ecology, bathymetry, topography, atmospheric chemistry, sustainable development, related to water, sediments, soil, air, biodiversity, bathymetry, hydromorphology and will cover a wide geographical area (2,000 km of the Danube navigable sector including wide coastal areas). Activities during research trip will be mainly collecting and preparing samples and performing physico-chemical and ecological analysis, bathymetric observations, atmospheric investigations. Research activities in on-land laboratories focus on in-depth analyses of water, soil, biological and zoological component, using state of the art equipment. A cloud remote sensing station is also part of the on-land research center, continuously investigating vertical atmospheric profiles of temperature, humidity, water vapour, planetary layer, aerosol composition.

Acknowledgements

We acknowledge the project An Integrated System for the Complex Environmental Research and Monitoring in the Danube River Area, REXDAN, SMIS code 127065, co-financed by the European Regional Development Fund through the Competitiveness Operational Programme 2014–2020, contract no. 309/10.07.2020.

References

REXDAN. (n.d.). https://www.rexdan.ugal.ro/index.php/en/

*Corresponding author, e-mail: Mirela.Voiculescu@ugal.ro

Abstract

INVESTIGATION OF THE ATMOSPHERIC CLOUDS AND BOUNDARY LAYER OVER THE WESTERN-INDIAN REGION

Dharmendra Kumar Kamat[1, 2], Som Kumar Sharma[1], Sourita Saha[3], Prashant Kumar[4], Kondapalli Niranjan Kumar[5]*

[1]Physical Research Laboratory, Space and Atmospheric Sciences Division, Ahmedabad, India; e-mails: dharmendrakamat@prl.res.in; somkumar@prl.res.in
[2]Indian Institute of Technology Gandhinagar, Department of Physics, Gandhinagar, India; e-mail: dharmendrak@iitgn.ac.in
[3]University of California, Scripps Institutions of Oceanography, California, USA; e-mail: souritasahasweta@gmail.com
[4]Space Applications Centre, Ahmedabad, India; e-mail: kam3545@gmail.com
[5]National Centre for Medium Range Weather Forecasting, Ministry of Earth Sciences, Noida, India; e-mail: nirukin2003@gmail.com

The changing climate has put atmospheric clouds and boundary layer in focus due to their potent role in the climate system. The atmospheric boundary layer (ABL) is the lowest layer in the troposphere which directly interacts with Earth's surface, influences weather and the hydrological cycle, and is associated with low-level clouds. Clouds play a crucial role in the atmosphere, and their properties, such as cloud base height (CBH), cloud top height (CTH), cloud fraction, and vertical layer structure, significantly affect radiative balance, atmospheric circulations, and other meteorological processes. Therefore, monitoring and investigating clouds and ABL parameters and their interaction is essential for climate diagnosis and predicting future climate.

This study uses ground-based Lidar, satellite, and reanalysis datasets to investigate the atmospheric clouds and boundary layer over the Western-Indian region. The study aims to get insights into the coupling of low-level clouds with ABL and to study the cloud formation and break-off factors under the influence of surface forces. Investigations over the Udaipur (24.58°N, 73.71°E) region showed that the boundary layer clouds (BLC) persist throughout the day by the transport of moisture to cloud heights by turbulent updrafts, and clouds deck broke off with the entrainment of free tropospheric air when the boundary layer deepens. On 21 July 2022, during the early hours, CBH was around 0.5 km and reached about 2 km during the peak sunshine and reduced after that. Due to strong coupling, the BLC sits atop the boundary layer throughout the day. This study will provide better insights into the cloud and boundary layer interaction and its impact on weather and climate sensitivity.

*Corresponding author, e-mail: dharmendrakamat@prl.res.in

Abstract

GEOMAGNETIC DISTURBANCE FORCING ON THE MIDDLE ATMOSPHERE

Irina Mironova[1]*

[1]St. Petersburg State University, Faculty of Physics, Department of Earth Physics, St. Petersburg, Russia; e-mail: i.a.mironova@spbu.ru

Information about the energetic electrons precipitation (EEP) from the radiation belt into the atmosphere is important for assessing the ozone variability and dynamics of the middle atmosphere during magnetospheric and geomagnetic disturbances. The exact values of energetic electron fluxes depending on their energy range are one of the most important problems in estimation of atmospheric ionization rates, which, in turn, are taken into account when evaluating ozone depletion in chemical-climatic models. Despite the importance of these processes for the high latitudes of the middle atmosphere, the precipitation of energetic electrons is still insufficiently studied. To better understand EEP and related processes in the atmosphere, it is important to have many realistic EEP observations in order to correctly characterize their spectra.

In this work, we compare the spectra of precipitating energetic electrons with energies from keV up to relativistic energies about 1 MeV, based on balloon observations in the high-latitude atmosphere and precipitation of energetic electrons recorded by the NOAA POES satellites in 2003. Here, we estimate the spectra and ionization rates of the atmosphere during energetic electron precipitation, according to various observations, in different periods of geomagnetic disturbances. Using a one-dimensional radiative-convective model with ion chemistry, we show the response to precipitation of energetic electrons in a polar atmosphere.

Acknowledgements

The work was carried out at the "Laboratory for the Study of the Ozone Layer and Upper Atmosphere" with the support of the Ministry of Science and Higher Education of the Russian Federation under contract No. 075-15-2021-583.

References

Grankin, D.; Mironova, I.; Bazilevskaya, G., Rozanov, E., & Egorova, T. (2023). Atmospheric Response to EEP during Geomagnetic Disturbances. *Atmosphere*, *14*(2), Article 273. https://doi.org/10.3390/atmos14020273

*Corresponding author, e-mail: i.a.mironova@spbu.ru

GeosciRA23
Book of Abstracts and Contributed Papers
International Conference on Recent Trends in Geoscience Research and Applications 2023
Belgrade, Serbia & Virtual, October 23–27, 2023
Editors: Aleksandra Nina, Snežana Dragović, and Dejan Doljak

Abstract

UNVEILING CONFLICT HERITAGE: EXAMINING THE INFLUENCE OF HUMAN CONFLICTS ON LAND DEGRADATION AND LANDSCAPE MODIFICATION

Ivan Lizaga [1], Borja Latorre[2], Montfort Bagalwa[3,4], Bossissi Nkuba[5], Kristof Van Oost[3], Pascal Boeckx[1]*

[1]Isotope Bioscience Laboratory (ISOFYS), Department of Green Chemistry and Technology, Ghent University, Gent, Belgium; e-mails: ivan.lizaga@ugent.be; pascal.boeckx@ugent.be
[2]Estación Experimental de Aula-Dei (EEAD-CSIC), Spanish National Research Council, Zaragoza, Spain; e-mail: borja.latorre@eead.csic.es
[3]Earth and Life Institute, Université Catholique de Louvain, Louvain-la-Neuve, Belgium; e-mail: montfort.bagalwa@uclouvain.be; kristof.vanoost@uclouvain.be
[4]Service Environnement, Observatoire Volcanologique de Goma (OVG), Goma, Democratic Republic of Congo; e-mail: montfortbagalwa2021@gmail.com
[5]University of Antwerp, Institute of Development Policy and Management (IOB), Antwerpen, Belgium; e-mail: bossissi.nkuba@uantwerpen.be

Human migrations, often driven by armed conflicts, have far-reaching and enduring impacts on landscapes, disrupting the natural environment, ecosystem health, food security, and biodiversity conservation. These conflicts disrupt traditional land practices, agriculture, and conservation efforts, limiting long-term conservation.

However, conflict-related instability hinders comprehensive ground-level impact assessments, making it nearly impossible to track and understand the evolving situation at big scales. While satellite-based remote sensing provides valuable insights, limitations in temporal and spatial resolution constrain our ability to capture subtle landscape changes.

In this context, inland deltas can serve as records of human activities and changes in land use. We propose monitoring their changes using remote sensing, fieldwork, and crowdsourced data to better understand the interplay between human actions and landscape degradation in post-conflict areas.

As a case study, we apply this method to the Lake Kivu region, a conflict-prone area between the Democratic Republic of Congo and Rwanda. Our research indicates that monitoring inland deltas has the potential to inform lasting landscape effects, aid in conflict resolution, promote sustainable development, and contribute to post-conflict reconstruction efforts, ultimately mitigating environmental degradation in conflict-affected regions.

*Corresponding author, e-mail: ivan.lizaga@ugent.be

Abstract

MODELING OF VERTICAL GRAVITY GRADIENT FOR PURPOSES OF GRAVIMETRIC SURVEY

Klemen Medved[1], Božo Koler[2], Sofija Naod[3], Oleg Odalović[3]*

[1]Surveying and Mapping Authority of the Republic of Slovenia, Ljubljana, Slovenia; e-mail: klemen.medved@gov.si
[2]University of Ljubljana, Faculty of Civil and Geodetic Engineering, Ljubljana, Slovenia; e-mail: Bozo.Koler@fgg.uni-lj.si
[3]University of Belgrade, Faculty of Civil Engineering, Department of Geodesy and Geoinformatics, Belgrade, Serbia; e-mails: sofijanaod@gmail.com; odalovic@grf.bg.ac.rs

The knowledge of the vertical gradient of the gravity field is of great importance in gravimetry and consequently in geodesy, since the gravity acceleration measured with the instrument must be reduced to a stabilized point. We can model vertical gravity gradient by using normal gravity field and different digital terrain models. In this research, we used an approach that belongs to the group of "forward modeling" methods and differs from the known and used vertical gravity gradient modeling procedures, as it does not contain data about the Earth's gravity field. We created various combinations of models from which we calculate the vertical gravity gradients. For all calculations, we assumed a constant density of topographic masses above the ellipsoid and included the effect of the Earth's curvatures, while using a square to determine the area of calculation and division into zones, all with the aim of improving calculation speed. In our approach, we model the gravitational influence of the topographic masses as the summation of the topographic masses between the ellipsoid and the geoid and the topographic mass between the geoid and the physical Earth surface, using the rectangular prism as the elementary body.

Based on the deviations between the measured and modeled values, we were able to perform analyzes and statistical evaluations of the results. This allows us to determine the optimal model and data selection criteria for modeling vertical gravity gradients.

Acknowledgements

The authors acknowledge the financial support from the Slovenian Research Agency (research core funding No. P2-0227 Geoinformational structure and sustainable spatial development in Slovenia).

References

Odalovic, O., Medved, K., & Naod, S. (2022). Modeling of vertical gravity gradient by normal gravity field and digital terrain models. *Journal of Geodesy, 96*, Article 74. https://doi.org/10.1007/s00190-022-01669-y

*Corresponding author, e-mail: klemen.medved@gov.si

Abstract

UAV-BAZED SURVEY OF THE NATURAL MONUMENT KUKLICA

Ivica Milevski[1], Slavoljub Dragicević[2], Bojana Aleksova[1]*

[1]Ss. Cyril and Methodius University, Faculty of Natural Sciences and Mathematics, Skopje, North Macedonia; e-mails: ivica@iunona.pmf.ukim.edu.mk, aleksova_bojana@yahoo.com
[2]University of Belgrade, Faculty of Geography, Serbia; e-mail: slavoljub.dragicevic@gef.bg.ac.rs

This paper presents methods and techniques for UAV-based survey of the geosite "Kuklica" near the town of Kratovo, North Macedonia. Kuklica is a rare natural complex of earth pyramids with exceptional scientific, educational, tourist, and cultural significance. In this area, it can study the intensity of geomorphological processes on this type of denudation landforms and different levels of morphological evolution, from initial ones (young stage) to almost total destruction (old stage). Because of its significance, Kuklica geosite is proclaimed a Natural monument and legally protected area in 2008. However, after the proclamation, the interest in visiting this site rapidly grew, as well as the threats of its potential degradation. Because of that, the anthropogenic impact starts to show through the numerous interventions that have been made in this area in the last years (paved paths, channels, info-house, toilets, etc.). With increased threats for degradation of Kuklica and destruction of individual landforms, the need for detailed inventory and monitoring of this site appears. Given the small size of the site (0.8 km^2), the freely available satellite images and digital elevation models do not allow its comprehensive analysis and monitoring, especially of the individual forms. Worldwide, for visual and 3D surveys or monitoring of similar geosites, new tools are increasingly used, including Unmanned Aircraft Vehicles (UAV) and Light Detection and Ranging (LiDAR). Given that professional LiDAR is very expensive and still poorly available, in this research, we used UAV (drone) for that purpose. First of all, the flight path and altitude of the UAV as well as ground markers (checkpoints), were precisely defined. Using Agisoft Metashape software, a digital elevation model and orthophoto imagery with ultra-high (sub-decimeter) resolution are produced. With the procedure, more than 100 earth pyramids were recorded, ranging in height from 1–2 m to 8.4 m. In this stage, a very accurate UAV-based 3D model of the five biggest earth pyramids will be realized (accuracy is checked with the iPhone 14 pro LiDAR module) and their morphometrical properties will be calculated and analyzed with the assessment of all important erosion parameters. Also, anthropogenic constructions that can cause degradation will be identified and recorded for further monitoring. The final goal is to follow the changes and to minimize the degradation of the unique landscape, thus protecting the geosite and its values much better.

*Corresponding author, e-mail: ivica@iunona.pmf.ukim.edu.mk

Abstract

RAINFALL EROSIVITY IN BULGARIA–SERBIA TRANSBORDER REGION

Nina Nikolova[1], Jelena Svetozarevic[1], Simeon Matev[1], Dimitar Krenchev[1], Rositsa Kenderova[1], Georgi Rachev[6]*

[1]Sofia University "St. Kl. Ohridski"/Faculty of Geology and Geography, Sofia, Bulgaria; e-mails: nina@gea.uni-sofia.bg; jelena.svetozarevic09@gmail.com; smatev@gea.uni-sofia.bg; dkrenchev@gea.uni-sofia.bg; rosica@gea.uni-sofia.bg; ratchevg@gea.uni-sofia.bg

The present study aims to analyze the influence of precipitation on soil erosion in the cross-border region Bulgaria–Serbia, which includes territories with different climatic and orographic conditions. To achieve this goal, the erosivity of precipitation has been evaluated by indices based on monthly and annual sums (Fournier index—FI and modified Fournier index—MFI) for which numerous authors (Amara et al., 2020; Bonilla & Vidal, 2011; Coman et al., 2019; Li et al., 2022; Lukić et al, 2019) prove that they give reliable results and reflect the climatic features of the specific areas. The results of the analyzes show that, in most of the studied areas, in general, it is characterized by a low to moderate level of rainfall erosivity, but in individual stations, several years with a strong and even a very strong level of erosivity were found. Strong rainfall erosivity was observed mainly in the 1980s and 1990s, which were generally characterized by drought, and in years of high rainfall, for example, 2005 and 2014. In both cases, the higher level of erosivity of precipitation is due to uneven distribution of precipitation over the years and to individual cases of intense precipitation. Future research will continue to clarify the trends and causes of extreme rainfall events, which will contribute to the creation of appropriate strategies and the development of preventive activities, to reduce and possibly eliminate the negative impacts of climate change.

Acknowledgements

This work was completed as part of the National Science Program "Environmental Protection and Reduction of Risks of Adverse Events and Natural Disasters", approved by the Resolution of the Council of Ministers № 577/17.08.2018 and supported by Ministry of Education and Science of Bulgaria (Agreement № Д01-271/09.12.2022).

References

Amara, D. M. K., Ullah, K., & Yushu, Z. (2020). Rainfall erosivity estimation for Sierra Leone using non-parametric indices. *Theoretical and Applied Climatology, 139*, 221–236. https://doi.org/10.1007/s00704-019-02960-3

Bonilla, C. A., & Vidal, K. L. (2011). Rainfall erosivity in Central Chile. *Journal of Hydrology*, *410*(1-2), 126–133. https://doi.org/10.1016/j.jhydrol.2011.09.022

Coman, A. M., Lacatusu G., Macsim A.M., & Lazar G. (2019). Assessment of soil erosion using Fournier indexes to estimate rainfall erosivity. *Environmental Engineering and Management Journal*, Vol. 18, (8), 1739-1745, http://www.eemj.icpm.tuiasi.ro/

*Corresponding author, e-mail: nina@gea.uni-sofia.bg

Li, J., Sun, R., Chen, L. (2022). Assessing the accuracy of large-scale rainfall erosivity estimation based on climate zones and rainfall patterns. *CATENA,* 217, Article 106508. https://doi.org/10.1016/j.catena.2022.106508

Lukić, T., Lukić, A., Basarin, B., Ponjiger ,T. M., Blagojević, D., Mesaroš, M., Milanovi,ć M., Gavrilov, M., Pavić, D., Zorn, M., Komac, B., Miljković, D., Sakulski, D., Babić-Kekez, S., Morar C., & Janićević, S. (2019). Rainfall erosivity and extreme precipitation in the Pannonian basin. *Open Geosciences*, 11, 664–681. https://doi.org/10.1515/geo-2019-0053

Abstract

DELAYED RESPONSE OF LOW LATITUDES TEC DURING THIRTY-SIX GEOMAGNETIC STORMS FROM 2014 TO 2017

Heba Salah Mohamed[1,2], Christine Amory-Mazaudier[3], Sampad Kumar Panda[4], O. M. Shalabiea[5], A. Mahrous[6]*

[1]Cairo University, Faculty of Science, Astronomy, Space Science and Meteorology Department, Giza, Egypt; e-mail: heba.salah@aucegypt.edu
[2]Canadian International College, Basic Science Department, Cairo, Egypt
[3]Sorbonne Universit é, Ecole polytechnique, Institut Polytechnique de Paris, Universit é Paris Saclay, Observatoire de Paris, CNRS, Laboratoire de Physique des Plasmas (LPP), Paris, France; e-mail: christine.amory@lpp.polytechnique.fr
[4]Department of ECE, KL Deemed to be University, Koneru Lakshmaiah Education Foundation, Vaddeswaram, Gun-tur, Andhra Pradesh, India; e-mail: sampadpanda@gmail.com
[5]Beni-Suef University, Faculty of Navigation Science and Space Technology, Alexandria, Egypt; e-mail: shalabiea@sci.cu.edu.eg
[6]Egypt Japan University of Science and Technology, Institue of Basic and Applied Science, Alexandria, Egypt; e-mail: ayman.mahrous@ejust.edu.eg

Ionospheric response to the onset of geomagnetic storms is an important aspect for developing models towards better understanding and prediction of ionospheric parameters, particularly over the equatorial and low latitude sectors that are associated with several complexities. Our paper discusses the time response of the ionosphere (Δtiono) where Δtiono is the time elapsed from the onset of sudden storm commencement (SSC) of a magnetic storm to the absolute maximum value of DVTEC (TEC: total electron content). Over the period from 2014 to 2017, thirty-six storms are reviewed and their Δtiono are analyzed along with the magnetic and solar parameters. We defined a threshold value of TEC to be eight TECU. Three storms are studied in detail as a reference for the entire range of storms (March 2015, June 2015, and September 2015). The stations used are Kourou (KOUR; 5.25°N/52.80°W) in the American longitude sector, Addis Ababa (AAE; 9.03N°/38.76°E) in the African longitude, Port Blair (PBRI; 11.63°N/92.71°E), and Patumwan (CUSV; 13.73°N/100.53°E) in the Asian longitude sector. In the Asian and American sectors, for all storms combined, there is no significant correlation (0.44 for the Asian sector and 0.22 for the American sector) between the delay (SSC time/time of maximum DVTEC) and the minimum of the Dst as found by previous studies. Instead, we considered geomagnetic storms satisfying the criteria: a) SSC occurs on the day side and b) the origin of the magnetic storm on the solar disk must be far from the limb or does not belong to the far side, to obtain a much better correlation. The highest correlation value is observed at Thailand (0.84), followed by India (0.79) and South America (0.759), and the minimum value at Africa (0.641). The average response time in our study was found to be

*Corresponding author, e-mail: heba.salah@aucegypt.edu

about 27.2 h. We observed positive and negative ionospheric storms, five negative storms in South America followed by two in Asia and a single negative storm in Africa from which it is realized that the most negative storms are in the time range of 9–15 LT. Nevertheless, there is hardly any relationship between the strength of DVTEC amplitude and the intensity of magnetic storms irrespective of longitude sectors.

Abstract

MULTI-GNSS GLOBAL AND LOCAL IONOSPHERIC MAPPING UTILIZING EXCLUSIVELY PHASE OBSERVATIONS

Artem Padokhin[1,2], Elena Andreeva[1]*

[1]Lomonosov Moscow State University, Faculty of Physics, Moscow, Russia; e-mail: padokhin@physics.msu.ru
[2]Pushkov Institute of Terrestrial Magnetism, Ionosphere and Radio Wave Propagation, Troitsk, Russia; e-mail: es_andreeva@mail.ru

Reliable ionospheric information is important for many scientific and practical applications. The talk proposes an original method for constructing global and local ionospheric TEC maps based on the analysis of solely phase measurements of GNSS signals at a pair of coherent frequencies, which does not require satellite/receiver DCBs estimations and thus makes it easier to combine different GNSS systems within single reconstruction algorithm. The proposed approach uses the representation of the ionosphere as a thin layer with the electron content given by a truncated expansion into a series of spherical harmonics in MODIP system. The expansion coefficients are determined by least squares with the inequality constrains representing the positivity of TEC, implemented by solving the corresponding linear complementarity problem. RHS of the solved system consists of TEC variations rather than from TEC biased by satellite/receiver DCBs as in commonly used strategies. Extensive testing of the proposed method on the data of synthesized observations using the real geometry of GNSS satellites and receivers and the ionosphere, given by NeQuick2 model showed mean deviation of reconstructed TEC values from modeled ones to be 0.03TECu with RMS 0.75TECu and maximum errors not exceeding 5TECu in the areas with poor coverage by GNSS receivers. The results of the comparison of global ionospheric maps obtained by the proposed method and maps of CODE center showed practically unbiased results with mean deviation 0.07TECu, RMS 1.75TECu and maximum deviations not exceeding 10TECu also in the areas with poor receiver coverage. The proposed algorithm is implemented as a set of Python scripts, which can be routinely used for ionospheric mapping given data form network of GNSS receivers. Those scripts are available by the request from authors.

Acknowledgements

The work is supported by Russian Science Foundation (project 22-27-00396).

*Corresponding author, e-mail: padokhin@physics.msu.ru

GeosciRA23
Book of Abstracts and Contributed Papers
International Conference on Recent Trends in Geoscience Research and Applications 2023
Belgrade, Serbia & Virtual, October 23–27, 2023
Editors: Aleksandra Nina, Snežana Dragović, and Dejan Doljak

Contributed paper

NON-EXTENSIVE TSALLIS ENTROPY ANALYSIS ON LONG-TERM VARIATION OF JOULE HEATING AT HIGH LATITUDES

Sumesh Gopinath[1], C. P. Anil Kumar[2], Prince P. R[3], Sherin Ann Abraham[4], S. Antony[4]*

[1]Sri Sathya Sai Arts and Science College, Department of Physics, Thonnakkal, Thiruvananthapuram, Kerala, India; e-mail:sumeshgopinath@gmail.com
[2]Indian Institute of Geomagnetism, Equatorial Geophysical Research Laboratory, Krishnapuram, Tirunelveli, Tamil Nadu, India; e-mail:cpanilegrl@gmail.com
[3]University College, Department of Physics, Thiruvananthapuram, Kerala, India; e-mail: princerprasad@gmail.com
[4]Mahatma Gandhi University, School of Pure and Applied Physics, Kottayam, Kerala, India; e-mail: ansherinn@gmail.com

Abstract: The high-latitude thermosphere-ionosphere system receives a notable portion of the solar wind energy that crosses the magnetopause as a result of Joule heating, with remarkable and global-scale effects. A useful tool for examining many characteristics of nonlinear dynamical systems is nonextensive Tsallis entropy, a generalisation of Shannon entropy. By describing the level of nonextensivity, it can provide degree of intrinsic fluctuations. The computation of the Tsallis entropy of Joule heating in the upper atmosphere at high latitudes is reported for the first time in this paper, and its yearly relationship with the solar wind forcing during solar maxima and minima periods is discussed. We have used theoretical models to calculate the Poynting flux flowing onto the Earth's ionosphere and associated Joule heating due to the solar wind-magnetosphere-ionosphere dynamo. The investigation reveals that the Tsallis entropy values clearly reflect the complexity variations during solar maxima and minima periods of solar cycle 23**.**

Keywords:Ionosphere; Tsallis entropy; Joule heating; Solar wind;

1. Introduction

A significant field of study in magnetosphere-ionosphere-thermosphere coupling investigations is the energy transference that occurs among the magnetosphere and the ionosphere-thermosphere region. Extreme ultraviolet radiation from the sun, auroral particle precipitation, Joule heating from electric currents, and gravity wave transmission from the lower atmosphere are all ways that energy is deposited in Earth's upper atmosphere and ionosphere at high latitudes. While auroral particle precipitation and Joule heating are dominant during geomagnetic storms, forcing from the lower atmosphere plays a larger role during geomagnetic quiet periods.

The energy input during the geomagnetic storm is by particle precipitation and Joule heating. Joule heating, however, accounts for the majority of energy injection and, at its peak, can absorb up to two-thirds of the energy placed onto the thermosphere (Knipp et al., 2004).

*Corresponding author, e-mail: sumeshgopinath@gmail.com

In accordance with earlier research, solar wind energy during a geomagnetic storm strengthens the convective electric field, and the enormous injection of high-energy particles raises ionospheric conductivity and, as a result, Pederson currents. Due to the auroral zone being the primary location of high-energy particle precipitation, the accompanying Joule heating also rises (Wilson et al., 2006). Due to the occurrence of massive gravity waves and wind surges, the heated thermosphere region at high latitudes increases, disrupting the thermospheric density globally. Due to inaccurate density predictions made by thermospheric models, the altered thermospheric density may have an impact on low-orbit spacecraft's ability to operate normally. Therefore, since the 1950s, a variety of semi-empirical thermospheric models that take these effects into account have been created in order to meet the rising precision demands of missile and space missions.

With this aim Anil et al. (2023) developed a linear regression analysis technique to obtain the quantitative response of polar magnetic potential (Ψ) generated by this dynamo as in Equation (1) and associated electric potential (Φ) in kV as in Equation (2).

$$\Delta\Psi = 26.12 + 4.5N_{SW}V_{SW}B_T sin^4(\Theta/2) \quad (1)$$

$$\Delta\Phi = 27.30 + 3.7N_{SW}V_{SW}B_T sin^4(\Theta/2) \quad (2)$$

where N_{SW} number density of charged particles, V_{SW} solar wind velocity, B_T the root mean square magnitude of the IMF, and Θ is the angle of the IMF projected onto the Y-Z plane. For calculating the Poynting flux pouring into the ionosphere and the associated Joule heating as a result of the solar wind-magnetosphere-ionosphere interaction, Weimer (2005) developed a combined electrical and magnetic potential model. Joule heating near the Polar Regions is thought to be more significant than auroral regions in the current study because it has received less study.

Many years back, Tsallis (1988) proposed a generalization of the Boltzmann-Gibbs-Shannon entropic measure and this entropy functional proposed by Tsallis along with its associated generalized statistics is still being hailed as the possible basis of a theoretical framework suitable to deal with nonextensive settings. Tsallis entropy is a non-logarithmic entropy formalism which takes the form $k(1/(q-1))(1-\Sigma p^q_j)$, where P_j is the probability of j th microstate, k is the Boltzmann constant and q is the degree of non-extensivity of the system. According to thermo-statistics, the number of microstates is a measure of organization of a system and if the number of possible microstates for a given macrostate is high (or low), less-organized (or more-organized) the system will become. The classical Boltzmann-Gibbs-Shannon entropy is related to the condition q = 1 where ordinary diffusion processes described by linear Fokker-Planck equations exist. According to Tsallis statistics, the case q > 1, corresponds to a regime with long-range correlations characterized by anomalous diffusion processes which can only be explained through nonlinear Fokker-Planck equations. For the subsystems, say M and N, the pseudo-additivity of non-extensive Tsallis entropy can be described as:

$$S_q(M + N) = S_q(M) + S_q(N) + (1–q)\, S_q(M)\, S_q(N) \quad (3)$$

which is in contrast with the ordinary additivity:

$$S_q(M + N) = S_q(M) + S_q(N) \quad (4)$$

of BGS entropy. The multiplicative term (1–q) $S_q(M)$ $S_q(N)$ accounts for non-extensive statistics that describes long-range correlations between subsystems where the degree of non-extensivity is dependent on index (Burlaga et al., 2006; Pavlos et al., 2012).

2. Data and methodology

We used Level-2 data of Advanced Composition Explorer(ACE) Satellite from 2001 to 2010 to calculate Joule heating. We downloaded data from the web (https://ace.srl.caltech.edu/ASC/level2/cris_l2desc.html) for the parameters: solar wind velocity (V_{sw}), number density (N_{sw}), IMF-By and Bz and clock angle (Φ) of IMF. We used spherical cap harmonic analysis (SCHA). This SCHA involves the fitting of a potential function (zonal harmonics) with a series of oscillating functions: sine waves along parallels of latitudes and Legendre polynomials along circles of polar longitudes, Haines, (1985). The magnitude of Joule heating (S) is obtained by the combined model of electric and magnetic potential model as per the solution Equation (5) in the Weimer model (Weimer, 2005).

$$S = E \times (\nabla B/\mu) \quad (5)$$

Since the height integrated ionospheric Joule heating is really the dot product of the electric field with the height integrated perpendicular current, hence it exhibits variations in both hemispheres with respect to season, solar activity and solar events. As per the modeling equation, the role of the ionospheric conductivity distribution in regulating the power delivered by the dynamo is implicitly contained within the statistical magnetic potential model. The hourly Joule heating for the high latitude region is estimated using the Weimer_05 model in IDL platform. This process requires corrected geomagnetic coordinates (CGM) of the locations, solar wind parameters (wind speed and number density), IMF (By and Bz) parameters, and date and time to calculate the dipole tilt angle. The time lag is corrected as suggested by Burns et al. (2012).

2.1. Wavelet Tsallis entropy

Time-frequency analysis methods such as wavelet transforms are applied to study the features of a non-stationary signal. The discrete wavelet transform (DWT) gives a non-redundant representation of the signal while its values represent the coefficients in a wavelet series. These wavelet coefficients could give complete information in an easy way while they provide direct

estimation of local energies at different scales. It is also possible to organize the information in a hierarchical way of nested subspaces namely multi-resolution analysis in L 2 (ℜ). In the present work, we employ orthogonal discrete wavelet family Daubechies as mother wavelets. After computing the probability distribution of the energy, Tsallis wavelet entropy can be defined in terms of it as:

$$S_q=(1/(q-1)\ (\Sigma_j[p_j-(p_j)^q]) \quad (6)$$

where q is a non-extensivity parameter. Many complex systems in nature are described by a non-Gaussian distribution with different values of parameter q.

3. Results and discussions

In polar ionosphere, variations in Joule heating are predominantly controlled by changes in plasma convection, like the ones brought about by changes in the interplanetary magnetic field. The ionospheric Joule heating computed for the polar region is depicted in Figure 1 for the years 2001.

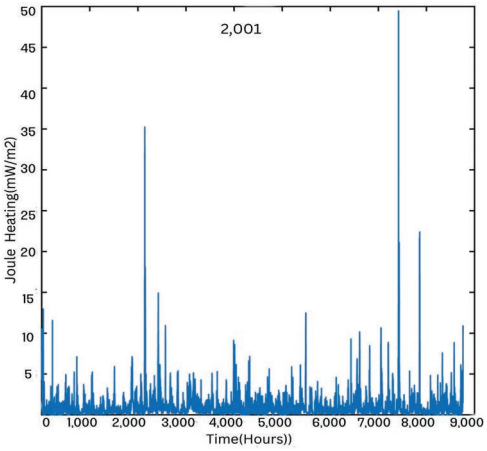

Figure 1. Joule heating rate in the ionosphere in southern hemisphere during the year 2001.

Joule heating exhibits marked variations, during summer months and it can be as small as few ten of mW/m2 to few hundreds of mW/m2 on background GW of the total Joule heating as shown in Figure 1. The conductivity of the ionosphere in the winter polar cap is ten order less than the conductivity in the summer polar cap. Billet et al. (2018) observed that solar-induced conductivity is higher in the hemispheric light months, resulting in higher magnitudes of Joule heating. Since, Earth's orbits is in its perihelia in the beginning of January and the region is lighted better. Therefore the ionospheric conductivity should slightly larger during this period. The perihelia-aphelion difference in the Sun-Earth distance is about three percent which means that the corresponding ionospheric electrodynamics will also differ. The consistently high conductivity of the sunlit summer ionosphere provides ideal conditions for the closure of field-aligned currents of any intensity (Akhila et al., 2020).

As the plasma velocities exceed mW/m^2 the neutral velocities by far, the role of neutral winds in Joule heating is usually ignored at high latitudes. Fujii (1981) studied the seasonal Birkeland current intensity and discovered that larger currents co-varies with both higher ionospheric conductivity and the efficiency of power output which is available. Most of the energy due to Joule heating in Polar Regions are dissipated to lower latitudes. It produces an

asymmetry in pattern geometry due to change in conductivity even though Weimer model provides realistic patterns parameterized by the IMF components direction and magnitudes. The perihelion-aphelion difference causes the difference in ionospheric electrodynamics.

In order to analyze the solar cycle dependence of the Joule heating rate, Tsallis entropy values can be compared for both solar minimum year 2008 (where solar radio flux at 2,800 MHz which is an excellent indicator of solar activity shows 70 sfu) and solar maximum year 2001 (solar radio flux shows 200 sfu). Figure 2 shows the first difference Joule heating time series for the year 2001.

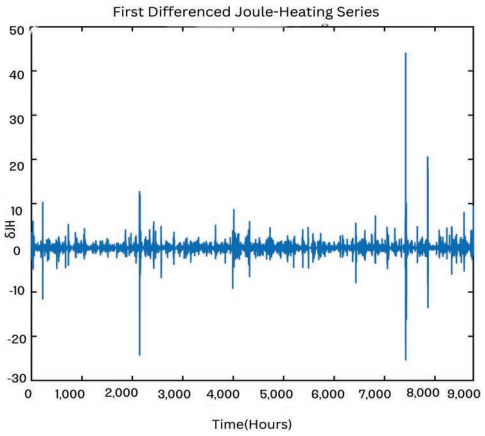

Figure 2. First difference Joule heating time series for the year 2001.

It is used to create the probability distribution function. Figure 3 shows PDF vs. q-Gaussian function (blue circles) and the nonlinear model fit (red solid line) for the Joule heating time series of 2001. For the solar maximum year 2001, the q = 1.5413 and β = 1.2044 with a mean squared error (MSE) of 0.00078. For the solar minimum year 2008, the q = 1.5402 and β = 1.2221 with an MSE of 0.0022. Similarly, the nonlinear fits were calculated independently for each year in order to give an account of the end values for other years also. It is found out that the average value of q is 1.54.

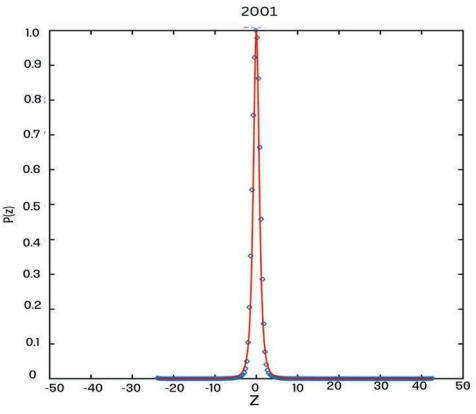

Figure 3. PDF P(z) vs. z q-Gaussian function (blue circles) and the nonlinear model (equation 15) fit (red solid line) for the joule heating time series of 2001.

Karakatsanis et al. (2013) have studied the phase transition process in the solar flare dynamics from a high dimensional non-Gaussian self-organized critical (SOC) state to a low dimensional non-Gaussian chaotic state. A magnetospheric phase transition associated with magnetic storms will produce a shift from high-dimensional quiet SOC state to a low-dimensional global chaotic state such that the non-extensive statistical character of the magnetospheric plasma is seen to be strengthened during storm periods. They have reported that the q index is higher in most cases during the storm period compared to the geomagnetically quiet periods preceding the storm in most cases.

Figure 4 shows the wavelet decomposition showing approximation coefficients and detail coefficients (levels 1–7) from Joule heating time series of 2001. Using wavelet entropy method, Tsallis entropy variations of Joule heating for the years 2001–2010 is depicted in Figure 5. During solar maximum year of 2001, the system was in a self-organized critical state which marks the reduction in Tsallis entropy which shows a value 0.1. As the system slowly comes out of the SOC state, during the subsequent waning of the sunspot cycle, entropy gradually increases. The entropy remained high during the period of 2004–2006, which is mid-way between the solar maxima and the succeeding minima. The decrease of the entropy during the onset of deep minimum at 2006, suggests a change in the organization level of the Joule heating—solar wind dynamics system connected with self-organization processes and the emergence of another newly developing self-organized state quite similar to the one that the system attained during solar maxima, with a lower complexity level, as evidenced by the loss of entropy. This is evident from the Tsallis entropy value of 0.14 during the year 2008. The entropy increases after the minimum, indicating a recovery of the global complexity of the system.

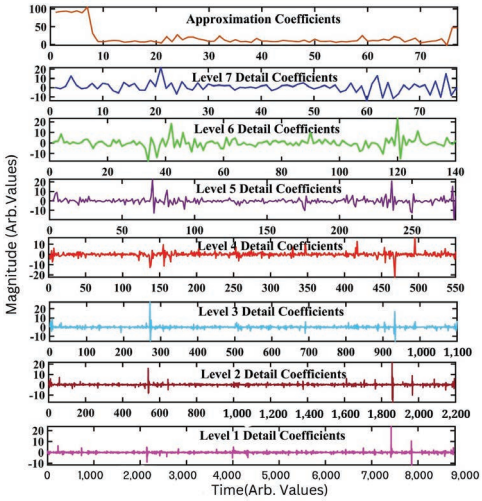

Figure 4. The wavelet decomposition showing approximation coefficients and detail coefficients (level1–7) from joule. Heating time series of 2001.

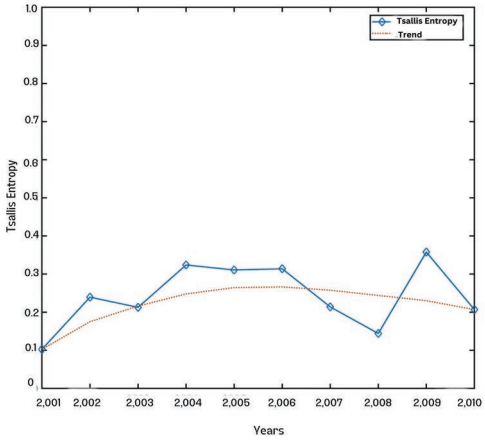

Figure 5. Tsallis entropy variations of joules heating for the years 2001–2010.

Joule heating depends on injection of large amount of energetic particle flux into the polar and auroral oval regions during magnetospheric disturbances as a result of losing of magnetospheric currents. The particle fluxes will collide with neutrals and eventually lose their kinetic energy through Joule heating. As this happens mainly in the high-latitude region, the concentration

of generated heat is high around this region. According to our results, it can be summarized as, for Joule heating, the existence of a non-extensive mechanism of energy dissipation/injection which can be characterized as fractal dissipation/energization mechanism as the variations in dissipation/energization corresponds to changes in fractal distribution.

4. Conclusion

According to our understanding, the Tsallis statistics is not only a simple generalization of thermodynamics for chaotic and complex systems, or a non-equilibrium generalization of Boltzmann-Gibbs statistics, but also serves as a powerful theoretical foundation for the unification of macroscopic and microscopic physical complexity. The present work will contribute to the understanding of non-extensivity and associated statistics related with the long-term variation of energy transfer in the high latitude ionosphere-thermosphere system. From the results, it is evident that, even though there is intermittent forcings by magnetospheric substorms and relative phenomena, non-extensive entropy of Joule heating rate predominantly depends on solar activity. The results of these analyses show that the non-extensive statistics are a general characteristic of Joule heating, suggesting that the associated system have a strong temporal correlation and a long-range interaction, such as with the solar wind-magnetosphere-ionosphere coupling.

Acknowledgements

The CPA is grateful to the Director, Indian Institute of Geomagnetism, Navi Mumbai for constant support and Ministry of Science and Technology, Government of India, for the financial assistance. He also thanks the Dr. D. R. Weimer for providing his IDL code, for SCHA-based model. The authors acknowledge ACE satellite team for the solar wind and IMF data.

References

Akhila, J. C. K., & Kumar, C. P. A. (2020). Investigation on High Velocity Plasmas and Field Aligned Currents at High Latitudes. *Asian Journal of Research and Reviews in Physics, 3*(2), 22–29. https://doi.org/10.9734/ajr2p/2020/v3i230117

Kumar, C. P. A., Ann, A. S., & Akhila, J. C. (2023). Investigation of Joule Heating in Polar Regions - Antarctica. *New Frontiers in Physical Science Research, 6*, 70–80. https://doi.org/10.9734/bpi/nfpsr/v6/17736D

Billett, D. D., Grocott, A., Wild, J. A., Walach, T., & Kosch, M. J. (2018). Diurnal Variations in Global Joule Heating Morphology and Magnitude Due To Neutral Winds. *Journal of Geophysical Research: Space Physics, 123*(3), 2398–2411. https://doi.org/10.1002/2017JA025141

Burns, G. B., Tinsley, B. A., Frank-Kamenetsky, A. V., Troshichev, O. A., French, W. J. R., & Klekociuk, A. R. (2012). Monthly Diurnal Global Atmospheric Circuit Estimates Derived from Vostok Electric Field Measurements Adjusted for Local Meteorological and Solar Wind Influences *Journal of the atmospheric sciences, 69*(6), 2061–2082. https://doi.org/10.1175/JAS-D-11-0212.1

Fujii, R., Iijima, T., Potemra, T. A., & Sugiura, M. (1981). Seasonal dependence of large-scale Birkeland currents. *Geophysical Research Letters, 8*(10), Article 11031106. https://doi.org/10.1029/GL008i010p01103

Karakatsanis, L. P., Pavlos, G. P., & Xenakis, M. N. (2013). *T*sallis non-extensive statistics, intermittent turbulence, SOC and chaos in the solar plasma. *Part two: Solar flares dynamics. Physica a: Statistical mechanics and its applications, 392*(18), 3920–3944. https://doi.org/10.48550/arXiv.1201.6498

Knipp, D. J., Tobiska, W. K. & Emery, B. A. (2004). Direct and Indirect Thermospheric Heating Sources for Solar Cycles. *Solar Physics, 224,* 495–505. https://doi.org/10.1007

The ace science center. (2023). *CRIS Level 2 Data Documentation*. https://ace.srl.caltech.edu/ASC/level2/cris_l2desc.html

Tsallis, C. (1988). *P*ossible generalization of Boltzmann-Gibbs statistics. *Journal of statistical physics, 52*, 479–487. https://link.springer.com/article/10.1007/BF01016429

Weimer, D. R. (2005). Improved Ionospheric Electrodynamic models and application to calculating Joule heating rates. *Journal of Geophysical Research, 110,* Article 05306. https://doi.org/10.1029/2004JA010884

Wilson, G. R., Weimer, D. R., Wise, J. O., & Marcos, F. A. (2006). Response of the thermosphere to Joule heating and particle precipitation. *Journal of Geophysical Research: Space Physics, 111*(A10). https://doi.org/10.1029/2005JA011274

GeosciRA23
Book of Abstracts and Contributed Papers
International Conference on Recent Trends in Geoscience Research and Applications 2023
Belgrade, Serbia & Virtual, October 23–27, 2023
Editors: Aleksandra Nina, Snežana Dragović, and Dejan Doljak

Contributed paper

TROPOSPHERIC REFRACTION AND ITS INFLUENCE THROUGH ZENITH TOTAL PATH DELAY AT DIFFERENT IGS STATIONS

Violeta Vasilić[1], Ljiljana Brajović[2], Dušan Petković[1], Dragan Blagojević[1]*

[1]University of Belgrade, Faculty of Civil Engineering, Department of Geodesy and Geoinformatics, Belgrade, Republic of Serbia; e-mail: tatic@grf.bg.ac.rs; dpetkovic@grf.bg.ac.rs; bdragan@grf.bg.ac.rs
[2]University of Belgrade, Faculty of Civil Engineering, Department of Mathematics, Physics and Descriptive Geometry, Belgrade, Republic of Serbia; e-mail: brajovic@grf.bg.ac.rs

Abstract: The propagation of the Global Navigation Satellite System (GNSS) signals through the atmosphere is affected by the electron content in the ionosphere and the air density in the electrically neutral troposphere, thus causing a signal delay and leading to errors in the GNSS observations and the estimated positions. Our research has been conducted related to the influence of the tropospheric layer of the Earth's atmosphere on signals at geodetic observation stations in the zenith direction. Since tropospheric refraction cannot be directly estimated, the signal delay has been quantified by applying several developed models. As the lowest layer of the atmosphere, the average height of the troposphere is approximately ten kilometers, and it is variable concerning the latitude of the measuring station and seasonal conditions. The tropospheric delay of the GNSS signal - Zenith Total Delay (ZTD), was analyzed on the examples of three International GNSS Service (IGS) stations at different latitudes. Two epochs in July 2022 and January 2023 for each IGS station are considered regarding seasonal differences in the atmospheric parameters. It was found that at each of the IGS stations, there is an oscillation of the ZTD amplitude with a half-day period. Different patterns were distinguished at each station, depending on the station latitude and epoch, i.e., summer or winter atmospheric conditions. For example, a random walk signal was dominant at the ROAG, San Fernando IGS station.

Keywords: IGS station; ZTD; GNSS signal

1. Introduction

The characteristics of the atmosphere's natural structure are variable in both space and time. Depending on them, the propagation of GNSS signal through the atmosphere is differently affected, and it is reflected in signal delay. High accuracy in the estimated positions of the geodetic stations will be enabled with appropriate modeling or with the reduction of signal delay errors. A simplified atmosphere model in the form of concentric layers of different heights is used to determine atmospheric parameters.

The lowest layer of the atmosphere is the troposphere, and according to Saastamoinen's model (Saastamoinen, 1972a, 1972b), the troposphere is the layer of the Earth's atmosphere with an average height of 10 km with a rate of temperature decrease of 6.5 degrees Celsius/km. Above the tropospheric layer, from the tropopause is a stratospheric layer with an average height of 70 km, in which the temperature is assumed to be constant.

*Corresponding author, e-mail: tatic@grf.bg.ac.rs

The analysis of ZTD of the GNSS signal was performed on the examples of three IGS stations at different latitudes METG, METSAHOVI, Finland, GOP6, ONDREJOV, Czechia and ROAG, SAN FERNANDO, Spain, for two epochs in July 2022 and January 2023. ZTD 5 min time series were downloaded from the NASA website (n.d.). This analysis has been performed regarding seasonal differences in the atmospheric parameters.

2. Theoretical aspects of ZTD and applied estimation models

At the zenith of GNSS stations, the tropospheric refraction is about 2.3 m, and the delay for signals closer to the horizon can be up to seven times higher. The basic mathematical expression of the correction for atmospheric refraction (Saastamoinen, 1972a, 1972b) in a spherically layered atmosphere is:

$$\Delta z = \int_{1}^{n_1} \frac{\tan z}{z}\, dn \; ; \left(0 \le z_1 \le 90^{\circ}\right) \tag{1}$$

Solving the integral of atmospheric refraction, the refractive index function n is expanded following the trigonometric function of the zenith distance z, that the equation for obtaining ZTD according to Saastamoinen (1972a, 1972b) has the following form:

$$\rho = 0.002277 \cdot \frac{\left(P_0 + \left(0.05 + \frac{1255}{T_0 + 273.15}\right) e_0\right)}{f(\varphi,h)}$$

$$e_0 = r_h \cdot 6.11 \cdot 10^{\frac{7.5 \cdot T_0}{T_0 + 273.3}} \tag{2}$$

$$f(\varphi,h) = 1 - 0.00266 \cdot \cos 2\varphi - 0.00028 \cdot h$$

where ρ denotes the ZTD, P_0, T_0, e_0, and r_h denote the pressure, the temperature, the water vapor pressure, and the relative humidity, respectively, f(φ,h) is the correction of gravity acceleration caused by the rotation of the Earth, φ denotes the latitude of the point, and h denotes the height, with the subscript 0 indicates the values of the parameters at the earth surface.

In addition to the Saastamoinen model, several models are used for modeling the tropospheric delay, such as the Hopfield model, the Herring model, and others. Tropospheric delay is generally considered the sum of two components: the tropospheric hydrostatic part or ZHD and the tropospheric wet part or ZWD (Blagojević, 2014; Cui et al., 2022). The hydrostatic component has a larger amplitude and contributes 90% to the total Zenith Total Delay, while the remaining portion is associated with the ZWD component. In the paper of authors Bevis et al. (1992), it is emphasized that according to most theorists, global warming will cause systematic changes in the total water vapor content of the atmosphere. In the paper of authors Labib et al. (2018), research on tropospheric delay related to different climate zones is presented.

The analysis of the ZTD time series was performed as follows. First, the linear trend was removed according to the model y = a + b*x*, and after that, the Fourier transformation was applied to the ZTD time series. Then ZTD time series were modeled using a fitting modeling function representing the sum of 8 sinusoidal oscillations. This fit function is used to approximate the time series and has the following form: y(*t*) = A1 sin (2π f1 t + φ1) + A2 sin (2π f2 t + φ2) + ... + A8 sin (2π f8 t + φ8), with the following notations: y(*t*) is the value of the time series at time t, A1–A8 are the amplitudes of the sinusoidal components, f1–f8 are the frequencies of the corresponding sinusoidal components, and φ1–φ8 are the phases of the corresponding sinusoidal components.

This fit function is used to explain ZTD's periodicity as well as allows the modeling and analysis of oscillations in the time series. Also, we have applied the autoregressive model of order 1 (AR (1)), y(*t*) = c + ϕ . y(*t*-1) + *ε*(*t*), with the following notations: y(*t*) is the current value, y(*t*-1) is the previous value, ϕ is the autocorrelation coefficient at lag 1, c is a constant, and *ε*(*t*) is white noise (Information technology laboratory, n.d.).

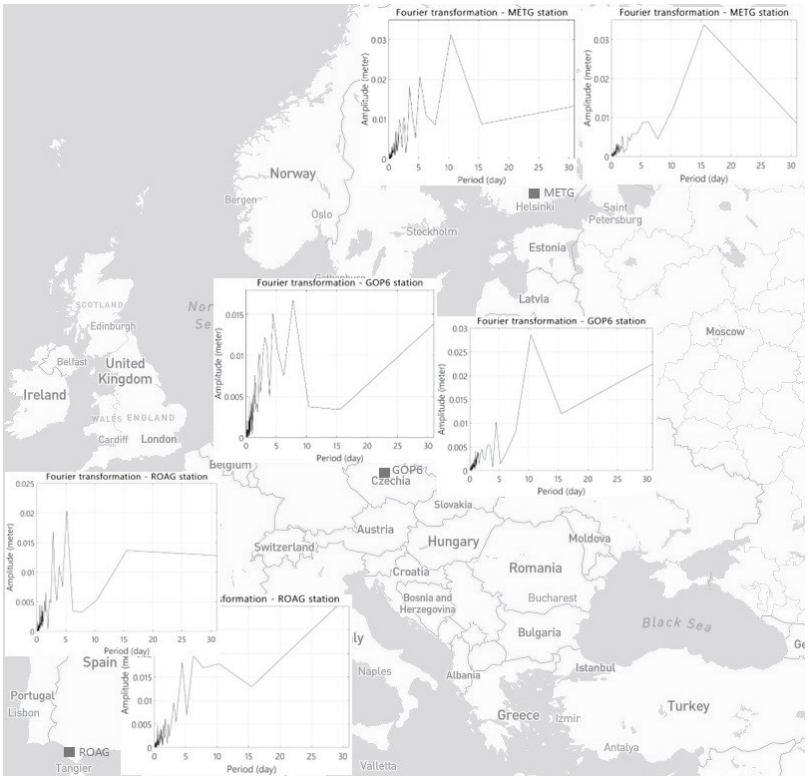

Figure 1. Spatial distribution and corresponding FFT of ZTD of IGS stations METG, GOP6, ROAG for July 2022 (left) and January 2023 (right).

3. The main ZTD characteristics of IGS stations in July 2022 and January 2023

The Fourier transformations of the ZTD time series for both epochs, July 2022 and January 2023, for all three stations are visually represented in Figure 1. They are listed in Table 1 with their main station data. ZTD time series with the modeled fit lines for both epochs are shown in Figure 2 for all three stations: METG, GOP6, and ROAG.

Table 1. The main characteristics of IGS stations

IGS station	Longitude	Latitude	Height
METG, METSAHOVI, Finland	24° 23' 03.0"	60° 14' 31.1"	59.7 m
GOP6, ONDREJOV, Czechia	14° 47' 08.2"	49° 54' 49.2"	592.6 m
ROAG, SAN FERNANDO, Spain	353° 47' 37.4"	36° 27' 48.1"	83.2 m

The shorter periods less than six days at station METG and less than five days at station GOP6, in both epochs, July and January, are approximately equal but have different amplitudes, indicating uniformity in periods across both epochs. Due to the convergence of the fit model for the July 2022 epoch at station GOP6, ZTD time series modeling was performed with 12 sinusoidal functions. In the case of station ROAG, the daily and semi-daily periods are the same and have approximately equal amplitudes in epochs July 2022 and with a slight difference in January 2023, while other periods with their appropriate amplitudes differ (Table 2). In July 2022, this station exhibited more oscillations with periods shorter than five days than in January 2023.

We estimated that ϕ autocorrelation coefficient at lag 1 is close to 1, and c constant term is zero for all ZTD time series. As the coefficient ϕ was slightly less than 1, we concluded that the ZTD time series exhibited exponential decay. The value of the autocorrelation coefficient at station ROAG in January 2023 was closest to 1, suggesting that a random walk-like type of signal was dominant. Based on their research, the authors Young et al. (2022), indicate the regional variability of the optimal random walk per station, which is determined by climatic, geographical, and weather factors.

The parameter values of several characteristic oscillations for three IGS stations in July 2022 indicate that the maximum amplitudes with their appropriate periods decrease with decreasing of the station's latitudes and are for station METG: 0.03166 m (period 11.30 days), station GOP6: 0.01635 m (period 7.94 days), and station ROAG: 0.01363 m (period 15.09 days) (Table 2). The amplitudes with approximately a three-day period increase with decreasing latitudes and increasing station heights. The smallest amplitude at station METG is less than 5 mm, while the largest amplitude at station GOP6, which has the greatest height, is less than 10 cm, while at station ROAG, it has an amplitude less than 2 cm. The amplitudes with daily periods increase with decreasing latitude and increasing station height, so the smallest amplitude value for station METG is approximately 1 mm, and the largest for station GOP6 is approximately 5 mm. The semi-diurnal amplitude values are approximately the same as the daily values, except for station METG, which has a value of approximately 3 mm. The obtained standard deviations of residuals for all three stations are less than 2 cm. The parameter values of several characteristic oscillations for three IGS stations in January 2023 indicate that the maximum amplitudes with their appropriate periods decrease with decreasing latitudes of the stations.

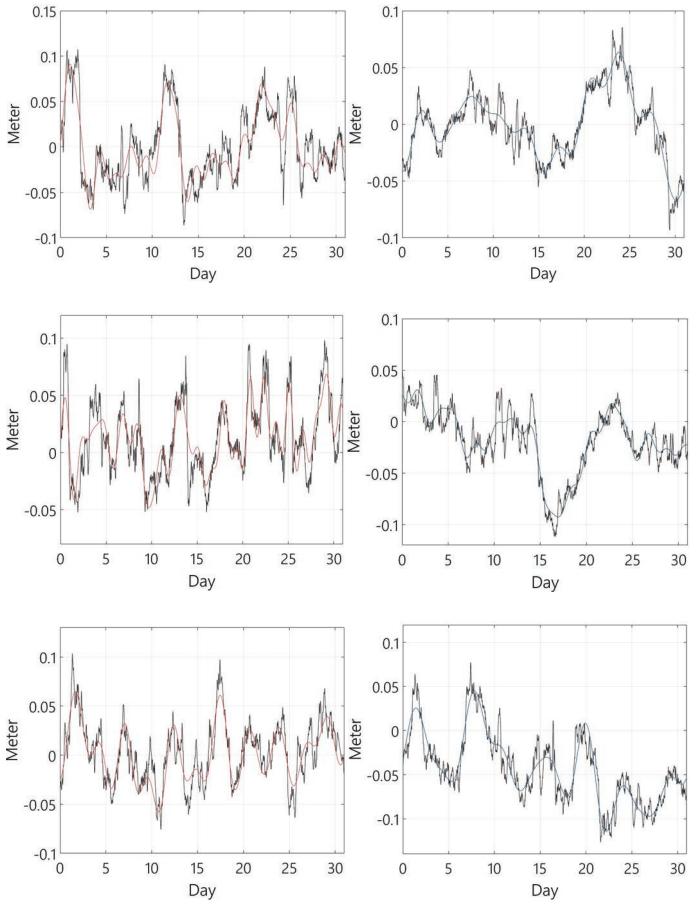

Figure 2. ZTD in July 2022 (left) and January 2023 (right) of IGS stations METG, GOP6, ROAG, and sine modeled lines.

Table 2. ZTD values of IGS stations for July 2022 and January 2023 concerning maximum amplitudes and approximately equal periods

IGS station	METG, July 2022				METG, January 2023			
Amplit. (m)	0.031656	0.001175	0.000928	0.003186	0.031859	0.003272	0.002486	0.000548
Period (day)	11.30	3.40	1.00	0.50	15.75	3.12	1.00	0.50
Phase (deg)	69.41	27.12	290.8782	291.28	263.22	268.85	5.68	103.09
IGS station	GOP6, July 2022				GOP6, January 2023			
Amplit. (m)	0.01635	0.09561	0.004723	0.00469	0.012153	0.00288	0.000462	0.001497
Period (day)	7.94	2.96	1.00	0.50	10.31	3.10	1.00	0.50
Phase (deg)	195.32	97.57	268.74	268.16	84.99	302.54	28.70	57.23
IGS station	ROAG, July 2022				ROAG, January 2023			
Amplit. (m)	0.013634	0.014301	0.004037	0.004533	0.010698	0.008588	0.001197	0.003596
Period (day)	15.09	2.81	1.00	0.50	11.01	3.10	1.00	0.50
Phase (deg)	51.21	319.50	210.20	208.99	81.25	245.52	245.44	114.66

Their values are as follows for station METG: 0.03186 m (period 15.75 days), station GOP6: 0.01215 m (period 10.31 days), and station ROAG: 0.01070 m (period 11.10 days). The amplitudes with a three-day period at stations METG and GOP6 are approximately equal and less than 5 mm, while the amplitude value for station ROAG is less than 1 cm. The amplitudes with daily periods decrease with decreasing latitude and increasing station height, so the smallest amplitude value for station GOP6, which has the greatest height, is 0.5 mm. Regarding semi-diurnal amplitude values, they increase with decreasing latitude of the station (Table 2). The obtained standard deviations of residuals for all three stations are less than 1.5 cm.

4. Conclusion

We have analyzed ZTD in two epochs in July 2022 and January 2023 of three IGS stations at different latitudes, and consequently of seasonal differences of the atmospheric parameters. At each IGS station, there are several oscillations of the ZTD amplitude with approximately three days, one-day, and half-day periods in both epochs. The values of maximum amplitudes and their periods differed in relation to summer or winter atmospheric conditions for all stations. This analysis could be useful in future investigations of the ZTD time series for an annual time period.

Acknowledgments

The Serbian Ministry of Science, Technological Development and Innovations, grant No. 200092, has supported the conducted research.

References

Bevis, M., Businger, S., Herring, T. A., Rocken, C., Anthes, R. A., & Ware, R. H. (1992). GPS Meteorology: Remote Sensing of Atmospheric Water Vapor Using the Global Positioning System. *Journal of Geophysical Research: Athmospheres, 97*(D14), 15787–15801. https://doi.org/10.1029/92JD01517

Blagojević, D. (2014). *Uvod u satelitsku geodeziju*. Građevinski fakultet Univerziteta u Beogradu.

Cui, B., Wang, J., Li, P., Ge, M., & Schuh, H. (2022). Modeling wide-area tropospheric delay corrections for fast PPP ambiguity resolution. *GPS Solutions*, *26*, Article 56. https://doi.org/10.1007/s10291-022-01243-1

Information technology laboratory. (n.d.). *NIST/SEMATECH e-Handbook of Statistical Methods*. http://www.itl.nist.gov/div898/handbook/, date.

Labib, B., Yan, J., Barriot, J-.P., Zhang, F., Feng, P. (2018). Monitoring Zenithal Total Delays over the three different climatic zones from IGS GPS final products: A comparison between the use of the VMF1 and GMF mapping functions. *Geodesy and Geodynamics, 10*(2), 93–99. https://doi.org/10.1016/j.geog.2018.11.005

NASA. (n.d.). *ZTD 5 min time series*. https://urs.earthdata.nasa.gov/home

Saastamoinen, J. (1972a). Atmospheric Correction for the Troposphere and Stratosphere in Radio Ranging of Satellites. In S. W. Henriksen, A. Mancini, & B. H. Chovitz (Eds.), *Use of Artificial Satellites for Geodesy* (pp. 247–251). American Geophysical Union. https://doi.org/10.1029/GM015p0247

Saastamoinen, J. (1972b). Contributions to the theory of atmospheric refraction, *Bulletin Géodésique, 105,* 279–298, https://doi.org/10.1007/BF02521844

Young, Z., Geoffrey, B., & Kreemer, C. (2022, December 12–16). *Application of Variable Random Walk Process Noise to Improve GPS Tropospheric Path Delay Estimation and Positioning at Local and Global Scales*. AGU22 fall meeting, Chicago IL, https://agu.confex.com/agu/fm22/meetingapp.cgi/Paper/1162048

GeosciRA23
Book of Abstracts and Contributed Papers
International Conference on Recent Trends in Geoscience Research and Applications 2023
Belgrade, Serbia & Virtual, October 23–27, 2023
Editors: Aleksandra Nina, Snežana Dragović, and Dejan Doljak

Contributed paper

CHANGES IN CONCENTRATION OF DTPA-EXTRACTABLE FORMS OF METALS IN RESPONSE TO SOIL TREATMENT WITH VARIABLE SEASHELL DOSES

Ivana Smičiklas[1], Marija Egerić[1], Mihajlo Jović[1], Snežana Dragović[1]*

[1]University of Belgrade, "VINČA" Institute of Nuclear Sciences - National Institute of the Republic of Serbia, Belgrade, Serbia; e-mails: ivanat@vin.bg.ac.rs, egericmarija@vin.bg.ac.rs, mjović@vin.bg.ac.rs, sdragovic@vin.bg.ac.rs

Abstract: Seashells piled in coastal areas worldwide, particularly near commercial mollusk farms, may pose a substantial environmental and health risk. Utilizing seashell waste (SW) as a natural liming material represents a meaningful contribution to the sustainable development of the aquaculture industry through resource recovery. This study assessed the effects of adding various doses of finely ground SW to acidic agricultural soil with elevated total concentration of Cu (219.2 mg/kg) on the bioavailability of selected metals (Cu, Zn, Fe, Mn, Co, Pb, Ni, and Cd). The concentration of DTPA-extracted forms of Cu and other elements decreased significantly with the increase in SW dose from 0.15% to 2%, whereas differences between 2% and 5% treatments were not significant. The association of metals' bioavailability with the agrochemical properties of control and treated soil samples revealed the leading influence of soil pH. Furthermore, the DTPA-extracted amounts of Cu and Zn were negatively correlated with carbonate and organic carbon content, and bioavailable Zn forms were negatively correlated with the content of accessible phosphorus. As a cost-effective, sustainable, and renewable source of calcium carbonate, organic carbon, and available phosphorus, SW is a candidate material for acidic soil amelioration, including the immobilization of a range of toxic and potentially toxic metals. However, the study's results underline that SW dose optimization through preliminary tests is a necessary research component that requires observing soil fertility parameters, particularly the status of essential metals.

Keywords: Soil remediation; seashell waste; metal immobilization; bioavailability; DTPA-extraction

1. Introduction

Increasing land degradation and decreasing productive land due to metal contamination and acidification incited a growing interest in readily available, economical, and highly effective technologies for soil remediation. Among these technologies, soil amendments as immobilizing agents and pH improvers have been developed extensively for large-scale applications because of their easy application and commercial viability. A variety of soil amendments have been widely employed to reduce the mobility and bioavailability of metals in contaminated soils by immobilizing them into stable forms via adsorption, precipitation, and complexation, including organic (e.g., animal wastes, biochar, biosolids, and compost) and inorganic (e.g., clay minerals, coal fly ash, liming materials, metal oxides, and phosphates) materials (Palansooriya et al., 2020).

*Corresponding author, e-mail: ivanat@vin.bg.ac.rs

The research on high-performance soil amendments that fulfill sustainable remediation principles has intensified in the last two decades. Naturally occurring waste materials and residues have received particular attention because of their availability, low cost, and relatively high efficiency in achieving remediation goals. Seashells have proven an emerging alternative to conventional liming materials for the remediation of acidic and metal-contaminated soils due to their high calcium-carbonate content (Barros et al., 2009). This approach also benefits the coastal ecosystems, by using the waste material from the growing seafood industry and enabling sustainable seashell aquaculture. Seashells act as soil conditioner, as they provoke changes in the fractionation of metals (e.g., Cd, Cu, Pb, Zn, Cr, and Ni) by increasing their sorption and precipitation, and improve soil nutrient contents and bacterial community structure (Jović et al., 2019). Nevertheless, adding seashells to agricultural soils demands caution and additional research to ensure the immobilization of toxic and potentially toxic metals while safeguarding the sufficient availability of essential ones (Santás-Miguel et al., 2022). In that sense, the behavior and bioavailability of Cu is of a particular significance, as this metal is a micronutrient essential for plant development and crop yield in certain low amounts while exhibiting high toxic potential at elevated concentrations.

Egerić et al. (2019) demonstrated that seashell waste (SW) could be employed to improve essential properties of the acidic agricultural soil with elevated Cu-concentration in terms of the increase in pH, carbonate, organic carbon, and available phosphate content and decrease in environmental mobility of Cu and other metals. This study aimed to evaluate the impact of different seashell doses on the availability of essential micronutrients (Cu, Fe, Mn, and Zn) and other selected metals (Cd, Co, Ni, and Pb) to plants, using the extraction with diethylenetriaminepentaacetic acid (DTPA). The relationship between the bioavailability of these elements and the agrochemical properties of the soil altered by various doses of the additive was assessed.

2. Materials and methods

The topsoil (0–20 cm) was sampled from an agricultural parcel in Slatina village, near the town of Bor (Serbia), in which a copper mining and smelting complex (Serbia Zijin Bor Copper, formerly known as RTB Bor) has been operating for more than a century. Dried soil was homogenized and sieved to <2 mm fraction. The composite SW, collected from the North Greek Aegean Sea coast, was washed from impurities, ground into a fine powder, and characterized as described previously (Egerić et al., 2017). The SW was mixed with soil at 0.15%, 0.3%, 2%, and 5% w/w bases (samples SW0.15, SW0.3, SW2, and SW5; Egerić et al., 2019). The treatments have been carried out in pots (triplicates), maintaining ~60% of soil water capacity for two months.

Ten grams of control soil (S) and treated samples were extracted with 20 ml of DTPA- solution (International Organization for Standardization, 2001). The extracting solution was prepared by dissolving 0.005 mol/L DTPA, 0.1 mol/L triethanolamine (TEA), and 0.01 mol/L $CaCl_2$ in deionized water and adjusting the final pH to 7.3 with 6 M HCl. Extractions were conducted at room temperature, for two hours, on a rotary shaker (15 rpm). Liquid phases were separated by membrane filtration (0.45 μm), and the concentrations of metals (Cu, Fe, Mn, Zn, Cd, Ni, Co, and Pb) were measured within 24 h by Inductively coupled plasma atomic emission spectroscopy (ICP-AES, Thermo Scientific iCAP 6500 Duo), with matrix-matched calibration standards. The concentrations of elements are presented on a dry matter basis.

3. Results and discussion

The results obtained from the DTPA test of the control and treated soil samples are graphically shown in Figure 1. The difference in metal availability between the samples was identified by Fisher's least significant difference (LSD) test.

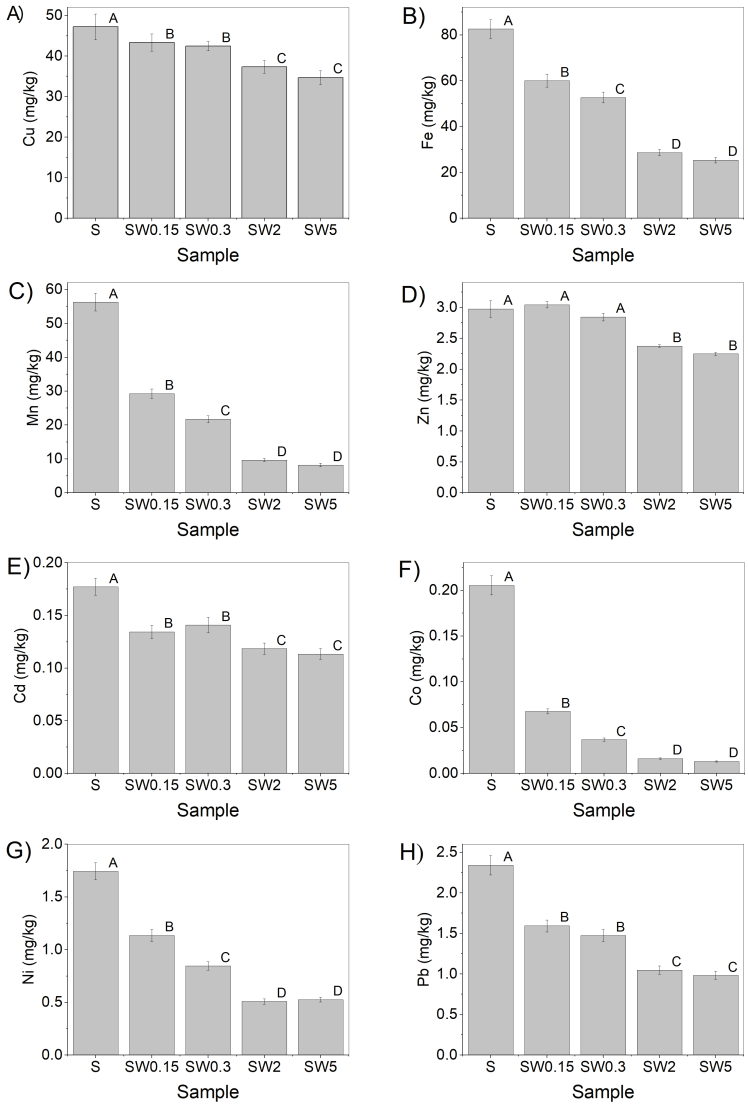

Figure 1. The DTPA-extracted concentrations of Cu (A), Fe (B), Mn (C), Zn (D), Cd (E), Co (F), Ni (G), and Pb (H) in the soil before and after treatment with different doses of SW, including one-way analysis of variance (ANOVA) and the Fisher's least significant difference (LSD) test at the level of significance α = 95% (p < .05).

Some of the metals are essential nutrient elements for the proper growth and development of plants (e.g., Cu, Zn, Fe, and Mn). Consequently, it is important to monitor their availability to plants. Determination of critical concentrations of bioavailable micronutrients in soil has been the focus of numerous studies, which pointed out variations across different extraction methods, soil types, properties, and specificities associated with plant species (Fageria et al., 2002). Recommended soil micronutrient values based on the results of the DTPA test (Barrett et al., 2017), are presented in Table 1.

Table 1. Recommended micronutrient concentration values in soil (mg/kg) based on the DTPA test (Barrett et al., 2017)

Metal	Very low	Low	Medium	High	Very high
Cu	0–0.3	0.3–0.8	0.9–1.2	1.3–2.5	>2.5
Fe	0–5	6–10	11–16	17–25	>25
Mn	0–4	5–8	9–12	13–30	>30
Zn	0–0.5	0.5–1.0	1.1–3.0	3.1–6.0	>6.0

The concentrations of available Fe (82.6 mg/g), Mn (56.3 mg/g), and Cu (47.2 mg/g) can be classified as very high in the control soil, and the bioavailability of Zn (2.9 mg/g) can be labeled as medium level. The bioavailability of Fe and Mn is commonly increased in acidic soils, while a very high level of bioavailable Cu signifies its anthropogenic input through mining and industrial activities in the vicinity of the sampling site. The DTPA extracted concentration of potentially toxic and toxic metals was generally low, highest for Pb (2.34 mg/kg), followed by Ni (1.74 mg/kg), Co (0.205 mg/kg), and Cd (0.177 mg/kg). These results agree with analyses of pseudo-total concentrations of trace elements in the soil (Egerić et al., 2019), showing that only Cu concentration was elevated (219.2 mg/kg) and above the remediation value (190 mg/kg) prescribed by Serbian legislation.

Statistically significant differences in the bioavailability of the investigated metals were detected between the control and treated soils, and the applied doses of SW had different effects on the availability of individual metals (Figure 1). Even after applying 0.15% SW, a significant reduction in the bioavailability of all elements, except for Zn, was observed. Generally, no significant differences in the bioavailability of essential micronutrients and other tested metals were found between the SW2 and SW5 samples.

Applying SW in all treatment variants did not decrease the bioavailability of microelements below the levels critical for plant growth and development. The SW dose had the greatest impact on the concentration of available Mn. According to Table 1, after the application of 0.15% and 0.3% SW, the concentration of available Mn was high and reached medium and low levels with a further SW dose increase (2% and 5%). Considering all treatments, Fe and Cu bioavailable concentrations remained very high. It is crucial to consider that these values are recommendations, which may not be in accordance with the actual requirements of specific crops, because the need for micronutrients depends on the type of crop, expected yield, pH value, and other soil properties (Barrett et al., 2017). For instance, bioavailable concentrations (DTPA test) over 50 mg/kg were found to reduce the dry matter yield of several vegetables (Yang et al., 2022). Finally, in all samples, the DTPA-extracted concentrations of Zn remained within the range of medium availability.

The bioavailability of other investigated metals, Pb, Cd, Co, and Ni, was simultaneously reduced by SW treatments (Figure 1), maximally by 33 % for Cd, 58 % for Pb, 70 % for Ni, and even 93 % for Co, at the highest SW dose of 5 %. The SW treatments induced changes in soil agrochemical attributes (Egerić et al., 2019). The descriptive statistics of selected essential properties are shown in Table 2. According to coefficients of variation, the addition of various amounts of SW most affected (i.e., increased) the content of carbonate, electrical conductivity (EC), the content of available phosphorus, organic carbon, and soil pH, while the total nitrogen content and cation exchange capacity (CEC) were least affected.

Table 2. Descriptive statistics of agrochemical properties of control and amended soil samples (Egerić et al., 2019)

Variable	Mean	Standard Deviation	Coefficient of variation	Minimum	Maximum
CaCO3 (%)	1.89	2.55	134.72	0.00	6.09
CEC (meq/100g)	11.58	0.172	1.48	11.40	11.85
Ntotal (%)	0.172	0.003	2.22	0.168	0.177
Corganic (%)	1.768	0.310	17.55	1.479	2.279
Available P (mgP2O5/100g)	4.210	1.102	26.17	2.880	5.400
pH	6.482	1.110	17.13	4.930	7.650
EC (dS/m)	0.684	0.314	45.94	0.378	1.122

The association between extracted metal concentrations and soil properties was analyzed using Pearson's correlation test (Table 3). A significant ($p < .05$) negative correlation has been observed between soil pH and metal bioavailability, which is in agreement with previous findings in the literature (Fageria et al., 2002). The EC exhibited a statistically significant ($p < .05$) negative correlation with the concentrations of Cu, Zn, and Fe in the DTPA extract. This can be attributed to the influence of the SW dose, which leads to an increase in soil pH and EC. Also, the bioavailability of Cu and Zn demonstrated a significant ($p < .05$) negative correlation with carbonate and organic carbon content.

Table 3. The Pearson's correlation coefficient between the agrochemical properties of soil samples and bioavailable concentrations of the investigated metals determined by DTPA extraction

Metal	$CaCO_3$	CEC	N_{total}	$C_{organic}$	Available P	pH	EC
Cu	–0.909*	–0.055	0.338	–0.928*	–0.858	–0.985*	–0.888*
Zn	–0.907*	0.170	0.550	–0.887*	–0.980**	–0.897*	–0.915*
Fe	–0.820	–0.044	0.183	–0.852	–0.830	–1.000*	–0.914*
Mn	–0.708	–0.082	–0.034	–0.770	–0.697	–0.974*	–0.830
Ni	–0.704	–0.008	–0.016	–0.762	–0.740	–0.977*	–0.858
Pb	–0.747	–0.126	0.027	–0.800	–0.719	–0.986*	–0.852
Co	–0.586	–0.127	–0.215	–0.670	–0.548	–0.911*	–0.720
Cd	–0.735	–0.297	0.012	–0.787	–0.632	–0.958*	–0.806

*Note. *p < .05, ** p < .01*

Soils with high $CaCO_3$ content generally exhibit lower bioavailability of micronutrients (Chatzistathis, 2014). On the other hand, depending on the total content and composition, organic matter can have different effects on the mobility and bioavailability of micronutrients. The high affinity of Cu to the organic phase of the soil often leads to reduced bioavailability

of this essential element, attributed to either the formation of insoluble organometallic complexes or soluble complexes, but difficult to uptake by plants (Fageria et al., 2002). A significant negative correlation ($p < .01$) was also found between bioavailable Zn and accessible phosphorus content. This indicates that in case of fertilizing the soil with phosphate fertilizers, the amount of bioavailable Zn potentially can be reduced below the concentrations critical for plants growth and development.

3. Conclusion

The application of waste seashells for improving soil pH and agrochemical properties affected the bioavailability of investigated elements. After the treatment with SW, and with SW dose increase, a decrease in the concentrations of all investigated elements in the DTPA extract was observed, indicating the suitability of using this additive to treat multiple metal contamination. The increase in soil pH value is the most significant factor affecting the immobilization of metals. The results indicate that selecting the amount of SW for treating a certain acidic soil must consider the bioavailability tests of essential elements. Adding 2% of SW was best for investigated soil, as a further increase in SW amount did not significantly reduce the bioavailable Cu fraction while affecting the excessive reduction of bioavailable Mn. Applying seashells with other amendments could improve Cu-immobilization capacity, thus, such an approach deserves further attention.

Acknowledgements

This work was supported by the Ministry of Science, Technological Development, and Innovation of the Republic of Serbia (Contract No. 451-03-47/2023-01/200017).

References

Barrett, W., Jones, N., Chu, P., Pohlman, K., Coleman, G., Poole, H., Goff, D., Spiva, C., Griffith, L., Zwiep, J., & Hohla, J. (2017). *Agronomy Handbook. Soil and Plant Analysis Resource Handbook*. Midwest Laboratories, INC.

Barros, M. C., Bello, P. M., Bao, M., & Torrado, J. J. (2009). From waste to commodity: transforming shells into high purity calcium carbonate. *Journal of Cleaner Production*, 17, 400–407. https://doi.org/10.1016/j.jclepro.2008.08.013

Chatzistathis, T. (2014). *Micronutrient Deficiency in Soils and Plants*. Bentham Science Publishers. https://benthamscience.com/ebook_volume/1540

Egerić, M., Smičiklas, I., Dojčinović, B., Sikirić, B., Jović, M., Šljivić-Ivanović, M., & Čakmak, D. (2019). Interactions of acidic soil near copper mining and smelting complex and waste-derived alkaline additives. *Geoderma*, *352*, 241–250. https://doi.org/10.1016/j.geoderma.2019.06.015

Egerić, M., Smičiklas, I., Mraković, A., Jović, M., Šljivić-Ivanović, M., Antanasijević, D., & Ristić, M. (2017). Experimental and theoretical consideration of the factors influencing cationic pollutants retention by seashell waste. *Journal of Chemical Technology and Biotechnology*, *93*(5), 1477–1487. https://doi.org/10.1002/jctb.5516

Fageria, N. K., Baligar, C., & Clark, R. B. (2002). Micronutrients in Crop Production. *Advances in Agronomy*, *77*, 185–268. https://doi.org/10.1016/s0065-2113(02)77015-6

International Organization for Standardization (2001). *Soil quality — Extraction of trace elements by buffered DTPA solution* (ISO Standard No. 14870:2001). https://www.iso.org/standard/25232.html

Jović, M., Mandić, M., Šljivić-Ivanović, M., & Smičiklas, I. (2019). Recent trends in application of shell waste from mariculture. *Studia Marina, 32*(1), 47–62. http://www.studiamarina.ac.me/pdf/32/Recent%20trends%20in%20application%20of%20shell%20waste%20from%20mariculture.pdf

Palansooriya, K. N., Shaheen, S. M., Chen, S. S., Tsang, D. C. W., Hashimoto, Y., Hou, D., Bolan, N. S., Rinklebe, J., & Ok, Y. S. (2020). Soil amendments for immobilization of potentially toxic elements in contaminated soils: A critical review. *Environment International*, *134*, Article 105046. https://doi.org/10.1016/j.envint.2019.105046

Santás-Miguel, V., Campillo-Cora, C., Núñez-Delgado, A., Fernández-Calviño, D., & Arias-Estévez, M. (2022). Utilization of mussel shell to remediate soils polluted with heavy metals. In I. Anastopoulos, E. C. Lima, L. Meili, & D. A. Giannakoudakis (Eds.), *Biomass-Derived Materials for Environmental Applications* (pp. 221–242). Elsevier. https://www.sciencedirect.com/book/9780323919142/biomass-derived-materials-for-environmental-applications

Yang, X.-E., Long, X.-X., Ni, W.-Z., Ye, Z.-Q., He, Z.-L., Stoffella, P.-J., & Calvert, D.-V. (2002). Assessing copper thresholds for phytotoxicity and potential dietary toxicity in selected vegetable crops. *Journal of Environmental Science and Health B, 37*(6), 625–635. https://www.tandfonline.com/doi/abs/10.1081/PFC-120015443

GeosciRA23
Book of Abstracts and Contributed Papers
International Conference on Recent Trends in Geoscience Research and Applications 2023
Belgrade, Serbia & Virtual, October 23–27, 2023
Editors: Aleksandra Nina, Snežana Dragović, and Dejan Doljak

Contributed paper

HISTORICAL AND INSTRUMENTAL SEISMIC ACTIVITY OF THE SKOPJE EPICENTRAL AREA

Ljubco Jovanov[1], Katerina Drogreška[1], Jasmina Najdovska[1], Dragana Cernih[1]*

[1]Ss. Cyril and Methodius University, Faculty of Natural Sciences and Mathematics, Seismological Observatory, Skopje, Republic of North Macedonia; e-mails: ljubco.jovanov@hotmail.com; katerinadrogreska@yahoo.con; najdovskaj@yahoo.com; dcernih@yahoo.com

Abstract: The seismicity of the Skopje epicentral area which has been analyzed in this study is characterized by the occurrence of weak to strong earthquakes based on a comprehensive database, cataloging 1,135 seismic events registered between 518 and 2021 with magnitude $M_w \geq 3.0$. The catalogue was divided into two periods: a macroseismic data part comprising 157 seismic events and an instrumental part containing 978 seismic events recorded during the period 1957–2021 by the Macedonian Seismological Network (SORM). The correlation between the macroseismic and instrumental seismicity with the seismotectonic features was performed by analyzing spatial distributions of seismic events. The current data allows observing two types of seismic activity in the selected area: Cluster-type and Occasional-type, contributing to a better understanding of the behavior of the seismically active faults. The return periods of large earthquakes ($M_w \geq 5$) and the instrumental seismicity of the Skopje area, allow us to fully research the considered area and to discover all the active faults in the area.

Keywords: seismic activity; earthquakes; active faults; Skopje epicentral area

1. Seismotectonic setting

The main neotectonic regions in the territory of the Republic of North Macedonia (RNM) are the Vardar zone, West Macedonia, and East Macedonia. (Arsovski, 1997). These regions, being developed within major, regional tectonic units, are permanently uplifting with different intensities. They also show differences in seismic activity, which is the reason to treat them as separate seismic zones (Hadžievski, 1976a; Jordanovski, 1998), named with the same names. The present seismic activity in the territory of the RNM is due to the permanent different intensities of movements of the higher-order tectonic units within the three seismic zones. The subject of this article, epicentral area Skopje, belongs to the Vardar seismic zone.

This epicentral area is presented by the sinking Skopje valley (depression). The depression is crisscrossed by neotectonic faults, oriented NW–SE and approximately E W, and the area is subjected to E–NE tectonic compression and N–NW tectonic dilation (Figure 1; Arsovski & Petkovski, 1975).

*Corresponding author, e-mail: ljubco.jovanov@hotmail.com

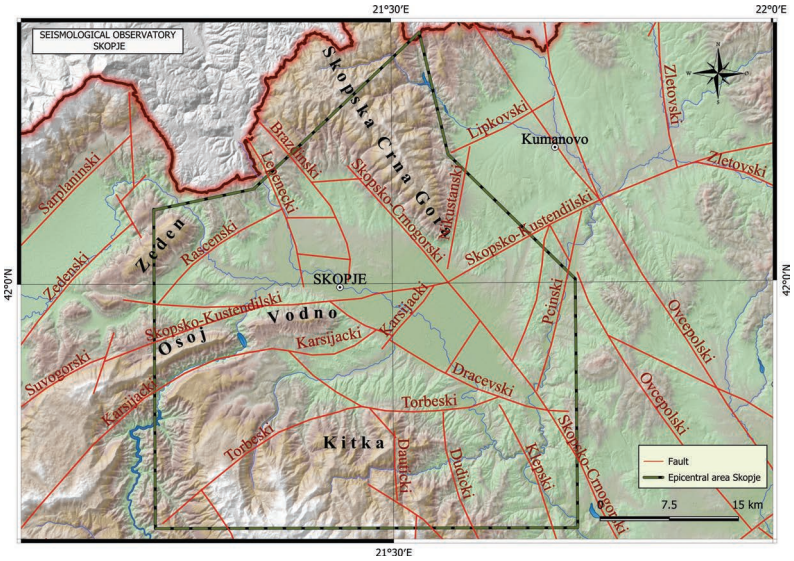

Figure 1. Seismotectonic map of Skopje epicentral area.

2. Data and methods

The seismicity of the Skopje area is based on instrumental seismological and macroseismic data available in the Seismological Observatory of the Faculty of Natural Sciences and Mathematics in Skopje. The Seismological Observatory of the RNM has a rich archive of seismological data (about 1500 years), including historical as well as instrumental data for the period up to the present day (Hadžievski, 1976a, b; Macedonian Seismological Network, n.d.). The historical development of seismological research depended mostly on the political conditions in the Balkans. Macroseismic data on the earthquakes that occurred were archived by the Turkish administration or individual foreign researchers (Mihajlovic, 1951, Watzof, 1923). The development of instrumental seismology began in 1957, when the Skopje Seismology Station start to operate. In the period up to today, we note the change of three generations of instruments, each with a different level of sensitivity.

The locations of the historical earthquakes are obtained mainly from the macroseismic data, i.e., from the corresponding maps of isoseismals, while the earthquakes that occurred after 1957 are included with instrumental locations. The data for all historical and instrumental earthquakes in the considered period that belong to the epicentral area of Skopje were used to complete and prepare a homogeneous catalog. During this period, part of macroseismic data includes 157 seismic events and instrumental data with 978 seismic events registered in the period 1957–2021, that is mean total 1,135 number of events for the epicentral area Skopje. The seismicity of the Skopje epicentral area is related to the activity of the faults, the largest number of epicenters of the earthquakes are located there. The grouping of epicenters around active faults defines several seismogenic sources, the main carriers of seismicity (Figure 2). Earthquakes occur when the Skopska Crna Gora and Vodno mountains meet. Because of this, the underground contact of these two mountains (above which the Skopje valley and the city

of Skopje are located) constantly acts and accumulates tectonic stresses. When the forces of these stresses overcome the frictional force of the blocks, Skopje Crna Gora and Vodno, these blocks move along their contact, causing earthquakes (Petkovski, 1992).

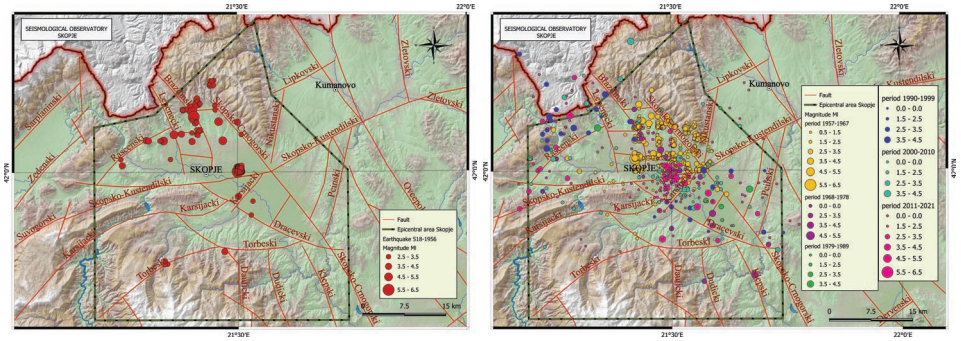

Figure 2. Epicentral map of Skopje area for the period 518–1957 (left) and 1957–2021 (right).

3. Detailed analysis of results

The availability of recent instrumental data together with macroseismic data allows to improve the knowledge about the seismicity and seismotectonic characteristics of the Skopje epicentral area. The spatial analysis is an important key, where a spatial comparison between the seismicity of an area and mapped fault locations allows to assessment of the possible activity along a given fault or group of faults. The hypocentral locations for the historical and instrumental events have been determined with a location uncertainty of less than 5 km, (Hadžievski, 1976c). The epicentral map (Figure 2), can be considered reliable for the following interpretation of the present work. According to the epicentral map, the historical and instrumental seismicity in Skopje area is characterized by many light to micro events ($M_w \leq 4.9$) and several moderate and strong events ($M_w \geq 5$). However, most of the events are low magnitude and can be qualified as micro ($M_w \leq 2$), where their average magnitude is approximately M_w 2.

A detailed analysis of the seismicity, in the present paper, allows observing some seismic types as follows: cluster type and occasional type. This classification could help to present in detail the properties of seismic activity and its relationship with the tectonic features of some specific areas, and to focus on the most important fault zones. The seismicity in the Skopje epicenter area (Figure 2) is characterized by several clusters of events with light to moderate and strong magnitude earthquakes ($M_w \geq 4.0$).

Cluster-type seismic activity is observed on or between the following fault/faults: Skopje–Kjustendil fault, Skopje–CrnaGora fault, Brazda fault, and Karshijacki fault. The Skopje–Kjustendil fault is characterized by an occurrence of both types of seismic activity: occasional-type or individual earthquakes and cluster type. These events form the new stable configuration of the local continuum (Figure 2). This fault in the area of the Skopje depression has an E–W direction, slope in the N–NE direction (toward Skopje Crna Gora) and is expressed in the relief in the western part of the Skopje depression, where it represents the northern

edge of the Vodno and Osoj mountains (Arsovski, 1997). Many clusters of events can be associated with this fault. From the epicentral maps we have located:

In the period from 518–1957, three clusters can be observed, one in the central part of the epicentral area, along the Skopje–Kjustendil fault, second in the northern part, whose occurrence can be attributed to the activity of the Brazda fault, and the third in the western part of the area, who can be attributed to the activity of the Torbeski fault. Fault activity is attributed to the proximity of epicenters to the fault line. In the period from 1957 to 2021, three clusters can be observed, along the Skopje–Kjustendil fault, one along the Brazda fault, two along the Skopje–CrnaGora fault, one along the Karshijacki fault.

The existence of cluster type of seismic activity can be proved using the Benioff diagram (Figure 3), for the energy released during the considered period, mainly represented by three huge leaps in the values of energy released during a period of a year. Some significant events can be classified as individual or occasional type. Earthquakes with magnitude between $3.0 \leq M_w \leq 4.9$, from some events of occasional type, such as the earthquake of 1992, M_w 4.1 and 2004, M_w 4.3, could be interpreted by the accumulation of seismic energy during a period of weak activity. Therefore, we can conclude that the period of weak seismic activity can accumulate seismic energy and at any time it can cause a small to light earthquake.

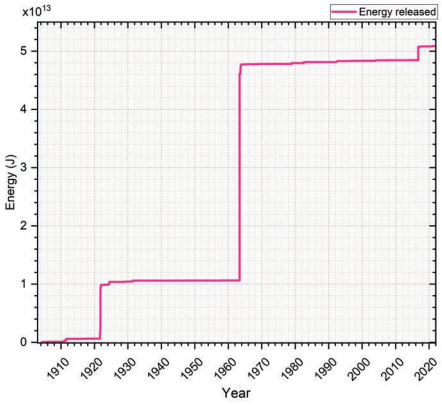

Figure 3. Benioff diagram for the energy released during the period 518–2021.

4. Discussion

During the period of study, from 518 to 2021, epicentral area Skopje, has about 1,135 local events that have been analyzed from the catalog of SORM (1901–2021). The catalog has part of macroseismic data including 157 seismic events, from 518 to1957, and instrumental data with 978 seismic events registered in the period from 1957 to 2021. The locations of these events can be considered reliable because most of the recorded events have relatively small location uncertainty values. The study of this local seismicity data of the Skopje epicenter area, has shown the general appearance of the seismicity in area and spotlighted some important observations:

- The seismicity of the Skopje epicentral area is due to the tectonic activity of all the faults in the Skopje depression and the surrounding area. The most active of all these faults is

the regional Skopje–Kjustendil faul. This fault in the area of the Skopje depression has an E–W direction, has a slope in the N-NE direction (toward Skopje Crna Gora), and is expressed in the relief in the western part of the Skopje depression, where it represents the northern edge of the Vodno and Osoj mountains;

- In the considered period from 518 to 2021, the seismicity of the Skopje epicentral area, according to the availability of seismic data, can be divided into two periods, 518–1957 when the locations of the events are determined according to macroseismic data, and from 1957–2021 when the locations of the events are determined instrumentally. That is why the number of events in the first period is much smaller than the number of events in the second period (Figure 4);
- The epicentral map (Figure 2), shows that the main seismicity with many micro to light, and several strong earthquakes with M_w 6.1, (518, 1555, and 1963) is apparently concentrated on the Skopje–Kjustendil fault: along the central segments of the fault. The Skopje–Kjustendil fault could be characterized by the highest recent instrumental seismicity in the Skopje epicenter area;
- In the period 518–1957, most of the recorded events are qualified as slight, where their average magnitude is approximately M_w 3.5, but in the period 1957–2021, most of the recorded events are qualified as weak, where their average magnitude is approximately M_w 2.0; and
- According to the epicentral map, the seismicity of Skopje epicenter area is characterized by a few clusters, in the central part of the area. The cluster from 1963 has been observed as event with a high magnitude M_w 6.1, and many slight events indicating the behavior of Skopje–Kjustendil faulting zone. Another cluster in 2016 with a magnitude more than M_w 5.0, was observed in the central part of Skopje area. The events show almost identical source mechanism solutions.

The light magnitude of some events of occasional type, such as the earthquake of 1992 and 2004 could be interpreted by accumulation of seismic energy during a long period.

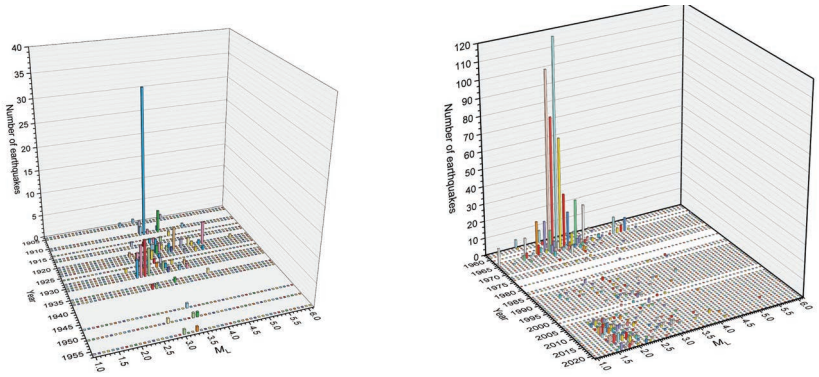

Figure 4. Time-spatial distribution of Skopje area for the period 518–1957 (left) and 1957–2021 (right).

5. Conclusion

The historical and instrumental seismicity of Skopje epicenter area during the period 518–2020, has been characterized and documented in the present paper with 1135 events. The correlation between the seismicity and the seismotectonic was performed through the analysis of spatial distributions of seismic events. The epicentral map has shown that the historical seismicity is concentrated on the Skopje–Kjustendil, Lepenecki, and Brazda faults, and the main instrumental seismicity with many micro to light earthquakes ($M_w > 1$) is concentrated on the faults system, Skopje–Kjustendil, Skopje–CrnaGora, and Brazda, where the highest instrumental seismicity in Skopje area has been observed.

This research allowed observing two types of seismic activity: cluster-type and occasional-type. The seismicity in Skopje epicenter area was characterized by many clusters of light to strong events ($4.0 \leq M_w \leq 6.9$) such as the clusters on the Skopje–Kjustendil fault. Some significant events could be classified as individual, such as the earthquakes of 1992 and 2004.

The geographical distribution of epicenters of a cluster could be related to the active fault. Therefore, many faults can be considered active in Skopje area. The occasional type of seismic activity could be interpreted as a temporary release of the accumulated seismic energy, which is also shown by the Benioff diagram.

References

Arsovski. M. (1997). *Tektonika na Makedonija* [Tectonics of Macedonia]. Faculty of mining and geology, Goce Delcev University of Stip.

Arsovski, M., & Petkovski, R. (1975). *Neotektonika na Socijalistička Republika Makedonija* [Neotectonics of the Socialist Republic of Macedonia], Univerzitet „Sv. Kiril i Metodij", Institut za zemjotresno inženerstvo i inženerska seizmologija.

Hadžievski, D. (1976a). *Katalog na zemjotresite vo Makedonija pred 1900 godina* [Catalog of earthquakes in Macedonia 1900 years ago]. Univerzitetot „Kiril i Metodij", Seizmološka opservatorija.

Hadžievski, D. (1976b). *Katalog na zemjotresite vo Makedonija, Del I, 1900-1930, Del II, 1931-1962, Del III, 1963-1974*v[Catalog of earthquakes in Macedonia, Part I, 1900-1930, Part II, 1931-1962, Part III, 1963-1974]. Univerzitetot „Kiril i Metodij", Seizmološka opservatorija.

Hadžievski, D. (1976c). Seizmičnost na teritorijata na S.R. Makedonija [Seismicity in the territory on S.R. Macedonia]. Univerzitet „Kiril i Metodij", Seizmološka opservatorija.

Jordanovski, Lj., Pekevski, L., Chejkovska, V., Chernih, D., Hristovski, B., & Vasilevski, N. (1998). *Osnovni karakteristiki na seizmicnosta na teritorijata na Republika Makedonija* [Basic characteristics of seismology on the territory of the Republic of Macedonia]. Seismological Observatory of the Faculty of Natural Sciences and Mathematics, University Ss. Cyril and Methodius.

Macedonian Seismological Network. (n.d.). *Katalozi na zemjotresite vo Republika Makedonija i pogranični̇te podrȧčja za godinite 1901–2021*. Fond na Seizmološkata opservatorija pri Prirodno-matematičkiot fakultet.

Mihajlović, J. (1951). *Zemjotresni oblasti vo Makedonija* [Earthquake zones in Macedonia]. Geoloshki Zavod.

Petkovski, R. (1992). *Seizmotektonske karakteristike Makedonije* [Seismotectonic characteristics of Macedonia]. Univerzitet u Beogradu, Rudarsko–geološki fakultet.

Watzof, S. (1923). *Zemjotresenija v Blgarija prez 1901, 1902, …, 1913-1916* [The earthquakes in Bulgaria. Report on the earthquakes felt during 1901, 1902,…, 1913-1916]. Central Meteorological Institute, Sofia.

Book of Abstracts and Contributed Papers
International Conference on Recent Trends in Geoscience Research and Applications 2023
Belgrade, Serbia & Virtual, October 23–27, 2023
Editors: Aleksandra Nina, Snežana Dragović, and Dejan Doljak

Contributed paper

DEVELOPMENT OF A LOW-COST PORTABLE INFRASOUND AND ENVIRONMENTAL ATMOSPHERIC DATA MEASUREMENT FOR MONITORING GEOPHYSICAL PARAMETERS

Mario Batubara[1], Masa-yuki Yamamoto[7], Islam Hosni Hemdan Eldedsouki Hamama[8], Thomas Djamaluddin[1], Timbul Manik[1], Peberlin Parulian Sitompul[1], Musthofa Lathif[1], Poki Agung Budiantoro[2], Ibnu Fathrio[3], Ednofri[4], Sutan Takdir Ali Munawar[5], Alit Daryana[6], Parid Saparudin[6]*

[1]Research Center for Space, National Research and Innovation Agency of Indonesia (BRIN), Bandung-West Java, Indonesia; e-mails: batubaramario@gmail.com; thom001@brin.go.id; timb001@brin.go.id; pebe001@brin.go.id; must009@brin.go.id
[2]Research Center for Satellite Technology, National Research and Innovation Agency of Indonesia (BRIN), Bogor-West Java, Indonesia; e-mail: poki001@brin.go.id
[3]Research Center for Climate and Atmosphere, National Research and Innovation Agency of Indonesia (BRIN), Bandung-West Java, Indonesia; e-mail: ibnu003@brin.go.id
[4]Space and Atmospheric Observation Station-Agam, National Research and Innovation Agency of Indonesia (BRIN), Agam-West Sumatera, Indonesia; e-mail: edno001@brin.go.id
[5]Remote Sensing Earth Station National Research and Innovation Agency of Indonesia (BRIN), Parepare-South Sulawesi, Indonesia; e-mail: suta006@brin.go.id
[6]Space and Atmospheric Observation and Technology Test Station, National Research and Innovation Agency of Indonesia (BRIN), Pameungpeuk-West Java, Indonesia; e-mails: pari002@brin.go.id; alit002@brin.go.id
[7]Kochi University of Technology, Kochi, Japan; e-mail: yamamoto.masayuki@kochitech.ac.jp
[8]National Research Institute of Astronomy and Geophysics Department of Egyptian, Egypt; e-mail: islamhamama@nriag.sci.eg

Abstract: Study on geophysical and natural hazards monitoring in real time involve analysis of multiple geophysical parameters. Currently, efforts to produce instruments apart from high performance, low power requirements and portable are also taken into account. In this paper, a low-power, portable and low-cost infrasound recording system is presented. Specifically, the system simultaneously measures barometric pressure, acceleration and local temperature synchronized by the Global Positioning System (GPS). In addition, a single board computer is integrated with an infrasound wave recording system for ease of control and monitoring of the overall system performance with remote access. After the prototype was packaged, a series of evaluation trials were carried out to verify the instrument's key parameters against the infrasound wave generator source. The experimental results show that the integrated design of the infrasound wave recording system with a single board computer as a whole can detect the source of infrasound waves. As evidence, profiles of infrasound wave measurements in mountainous, urban and coastal areas are discussed.

Keywords: infrasound; raspberry-pi; sensors; campaign; embedded ethernet server

*Corresponding author, e-mail: batubaramario@gmail.com

1. Introduction

Real-time monitoring of natural hazards, such as earthquakes resulting in tsunamis, volcanic eruptions or severe weather events benefits from the joint analysis of multiple geophysical parameters. In recent times, geophysical measurements are carried out through independent single parameter measurements due to the high cost of procuring the instrument and its fixed placement. In addition, the high demand for electric power and the stability of the continuity of the power supply as well as the dimensions and weight of the instrument require higher research and development capital to achieve higher equipment quality.

Several meteorological agencies often place several sensors in the same location to measure various meteorological parameters for local weather dynamic studies and weather forecast model improvement. The International Monitoring System (IMS) under the auspices of the Comprehensive Nuclear Test Ban Treaty Organization (CTBTO), continuously performs various seismic, hydroacoustic, infrasonic and radionuclide geophysical measurements (Marty, 2019). Infrasound Development Laboratory-Kochi University of Technology (KUT), Japan is collaborating to develop integrated infrasound sensors to support the construction of infrasound observation networks in Japan (Batubara & Yamamoto, 2020). The multi-instrument network has shown useful information for the vertical dynamic structure of the mid and upper atmosphere when supplemented with complementary upper atmosphere remote sensing, such as Ionosondes (Alfonsi et al., 2013), doppler sounding (Zalizovski et al., 2021), lidar (Blanc et al., 2018), GPS (ReVelle, 2010). Other studies involving analysis of multi-parameter geophysics such as analysis of the characteristics of earthquakes (Shani et al., 2018), volcanoes (Johnson & Ripepe, 2013), and seismo-acoustics caused by explosions (Assink et al., 2018).

The measurement requirement allows for higher resolution measurements which will contribute to the increased capacity for analysing geophysical object characteristics as well as the resolution and accuracy of conventional numerical prediction models. It is therefore essential to produce a low-cost, low-power and flexible mobility multi-parameter instrument platform that can complement existing geophysical sensor networks.

The purpose of creating this system is to support disaster research programs and satellite payload space in geological disaster mitigation missions in Indonesia as well as study the dynamics of the Earth's atmosphere through observing and detecting infrasound waves from various sources. The innovation of the infrasound wave observation system has undergone development in recent years and the experimental system has been flown on the sounding rocket for the purpose of wave propagation research (Pilger et al., 2021). However, the utilization of infrasound wave propagation has not been widely used in atmospheric science missions.

In this paper, the design and implementation of the system are discussed. Due to the design of the data communication lines, the infrasound sensors used can be easily integrated into the existing single board computer infrastructure so that the results of the integration result in a system that is low in power and easily movable. The structure of writing this article is structured as follows. Section 2 introduces the infrasound sensor system used. Section 3 describes the single board computer system used. Section 3 describes the process of integrating an infrasound sensor with a single board computer system and several other supporting components. While some of the initial results of the implementation of system integration are explained in Section 4, followed by some conclusions from this paper presented in Section 5.

2. Simple Platform Design

2.1. Infrasound Sensor

Infrasound is an Ultra-low Frequency sound (1 mHz to 100 Hz) lower than the human audio frequency range (20 Hz to 20 kHz), and it is possible to grasp various conditions related to geophysics. Typical examples include tsunamis, volcanic eruptions, earthquakes, landslides, meteorites and satellites entering the atmosphere, various artificial noises (wind power generation, explosion sounds, nuclear tests, etc). In general, low-frequency sounds can reach far without decaying.

Although analysis technology is also important, the SAYA company have succeeded in developing an integrated technology that can detect an infrasound generator with a single infrastructure sound sensor (SAYA, n.d.). Infrasound deals with frequencies much lower than the frequency range that can be measured by the microphone, so it is need a dedicated sensor that is completely different from the microphone.

2.2. Single Board Computer

The design of the device uses a single board computer unit to pursue streamlined, mobility as well as low power requirements and costs with capabilities that resemble ordinary computer units. The core of this device lies in the processing section which is used to monitor device performance both in the data acquisition process and in its connectivity. A single board computer based on Raspberry Pi zero was chosen in the design of this device, to achieve the above requirements. In addition, the Raspberry Pi device has a number of advantages such as high computing power in addition to power consumption and cost which provides various development opportunities and the development of many functional devices/prototypes based on this platform.

The board has a quad-core 64-bit Arm Cortex-A53 CPU, clocked at 1 GHz, Broadcom BCM2710A1 die with 512 MB of LPDDR2 SDRAM. Its upgraded processor provides Raspberry Pi Zero 2 W with 40% more single-threaded performance, and five times more multi-threaded performance, than the original single-core Raspberry Pi Zero. For the line communication, the board offers 2.4 GHz 802.11 b/g wireless LAN and Bluetooth 4.2, along with support for Bluetooth Low Energy (BLE), and modular compliance certification. The other specification, the board has a microSD card slot, a CSI-2 camera connector, a USB On-The-Go (OTG) port, and an unpopulated footprint for a HAT-compatible 40-pin GPIO header. A micro-USB socket is also suitable for its input power in the range of 5VDC 2.5A. The board has also mini-HDMI port for video output which can be easily made an innovative display if needed.

3. System Integration

This section contains the different subsections where the design and creation of the prototype together with the algorithm's implementation are explained.

3.1. Construction Work

3.1.1. Wiring Schematic

Top panel of Figure 4 shows the wiring schematic of the system being built. The systems are combined into one unit via an Ethernet hub. The GPS connects directly to the sensor via the

DB9 port. Meanwhile the Raspberry-pi is connected to an ethernet hub, Real Time Component (RTC) and display. All system components receive a low-power DC voltage source. Raspberry-pi can also connect to an ethernet hub via WIFI. RTC functions as a backup of universal time data, so there are 2 (two) universal time records, namely GPS and RTC.

The implementation of this wiring scheme design is realized in a prototype system for observing infrasound waves (Figure 1A). All components in the prototype are stored in one small box and have been tested in various observation campaign activities in several locations. One of the conditions for placing a prototype system in observation campaign activities can be seen in Figure 1B. The system should be placed in one room to avoid the disturbing effects of wind factors on the ground.

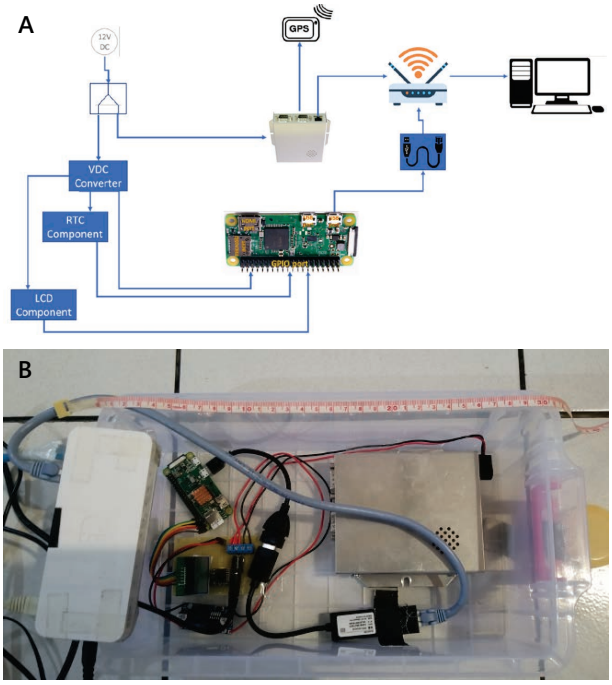

Figure 1. Implementation of system integration.

Note. Panel A: System wiring schematic. Panel B: The resulting system prototype is based on the wiring scheme.

3.1.2. Software Algorithm

All performance of the prototype is controlled by raspberry-pi. So, the prototype can of course work based on the programming system created and embedded in Raspberry Pi. There are five software that work on the Raspberry-pi: (1) "main" acts as the main prototype software which consists of initiating and checking the Raspberry-pi connection with sensors, RTC and GPS, transferring data from the sensor's internal memory to the Raspberry-pi's memory, and displaying operating status of the prototype on the display used; (2) "rtc" functions to provide universal time data; (3) "log" functions to record all prototype work processes; (4) "zip"

functions to compress observation data in one day; (5) and, the four software above are set in the order of activation in the "watchdog" software. Then these five pieces of software are operated periodically and automatically based on the crontab settings in the Raspberry-pi operating system. The "rtc" and "log" software are activated every system reboot. Meanwhile the "zip" and "watchdog" software are respectively run at 00:05 and at the 0th minute.

3.1.3. Data Formats

Gradually the data stored in the sensor's internal memory is stored in the raspberry-pi's internal memory. This is because the sensor's internal memory is always emptied automatically every time it reaches its maximum capacity. The type of observation file stored is binary and numeric CSV. These two files are saved once every hour and given file names based on the time of observation. Each observation file gradually increases in capacity to such an extent that the clock changes. Each observation file records several measurement parameters such as the amplitude of infrasound waves, three directions of acceleration in sensor movement, air pressure and temperature of the surrounding air, as well as the universal time of observation.

4. System Testing and Discussion

The prototype was functionally tested in a series of infrasound wave observation campaign activities in three locations, namely Pameungpeuk and Subang - West Java and Ancol, North Jakarta. The location of this observation can be seen in Figure 2.

Figure 2. Spatial distribution of the infrasound stations consists of Ancol Jakarta (red triangle), Subang (Green triangle), and Pamengpeuk (blue triangle).

Observations in Pameungpeuk-West Java and Ancol-North Jakarta are intended to see the characteristics of infrasound waves from sea waters known as microbarom waves. Meanwhile, observations in Subang and Bandung (yellow pins)—West Java aim to see the characteristics of infrasound waves caused by mountain waves. These two types of infrasound wave sources are very important in the study of infrasound wave propagation and the study of atmospheric dynamics. These three observation locations form a simple observation array geometric configuration that can be used to determine the location of the infrasound wave source.

4.1. Measurement at Pameungpeuk, West Java Indonesia

Figure 3 shows the power spectral density profile of the infrasound signal recorded for 24 hours at Pameungpeuk on May 15, 2023. The image shows that the spectrum at 0.4 Hz (microbarom frequency) begins to appear between 10 and 23 UTC. However, the spectrum at this range began to distruct at 19 UTC, affected by the ambient temperature and local wind structure (Figure 4).

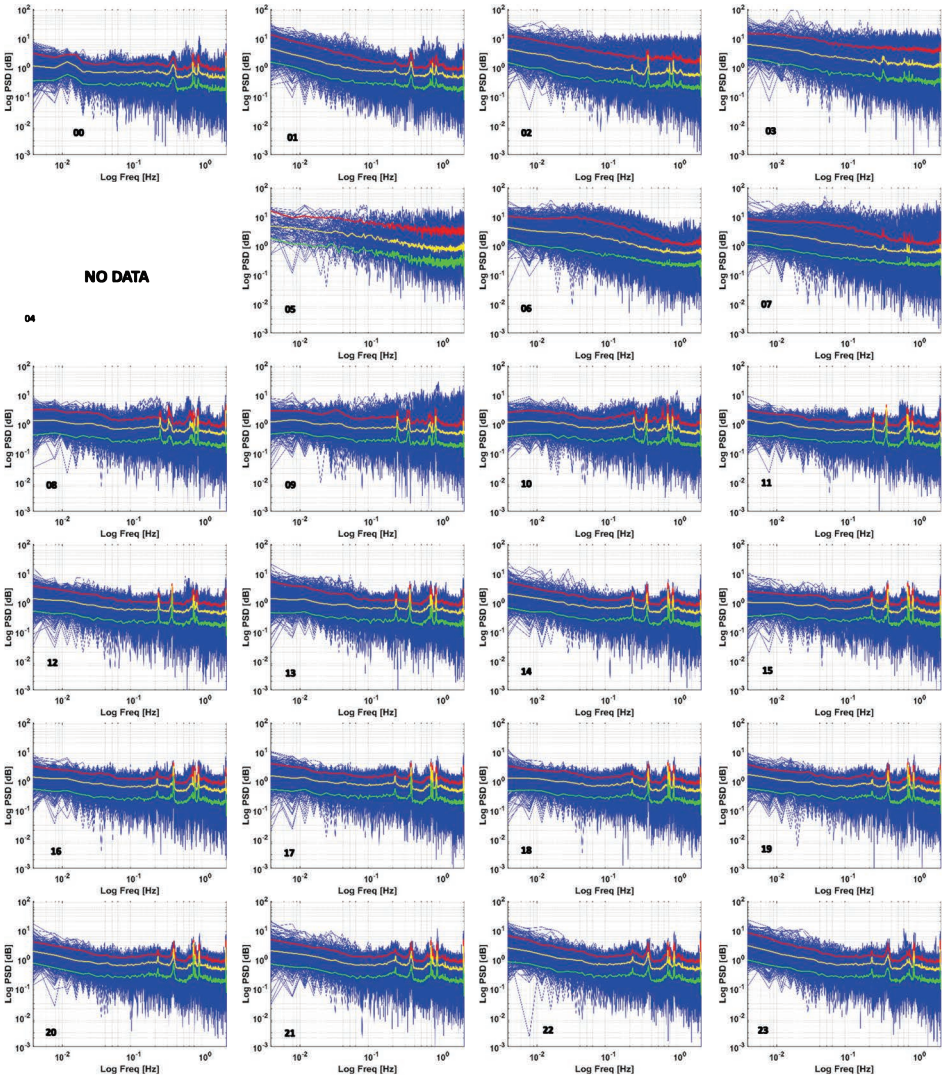

Figure 3. Power Spectral Density of Infrasound signals observed at Pameungpeuk, West Java on 15 May 2023 (0 –23 UTC) with 0.9 percentile (red line), 0.5 percentile (yellow line), and 0.1 percentile (green line).

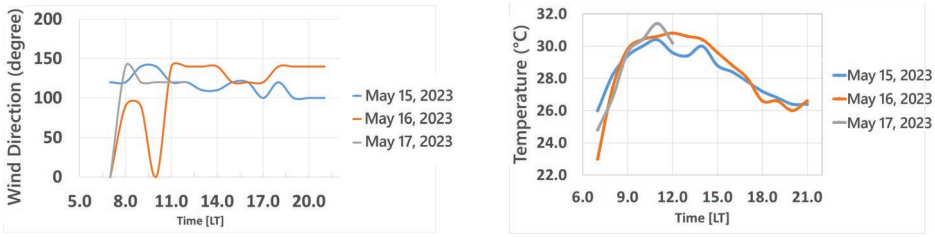

Figure 4. Two surface meteorology profiles using AWS in the Pameungpeuk area. Profile of wind direction (left panel) and temperature (right panel) for 3 (three) days.

4.2. Measurement at Ancol, Jakarta Indonesia

The power spectral density profile of the infrasound waves on 09–11 August 2023 is shown in Figure 5–7. The microbarom frequency spectrum appears around 0.4 Hz starting at 10 UTC to 02 UTC. This appearance is also in the same condition as the previous results of infrasound wave observations conducted in Pameungpeuk, West Java.

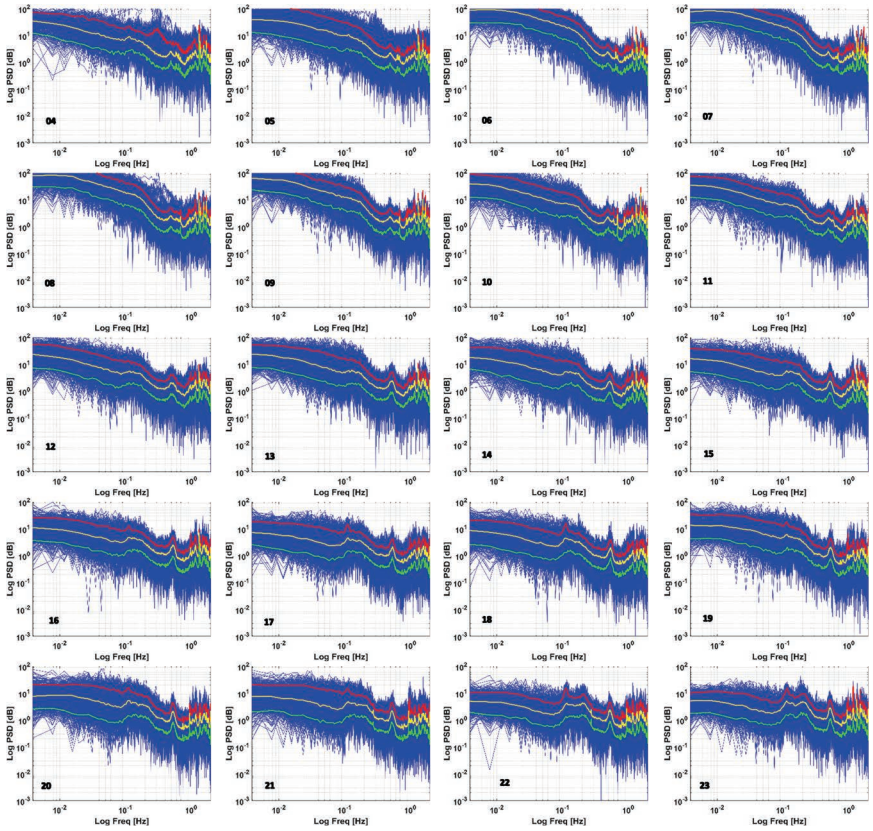

Figure 5. Power Spectral Density of Infrasound signals observed at Ancol, North Jakarta on 9 August 2023 with 0.9 percentile (red line), 0.5 percentile (yellow line), and 0.1 percentile (green line).

Figures 8 show wind speed along with its direction based on AWS measurements at Ancol, Jakarta in the period 9–11 August 2023. Specifically for wind speed, where at 10 UTC the wind began to change direction to the south, which was followed by a weakening of the strength of the gusts so that the propagation speed of the microbial column increased towards the observation location.

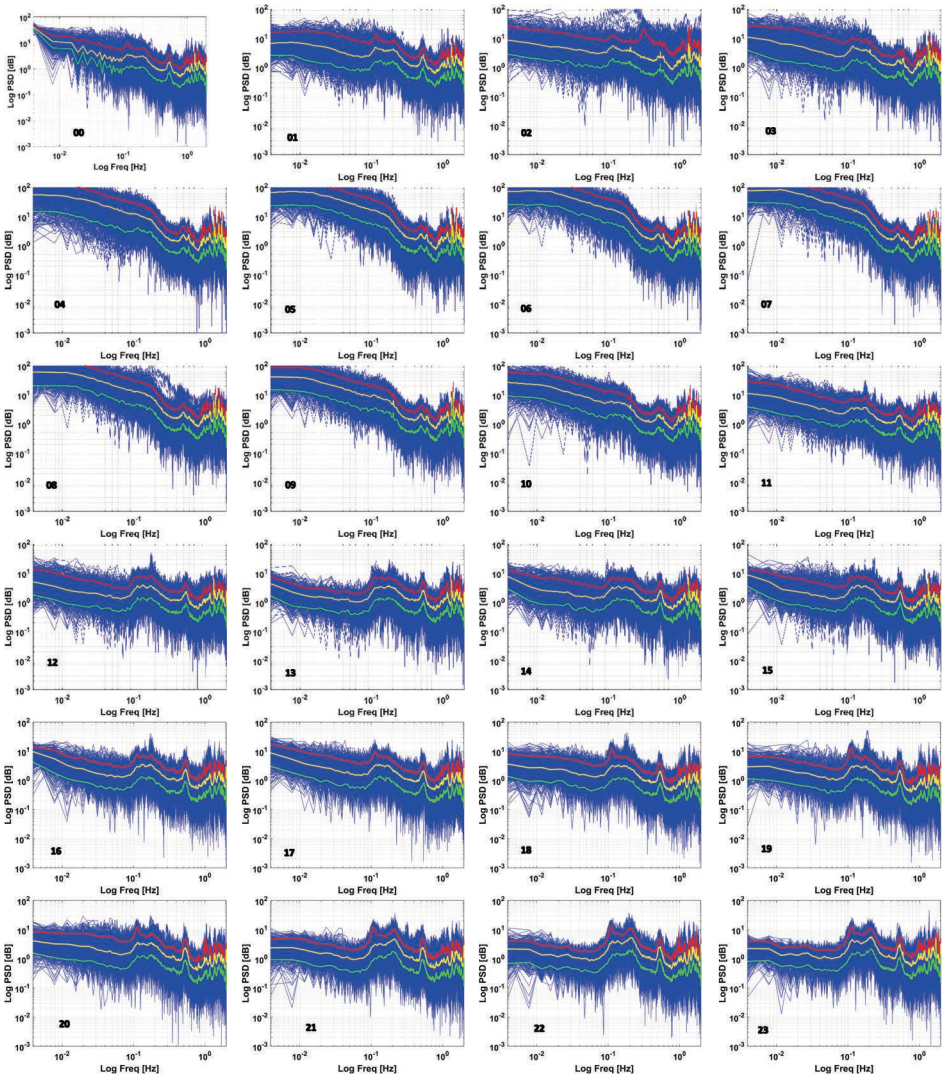

Figure 6. Power Spectral Density of Infrasound signals observed at Ancol, North Jakarta on 10 August, 2023 with 0.9 percentile (red line), 0.5 percentile (yellow line), and 0.1 percentile (green line).

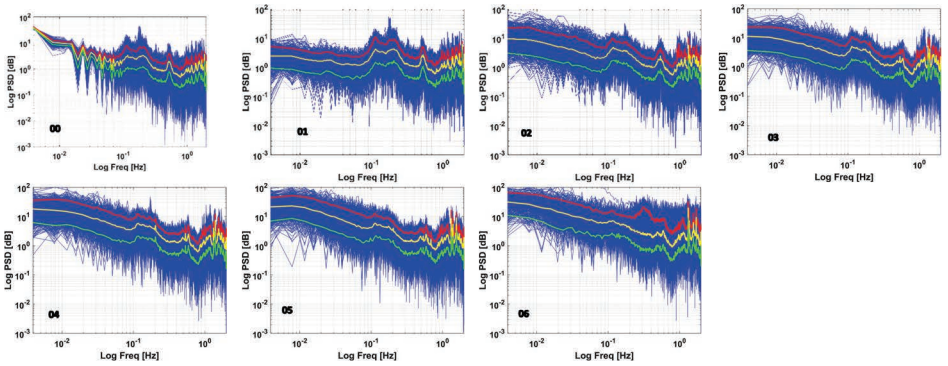

Figure 7. Power Spectral Density of Infrasound signals observed at Ancol, North Jakarta on 11 August, 2023 with 0.9 percentile (red line), 0.5 percentile (yellow line), and 0.1 percentile (green line).

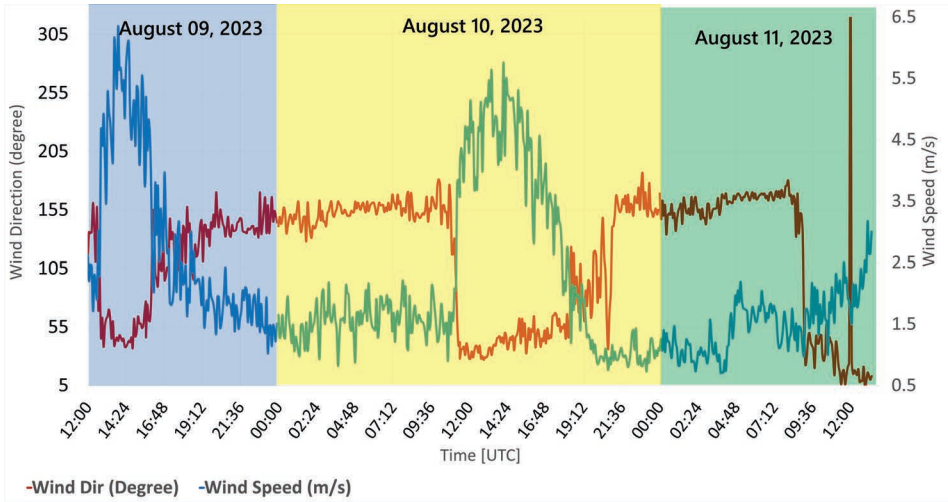

Figure 8. Profile of standard meteorology at KS Ancol Jakarta for the period 9–11 August 2023 using AWS. Wind direction in degree unit and Wind speed in m/s are shown in blue and red lines, respectively.

5. Conclusions

In this research, construction efforts and testing of a prototype integrated infrasound wave observation system are presented. This system is an integrated multidisciplinary observation platform that has low cost and low power consumption and is flexible in operation to monitor geophysical quantities. This includes instruments for measuring infrasound, acceleration, barometric pressure and temperature. This platform uses the latest sensor technology which is formed from embedded Ethernet device server components, making it easier for sensors to be monitored remotely. The programmable raspberry-pi unit controls overall system performance and retrieval and storage of observation data. Observation times are recorded based on the GPS and RTC data used where these two components are mutually supportive. Therefore, this

prototype can contribute well to multi-spatial observations by expanding the existing sensor network. This prototype system is specifically designed to measure infrasound. Infrasound wave measurements from three locations show results that prove the prototype system can function as intended. Two observations at locations close to sea waters showed that microbarom waves were successfully detected by this system in the afternoon until the following morning. It is indicated, when wind noise levels are high, infrasound signals can disappear and remain undetected. The use of this system in coastal areas is ideal for monitoring marine geophysical parameters, comparing in situ measurements, and comparing prototype output data with current model data. Therefore, as long as this platform is supported by simultaneous surface meteorological observations and model-based mathematical estimation support, studies of the dynamics of the Earth's atmosphere that utilize infrasound wave propagation can be carried out.

Acknowledgements

The authors would like to thank to Laboratory member at Kochi University of Technology (KUT), Japan, who initially built the infrasound sensor. This work was supported by research grant of the National Research and Innovation Agency (BRIN). The research grants are provided by the Research Organization of Aeronautics and Space as well as the Research Organization of Disaster and Maritim – BRIN. Finally, the author thanks all those who helped prepare field observations, especially the Coordinator of the Ancol Science Area, Jakarta; the coordinator of the Subang Science Area, West Java, and the Pameungpeuk Botanical Garden Area, West Java.

References

Marty, J. (2019). The IMS Infrasound Network: Current Status and Technological Developments. In A. Le Pichon, E. Blanc, & A. Hauchecorne (Eds.), *Infrasound Monitoring for Atmospheric Studies*. Springer, Cham. https://doi.org/10.1007/978-3-319-75140-5_1

Batubara, M., & Yamamoto, M. Y. (2020). Infrasound Observations of Atmospheric Disturbances Due to a Sequence of Explosive Eruptions at Mt. Shinmoedake in Japan on March 2018. *Remote Sensing, 12*(4), Article 728. https://doi.org/10.3390/rs12040728

Alfonsi, L., Spogli, L., Pezzopane, M., Romano, V., Zuccheretti, E., De Franceschi, G., Cabrera, M. A., & Ezquer, R. G. (2023). Comparative analysis of spread-F signature and GPS scintillation occurrences at Tucumán, Argentina. *Journal of Geophysical Research: Space Physics, 118*(7), 4483–4502. https://doi.org/10.1002/jgra.50378

Zalizovski, A. V., Yampolski, Y. M., Mishin, E., Kashcheyev, S. B., Sopin, A. O., Koloskov, A. V., Lisachenko, V. N., & Reznychenko, A. I. (2021). Multi-position facility for HF Doppler sounding of ionospheric inhomogeneities in Ukraine. *Radio Science, 56*(10), Article e2021RS007303. https://doi.org/10.1029/2021RS007303

Blanc, E., Ceranna L., Hauchecorne, A., Charlton-Perez, A., Marchetti, E., Evers, L. G., Kvaerna, T., Lastovicka, J., Eliasson, L., Crosby, N. B., Blanc-Benon, P., Le Pichon, A., Brachet, N., Pilger, C., Keckhut, P., Assink, J. D., Smets, P. S. M., Lee, C. F., Kero. J., . . . Chum, J. (2018), Toward an improved representation of middle atmospheric dynamics thanks to the ARISE project. *Surveys in Geophysics, 39*, 171–225. https://doi.org/10.1007/s10712-017-9444-0

ReVelle, D. O. (2010). Acoustic-Gravity Waves from Impulsive Sources in the Atmosphere. In A. Le Pichon, E. Blanc, & A. Hauchecorne (Eds.), *Infrasound Monitoring for Atmospheric Studies* (pp. 301–354). Springer, Dordrecht. https://doi.org/10.1007/978-1-4020-9508-5_11

DasGupta, A., Das, A., Hui, D., Bandyopadhyay, K. K., & Sivaraman, M. R. (2006). Ionospheric perturbations observed by the GPS following the December 26th, 2004 Sumatra-Andaman earthquake. *Earth, Planets and Space, 58*, 167–172. https://doi.org/10.1186/BF03353374

Shani-Kadmiel, S., Assink, J. D., Smets, P. S. M., & Evers, L. G. (2018). Seismoacoustic Coupled Signals From Earthquakes in Central Italy: Epicentral and Secondary Sources of Infrasound. *Geophysical Research Letters, 45*(1), 427–435. https://doi.org/10.1002/2017GL076125

SAYA. (2023). *Infrasound Sensor ADXIII - INF04LE*. SAYA. https://www.saya-net.com/products/inf04.html

Johnson, J. B., & Ripepe, M. (2011). Volcano infrasound: A review. *Journal of Volcanology and Geothermal Research, 206*(3–4), 61–69. https://doi.org/10.1016/j.jvolgeores.2011.06.006v

Assink, J., Averbuch, G., Shani-Kadmiel, S., Smets, P., and Evers, L.: A Seismo-Acoustic Analysis of the 2017 North Korean Nuclear Test. S*eismological Research Letters, 89*(6), 2025–2033. https://doi.org/10.1785/0220180137

Pilger, C., Hupe, P., Gaebler, P., & Ceranna, L. (2021). 1001 Rocket Launches for Space Missions and Their Infrasonic Signature. *Geophysical Research Letters, 48*, Article e2020GL092262. https://doi.org/10.1029/2020GL092262

POSTERS

Abstract

IONOSPHERIC D-REGION DISTURBANCES INDUCED BY OUTER SPACE EVENTS

Aleksandra Nina[1], Vladimir Čadež[2], Luka Č. Popović[2,3]*

[1]Institute of Physics Belgrade, University of Belgrade, Belgrade, Serbia; e-mail: sandrast@ipb.ac.rs
[2]Astronomical Observatory, Belgrade, Serbia; e-mails: vcadez@aob.ac.rs, lpopovic@aob.rs
[3]Department of Astronomy, Faculty of mathematics, University of Belgrade, Belgrade, Serbia; e-mail: lpopovic@matf.bg.ac.rs

In the ionospheric D-region, which extends within the altitude domain of about 50–90 km above the Earth's surface, there is a weakly ionized plasma whose characteristics are spatially and temporally variable. The main source of these variations is solar radiation, which causes both periodic variations due to changes in incoming solar hydrogen Lyα radiation (daily, seasonal, and variations during a solar cycle) as well as non-periodic changes due to sudden processes on the Sun (from these processes, solar X-ray flares have the most significant influence on the D-region). In addition to solar radiation, this ionospheric layer is influenced by galactic and extragalactic radiation from space as well as processes in the different terrestrial layers. Monitoring of the D-region is carried out using very low/low frequency (VLF/LF) radio signals. In this paper, we present the changes in the characteristics of VLF/LF signals that are detected by the receiver in Belgrade, Serbia, and induced by solar radiation and gamma ray bursts. In addition, we present the modeling of the periodic changes in the D-region electron density, as well as changes in this parameter during the influence of the solar X-ray flare.

Acknowledgements

The authors acknowledge funding provided by the Institute of Physics Belgrade, and the Astronomical Observatory (the contract 451-03-47/2023-01/200002) through the grants by the Ministry of Science, Technological Development and Innovation of the Republic of Serbia.

[*]Corresponding author, e-mail: sandrast@ipb.ac.rs

Abstract

GROUND-BASED RADAR INTERFEROMETRY: EXAMPLES OF APPLICATION TO THE MONITORING OF LANDSLIDES AND INFRASTRUCTURE

Olimpia Masci[1], Giovanni Nico[2], Giuseppina Prezioso[3]*

[1]DIAN S.r.l., Matera, Italy; e-mail: o.masci@dianalysis.eu
[2]Italy's National Research Council, Institute of Applied Mathematics, Bari, Italy; e-mail: giovanni.nico@cnr.it
[3]University of Naples "Parthenope", Department of Science and Technology, Naples, Italy; e-mail: pina.prezioso@uniparthenope.it

This presentation focus on the monitoring of landslides and man-made infrastructures which could be affected by the occurrence of landslides. Mass movements due to landslides and surface deformation, as well as vibrations frequencies of man-made structures are estimated by the radar interferometry technique applied to both Synthetic Aperture Radar (SAR) and Real Aperture Radar (RAR) data collected by a ku-band ground-based radar (Anghel et al., 2019; DiPasquale et al., 2018). SAR images are used to provide maps of terrain displacements and infrastructure deformations with a spatial resolution of 0.75 m in range direction. The cross-range resolution decreases with the range distances up a few meters at the maximum range distance of four kilometers. RAR profiles are used to estimate the vibration frequencies of infrastructures up to about 10 Hz (Nico et al., 2020). The precision of displacements is of a few millimeters depending on the phase decorrelating effects in the scene (e.g., vegetation). Examples of application of ground-based radar interferometry to the monitoring of landslides and man-made infrastructure are shown and commented.

References:

Anghel, A., Tudose, M., Cacoveanu, R., Datcu, M., Nico, M., Masci, O., Dongyang, A., Tian, W., Hu, C., Ding, Z., Nies, H., Loffeld, O., Atencia, D., Huaman, S. G., Medella, A., & Moreira, J. (2019). Compact ground-based interferometric synthetic aperture radar: Short-range structural monitoring. *IEEE Signal Processing Magazine, 36*(4), 42–52. https://doi.org/10.1109/MSP.2019.2894987

DiPasquale, A., Nico, G., Pitullo, A., & Prezioso, G. (2018). Monitoring Strategies of Earth Dams by Ground-Based Radar Interferometry: How to Extract Useful Information for Seismic Risk Assessment. *Sensors, 18*(1), Article 244. https://doi.org/10.3390/s18010244

Nico, G., Prezioso, G., Masci, O., & Artese, S. (2020). Dynamic Modal Identification of Telecommunication Towers Using Ground Based Radar Interferometry *Remote Sensing, 12*(7), Article 1211. https://doi.org/10.3390/rs12071211

*Corresponding author, e-mail: giovanni.nico@cnr.it

Abstract

UNDERSTANDING THE EFFECTS OF ANTHROPOGENIC AEROSOLS AND CONTROL IN AIR QUALITY DURING COVID-19 LOCKDOWN PERIOD

Arul Asir Jebakumar[1]*, *Johnson Jeyakumar Henry Duraisamy*[1], *Anil Kumar Chakkalayil Parameswaran*[2]

[1]Manonmaniam Sundaranar University, Pope's College, P.G. and Research Department of Physics, Tirunelveli, India; e-mails: arulasir1997@gmail.com; hjohnsonjeyakumar@gmail.com
[2]Indian Institute of Geomagnetism, Equatorial Geophysical Research Laboratory, Tirunelveli, India; e-mail: anilkumar.cp.iig@nic.in

We got unique opportunity to carry out air pollution studies during lockdown phases of the Covid-19 pandemic from Alandur (13.03°N, 80.21°E), Tamil Nadu, India. A comparative study has been made in atmospheric pollutants between pre-pandemic period and during the lock-down period (imposed to control the spread of novel Corona Virus infection) and with the aid of ground based atmospheric pollution monitoring instruments. We used the Blackman-Tukey power spectrum analysis for estimating the power spectrum of pollutants during Pre-Covid-19 and during Covid-19 time domains for the selected station. The data was obtained from the Central Pollution Control Board (CPCB). Since we learn a lesson from pollution under control during Covid pandemic, as such the power spectrum gives access to top to bottom analysis of anthropogenic pollutants to quantifying the peaks and periodicities present in the series for in depth analysis and control for the future. First, we normalized the time series which show the general trend of the pollution parameters. Then the spectral estimation was carried out for its eigen values and periodicities during pre-covid period and during lock-down period. These results show a particular trend at a peak business hour (IST) in diurnal pattern where the prominent pollutants played a dominant role in both timelines showing a significant drop (~42.5%) in the level of most of the prominent pollutants during lock-down period. Significant drop in levels of CO, NO_2, and $PM_{2.5}$, reflected in the power spectral windows of both timelines. However, O_3 and No_2 showed no substantial variation during this period. The future studies will envisage the pollution control technicalities and strategies Based on the Air Quality Index (AQI).

*Corresponding author, e-mail: arulasir1997@gmail.com

Book of Abstracts and Contributed Papers
International Conference on Recent Trends in Geoscience Research and Applications 2023
Belgrade, Serbia & Virtual, October 23–27, 2023
Editors: Aleksandra Nina, Snežana Dragović, and Dejan Doljak

Abstract

UTILIZATION OF REMOTE SENSING AND NUCLEAR TECHNIQUES FOR DETAILED MODELING AND QUANTITATIVE ASSESSMENT OF GULLY EROSION WITHIN THE FORESTED AREA OF THE MALČANSKA RIVER BASIN, EASTERN SERBIA

Mrđan Đokić[1], Miloš Manić[2], Milan Đorđević[1], Milena Gocić[1], Aleksandar Čupić[3], Mihajlo Jović[3], Ranko Dragović[1], Boško Gajić[4], Ivana Smičiklas[3], Snežana Dragović[3]*

[1]University of Niš, Faculty of Sciences and Mathematics, Department of Geography, Niš, Serbia; e-mails: mrdjan.djokic@pmf.edu.rs; milan.djordjevic@pmf.edu.rs; milena.gocic@pmf.edu.rs; dragovicr@pmf.ni.ac.rs
[2]University of Belgrade, Faculty of Geography, Belgrade, Serbia; e-mail: milos.manic@pmf.edu.rs
[3]University of Belgrade, "VINČA" Institute of Nuclear Sciences – National Institute of the Republic of Serbia, Belgrade, Serbia; e-mails: aleksandar.cupic@vin.bg.ac.rs; mjovic@vin.bg.ac.rs; ivanat@vin.bg.ac.rs; sdragovic@vin.bg.ac.rs
[4]University of Belgrade, Faculty of Agriculture, Beograd, Serbia; e-mail: bonna@agrif.bg.ac.rs

The gully erosion is one of the most significant land degradation processes. Although gully erosion significantly threatens agricultural productivity and natural ecosystems, European land management strategies frequently need more reliable data on environmental conditions governing this process. This study presents a methodology that integrates remote sensing and nuclear techniques for examining gully erosion (Đokić et al., 2023). It introduces a novel approach to erosion research by employing 360-degree camera photogrammetry to characterize gullies morphometrically. The main objectives of this approach are to evaluate the applicability of unmanned aerial vehicles and terrestrial photogrammetry for modeling gullies, to study small-scale erosion processes within gullies, compare erosion intensity between adjacent gullies, and determine the most effective and cost-efficient method for monitoring gullies. A total of 39 soil samples were taken in three studied gullies. The results revealed an average soil redistribution rate of 16.2 $t\ ha^{-1}\ yr^{-1}$ and coefficients of variation of 32%, 59%, and 91% for the gullies. The estimated erosion rate varies from a minimum of 0.1 $t\ ha^{-1}\ yr^{-1}$ to a maximum of 34.3 $t\ ha^{-1}\ yr^{-1}$. Soil deposition was identified at only two sampling sites, 1.1 and 2 $t\ ha^{-1}\ yr^{-1}$. Highly detailed 3D models of the gullies were created using 360-degree photogrammetry. The micro-relief obtained through modeling proved to be an essential aspect of advanced erosion research.

Acknowledgements

This paper was supported by the Ministry of Science, Technological Development and Innovation of the Republic of Serbia contracts 451-03-47/2023-01/200124, 451-03-47/2023-01/200017, and 451-03-47/2023-01/200116. The authors acknowledge the support of the Joint FAO/IAEA Division of

*Corresponding author, e-mail: mrdjan.djokic@pmf.edu.rs

Nuclear Techniques in Food and Agriculture in providing equipment for gamma-ray spectrometry and UAV remote sensing within the project SRB5003.

References

Đokić, M., Manić, M., Đorđević, M., Gocić, M., Čupić, A., Jović, M., Dragović, R., Gajić, B., Smičiklas, I., & Dragović, S. (2023). Remote sensing and nuclear techniques for high-resolution mapping and quantification of gully erosion in the highly erodible area of the Malčanska River Basin, Eastern Serbia. *Environmental Research*, *235*, Article 116679. https://doi.org/10.1016/j.envres.2023.116679

Abstract

DETERMINATION OF IONOSPHERIC MODELS USING GLOBAL NAVIGATIONAL SATELLITE SYSTEMS AND BERNESE GNSS SOFTWARE

Dušan Petković[1]*, *Sanja Grekulović*[1], *Miljana Todorović-Drakul*[1], *Oleg Odalović*[1]

[1]University of Belgrade, Faculty of Civil Engineering, Department of Geodesy and Geoinformatics, Belgrade, Serbia; e-mail: dpetkovic@grf.bg.ac.rs; sanjag@grf.bg.ac.rs; mtodorovic@grf.bg.ac.rs; odalovic@grf.bg.ac.rs

Since the last few decades of the 20th and the beginning of civilian application of NAVigation Satellite Timing And Ranging Global Positioning System (NAVSTAR GPS) established by the United States Department of Defense, satellite positioning is the most widespread technology for position determination on any place in the Earth's surface (Hofmann-Wellenhof et al., 2008). Besides positioning, a Global Navigation Satellite Systems (GNSS; a common name for all operational navigation systems worldwide) technology is used for other research applications such as atmospheric parameter estimation, i.e., ionospheric determination (Seeber et al., 2003). This paper presents the possibility of the GNSS technology as a tool for determining ionospheric models by the Bernese GNSS Software (Dach et al., 2015). Bernese supports three types of models to represent the ionosphere: local models based on Taylor series expansions, and station-specific and global (or regional) models based on spherical harmonic expansions (Schaer, 1999). Mentioned Ionospheric models (also called Ionospheric maps) can be produced in Bernese ION format or as a common data-exchange IONosphere EXchange (IONEX) format (Schaer et al., 1998). Based on these formats, it is possible to determine the quantity that characterizes the current state of the ionosphere, the so-called Total Electron Content (TEC).

Acknowledgments

The authors acknowledge funding provided by the Faculty of Civil Engineering, University of Belgrade, through the Ministry of Science, Technological Development and Innovations, grant No. 200092.

References

Hofmann-Wellenhof, B., Lichtenegger, H., & Wasle, E. (2008). *GNSS – Global Navigation Satellite Systems: GPS, GLONASS, Galileo, and more*. Springer Vienna.

Dach, R., Lutz, S., Walser, P., & Fridez P. (Eds). (2015). *Bernese GNSS Software Version 5.2. User manual*. Astronomical Institute, University of Bern.

Schaer, S., Gurtner, W., & Feltens, J. (1998). *IONEX: The IONosphere Map EXchange Format Version 1.1*. http://ftp.aiub.unibe.ch/ionex/draft/ionex11.pdf

Schaer, S. (1999). *Mapping and Predicting the Earth's Ionosphere Using the Global Positioning System*. University of Bern.

Seeber, G. (2003). *Satellite Geodesy*. Walter de Gruyter.

*Corresponding author, e-mail: dpetkovic@grf.bg.ac.rs

Book of Abstracts and Contributed Papers
International Conference on Recent Trends in Geoscience Research and Applications 2023
Belgrade, Serbia & Virtual, October 23–27, 2023
Editors: Aleksandra Nina, Snežana Dragović, and Dejan Doljak

Abstract

COVERAGE OF DATA RELEVANT FOR ATMOSPHERIC RESEARCH IN BEAM DATABASE

Bratislav P. Marinković [1,2]*

[1]Institute of Physics Belgrade, University of Belgrade, Laboratory for Atomic Collision Processes, Belgrade, Serbia; e-mail: bratislav.marinkovic@ipb.ac.rs
[2]The author is a member of EuroPlanet Society (Southeast Europe Hub)

Ensuring reliable atomic and molecular (A&M) data is of paramount importance for analyzing and modelling processes in science fields as plasma (Dujko et al., 2021; Marinković et al., 2007), astrophysics (Dimitrijević et al., 2021; Marinković et al., 2017) or atmosphere and environment (Marinković, 2009; Campbell & Brunger, 2016; Campbell & Brunger, 2023). A large consortium of research groups and institutions has been established in order to provide a unique entry point for A&M data distributed along different databases via a single portal known as VAMDC—Virtual Atomic and Molecular Data Centre (Albert et al., 2020; Dubernet et al., 2016). One of the databases specialized for electron-atom(molecule) interactions is the BEAMDB—Belgrade Electron/Atom(Molecule) Data Base (Marinković et al., 2019).

Molecular species that are covered in BEAM database and are relevant for atmospheric research include triatomic molecules (H_2O, H_2S, N_2O) and larger organic molecules (methane, formaldehyde). Beside carbon dioxide, these molecules represent powerful greenhouse gases. Especially methane (Vukalović et al., 2021) has a large impact on climate albeit its concentration in atmosphere is relatively small. Once in atmosphere, its potential to absorb heat via vibrational excitation is much larger than for CO_2 and also when it is consumed as a fuel, it releases carbon dioxide. Further plans to feed data in BEAMDB are to cover some of inhalation anesthetics such as halothane (Maljković et al., 2023), sevoflurane (Vukalović et al., 2022) and desflurane. These molecules have a prominent role in depletion of stratospheric ozone.

Acknowledgements

The author acknowledges funding provided by the Institute of Physics Belgrade and the Astronomical Observatory Belgrade, through the grants by the Ministry of Science, Technological Development and Innovation of the Republic of Serbia.

References

Albert, D., Antony, B. K., Ba, Y. A., Babikov, Y. L., Bollard, P., Boudon, V., Delahaye, F., Del Zanna, G., Dimitrijević, M. S., Drouin, B. J., Dubernet, M.-L., Duensing, F., Emoto, M., Endres, C. P., Fazliev, A. Z., Glorian, J.-M., Gordon, I. E., Gratier, P., Hill, C., . . . Zwölf, C. M. (2020). A Decade with VAMDC: Results and Ambitions. *Atoms, 8*(4), Article 4. https://doi.org/10.3390/atoms8040076

*Corresponding author, e-mail: bratislav.marinkovic@ipb.ac.rs

Campbell, L., & Brunger, M. J. (2023). Modelling of Energy-Dependent Electron Interactions in the Earth's Mesosphere. *Atmosphere, 14*, Article 611. https://doi.org/10.3390/atmos14040611

Campbell, L., & Brunger, M.J. (2016). Electron collisions in atmospheres. *International Reviews in Physical Chemistry, 35*, 297–351. https://doi.org/10.1080/0144235X.2016.1179002

Dimitrijević, M. S., Srećković, V. A., Ignjatović, Lj. M., & Marinković, B. P. (2021). The role of some collisional processes in AGNs: Rate coefficients needed for modeling. *New Astronomy, 84*, Article 101529. https://doi.org/10.1016/j.newast.2020.101529

Dubernet, M. L., Antony, B. K., Ba, Y. A., Babikov, Y. L., Bartschat, K., Boudon, V., Braams, B. J., Chung, H.-K., Daniel, F., Delahaye, F., Zanna, G. D., Urquijo, J. de, Dimitrijević, M. S., Domaracka, A., Doronin, M., Drouin, B. J., Endres, C. P., Fazliev, A. Z., Gagarin, S. V., . . . Zwölf, C. M. (2016). The virtual atomic and molecular data centre (VAMDC) consortium*. *Journal of Physics B: Atomic, Molecular and Optical Physics, 49*(7), Article 074003. https://doi.org/10.1088/0953-4075/49/7/074003

Dujko, S., Atić, S., Bošnjaković, D., White, R. D., Stokes, P., Hamilton, K. R., Zatsarinny, O., Bartschat, K., Rabasović, M. S., Šević, D., Marinković, B. P., Fursa, D. V., Bray, I., McEachran, R. P., Blanco, F., García, G., Jones, D. B., Campbell, L., & Brunger, M. J. (2021). Transport of electrons and propagation of the negative ionisation fronts in indium vapour. *Plasma Sources Science and Technology, 3*0, Article 115019. https://doi.org/10.1088/1361-6595/ac3343

Maljković, J. B., Vukalović, J., Pešić, Z. D., Blanco, F., García, G., & Marinković, B. P. (2023). Experimental and theoretical study on elastic electron interaction with halothane molecule in the intermediate energy range. Eur. Phys.J. Plus, 138, 349. https://doi.org/10.1140/epjp/s13360-023-03967-6

Marinković, B. P. (2009). Study of Higher Excited States of Some Polyatomic Molecules Relevant for Plasma Physics and Environment. *Journal of Physics: Conference Series, 162*, Article 012001. http://dx.doi.org/10.1088/1742-6596/162/1/012001

Marinković, B. P., Bredehöft, J. H., Vujčić, V., Jevremović, D., & Mason, N. J. (2017). Rosetta Mission: Electron Scattering Cross Sections—Data Needs and Coverage in BEAMDB Database. *Atoms, 5*(4), Article 46. https://doi.org/10.3390/atoms5040046

Marinković, B. P., Pejčev, V., Filipović, D. M., Šević, D., Milosavljević, A. R., Milisavljević, S., Rabasović, M. S., Pavlović, D., & Maljković, J. B. (2007). Cross section data for electron collisions in plasma physics. *Journal of Physics: Conference Series, 86*, Article 012006. http://dx.doi.org/10.1088/1742-6596/86/1/012006

Marinković, B. P., Srećković, V. A., Vujčić, V., Ivanović, S., Uskoković, N., Nešić, M., Ignjatović, Lj. M., Jevremović, D., Dimitrijević, M. S., & Mason, N. J. (2019). BEAMDB and MOLD—Databases at the Serbian Virtual Observatory for collisional and radiative processes. *Atoms, 7*(1), 11. https://doi.org/10.3390/atoms7010011

Vukalović, J., Maljković, J. B., Blanco, F., García, G., Predojević, B., & Marinković, B. P. (2022). Absolute differential cross-sections for elastic electron scattering from sevoflurane molecule in the energy range from 50–300 eV. *International Journal of Molecular Sciences, 23*(1), Article 21. https://doi.org/10.3390/ijms23010021

Vukalović, J., Maljković, J. B., Tökési, K., Predojević, B., & Marinković, B. P. (2021). Elastic electron scattering from methane molecule in the energy range from 50–300 eV. *International Journal of Molecular Sciences, 22*(2), Article 647. https://doi.org/10.3390/ijms22020647

GeosciRA23
Book of Abstracts and Contributed Papers
International Conference on Recent Trends in Geoscience Research and Applications 2023
Belgrade, Serbia & Virtual, October 23–27, 2023
Editors: Aleksandra Nina, Snežana Dragović, and Dejan Doljak

Contributed paper

FEATURE IMPORTANCE ANALYSIS IN RANDOM FOREST REGRESSION FOR AIR QUALITY FORECASTING IN BELGRADE, SERBIA

Filip Arnaut[1]*, *Aleksandra Kolarski*[1]

[1]Institute of Physics Belgrade, University of Belgrade, Belgrade, Serbia; email: filip.arnaut@ipb.ac.rs

Abstract: The significance of feature importance is crucial in determining the effectiveness of a machine learning algorithm during both its training and testing stages, especially with regards to the duration of the model's training process. This brief communication conducted feature importance analysis using a Random Forest regression algorithm on air quality data collected from the measuring station Mostar, Belgrade, Serbia. The input features utilized in this study consist of PM_{10}, CO, NO_2, and SO_2 air quality parameters, whereas the target was set to the $PM_{2.5}$ parameter. The utilized dataset consists of data collected over a three-year period (2019–2021), in which all five parameters were measured (23660 instances). The findings indicate that the model utilizing all four parameters as features exhibits the lowest root-mean-square-error (5.093 $\mu g \cdot m^{-3}$), whereas the model using only PM_{10} and CO as input features demonstrates the highest root-mean-square error (5.509 $\mu g \cdot m^{-3}$). The differences in errors are indicative of a 7.5% disparity, whereas the duration of model training exhibited a decline of 39.6%. The analysis of feature importance revealed that a viable compromise could be achieved between the quantity of features utilized for model training and the duration of the training process, with a slight reduction in model accuracy. The conducted correlation analysis revealed that the $PM_{2.5}$ parameter exhibited strong to very strong correlation coefficients with the PM_{10} (ρ_s=0.91) and CO (ρ_s=0.71) parameters, while displaying weak correlation coefficients with the SO_2 (ρ_s=0.25) and NO_2 (ρ_s=0.39) parameters, which can serve as a potential explanation for the feature importance analysis results.

Keywords: Machine learning; Network analysis; Air quality data analysis; $PM_{2.5}$

1. Introduction

Air quality has emerged as a significant environmental and public health concern, particularly in urban centers, industrialized regions, and areas with high traffic and industrial activity. The Republic of Serbia's cities with their frequent appearance on the list of top polluted cities globally, has one possible prevalent factor which is the increased use of personalized motor vehicles. Between 2011 and 2022, a 30% increase in the total number of registered passenger vehicles can be observed (Statistical Office of the Republic of Serbia, 2011; 2022). This pattern has the potential to contribute to increased air pollution levels.

Environmental or atmospheric air pollution forecasting research is considered advantageous due to the potential to develop a reliable, stable, and accurate method for forecasting air pollution. This could provide valuable information for vulnerable populations, including individuals with chronic respiratory illnesses and elderly individuals.

*Corresponding author, e-mail: filip.arnaut@ipb.ac.rs

Recent approaches to air pollution forecasting have utilized time series forecasting (Samal et al., 2019; Shen et al., 2020; Ye et al., 2019; Zhao et al., 2018) or a combination of time series forecasting and machine learning techniques i.e., hybrid methods (Ejohwomu et al., 2022).

In the realm of feature importance or feature selection research, Sethi and Mittal (2019) have highlighted CO and NO_2 as significant parameters for air quality pollution concerning $PM_{2.5}$. Conversely, Mahajan et al. (2021) have emphasized that NO_2 and particulate matter are the primary contributors to the air quality index (AQI). This study utilizes a commonly employed machine learning algorithm to analyze data gathered from a high-traffic location. The objective is to predict future values and implement feature importance and selection techniques to isolate the most significant features for subsequent research.

2. Methods and data

The Random Forest (RF) algorithm was first introduced by Breiman (2001), and since has become a widely used machine learning classification and regression algorithm. A notable advantage of the RF algorithm is its minimal number of hyperparameters that necessitate tuning, with the sole hyperparameter being the number of trees. In machine learning research utilizing the RF algorithm, the determination of the number of trees can typically be achieved through iterative modeling and the minimization of a loss function in this example the out-of-bag mean squared error. Once the loss function begins to converge, the effective number of trees can be established. The present study employed JASP software (JASP Team, 2023) to automatically determine the number of trees, with the restriction that the maximum number of trees could not surpass 500.

The RF modeling procedure was conducted utilizing data that was partitioned into three distinct groups, namely the training, validation, and testing sets. The allocation for this study was divided into a ratio of 64-16-20. During the training phase, the RF algorithm utilizes input features comprising of PM_{10}, CO, NO_2, and SO_2 to "learn" of the patterns in the data with respect to the $PM_{2.5}$ parameter, which serves as the target variable. During the testing phase, the algorithm is provided with input features and attempts to forecast the value of the target variable. Upon utilizing the RF algorithm to forecast the target variable and comparing the forecasted values with the actual values, a variety of assessment measures can be computed, including the root mean square error (RMSE), mean absolute error (MAE), mean absolute percentage error (MAPE), and the coefficient of determination (R^2). In the context of comparing multiple RF models that were trained and tested on identical data, the evaluation metric parameters play a critical role in model interpretation. In this study, where various models were trained on the same data but with different features (some of which were excluded), the evaluation metric parameters are essential in identifying the optimal model.

The process of feature importance or feature selection involves assigning a score to each utilized feature based on a given metric. In this study, the two metrics employed were Mean Decrease in Node Accuracy (MDNA) and Total Increase in Node Purity (TINP). The straightforward interpretation of both parameters is that features with higher scores hold greater significance in effectively modeling the target variable. Regarding MDNA, the score denotes the significance of a particular feature in relation to the model's overall accuracy. Conversely, the TINP score reflects the improvement in the quality of tree splits that result from utilizing a specific feature. Modelling was undertaken with respect to the MDNA and TINP parameters. Each

successive model excluded the least informative feature from the previous model. As a cost effective or efficiency parameter the time taken to train and test the model was used.

The data utilized in this study was obtained from the Environmental Protection Agency of the Republic of Serbia (n.d.) for the air quality monitoring station Mostar, situated in Belgrade, Serbia. The monitoring station is in a heavily transport-oriented part of the city where the number of vehicles is great. The dataset utilized in this study encompasses a three-year timeframe spanning from 2019 to 2021, during which air quality was monitored. It is noteworthy that solely those instances in which all five parameters were measured were considered for the purposes of the RF modelling. A total of 23660 data points (instances) were used.

3. Results and discussion

The three RF regression models were trained with the same input data, but different features used to forecast $PM_{2.5}$ values. The initial model (RF_1) was trained utilizing all input features (SO_2, NO_2, PM_{10}, and CO) with a total data count of 23660 instances per feature. Subsequently, the RF_2 and RF_3 models were trained with one less feature, contingent on the feature importance analysis of the preceding model.

The RF_1 model exhibits the lowest RMSE value of 5.093 $\mu g \cdot m^{-3}$ (Table 1), while the succeeding models (RF_2 and RF_3) manifest an increase in the RMSE value. It is noteworthy, however, that the most significant disparity in the RMSE value is observed between models RF_1 and RF_3, with a mere 7.5% variation. The MAE exhibits a comparable pattern to that of the RMSE, whereby the error parameter values demonstrate an increase as the quantity of features decreases. Notably, the most significant deviation is observed between the RF_1 and RF_3 models, with a discrepancy of approximately 8.8%.

The analysis of feature importance using the MDNA and the TINP for the initial model indicates that PM_{10} and CO are the most significant features, whereas NO_2 and SO_2 may be deemed insignificant. Feature importance analysis that was performed on the RF_2 model, wherein the NO_2 parameter was selected for exclusion. According to the RF_3 model, the features of CO and PM_{10} hold similar levels of significance in predicting $PM_{2.5}$ values.

Conversely, there is a notable reduction in the duration required for model training, with the RF_3 model taking approximately 39.5% less time to train than the RF_1 model. A feasible compromise may be achieved by reducing the number of features, shortening the model training time, and accepting a relatively minor rise in the model's error metrics. In this scenario, the compromise would entail accepting a model with a 7.5% reduction in accuracy while simultaneously reducing the time required to train the model by approximately 40%. The case presented in Table 1 serves as a mere illustration of a trade-off. Given that the discrepancies in the maximum time required are approximately one minute, the trade-off does not appear to confer significant advantages. Conversely, if the analysis were to incorporate a broader range of features, such as meteorological data comprising precipitation, temperature, humidity, among others, as well as other pertinent factors that could impact air quality, such as traffic information, and if the analysis were to span a time frame, the potential trade-off could prove to be highly advantageous in terms of the overall time saved for the analysis.

Table 1. Random Forest modelling results

Model	Feature	MDNA	TINP	RMSE [µg·m^{-3}]	MAE [µg·m^{-3}]	MAPE [%]	R^2	Time [sec]
RF_1	PM_{10}			5.093	3.371	22.25	0.93	159
	CO							
	NO_2							
	SO_2							
RF_2	PM_{10}			5.25	3.515	23.49	0.92	130
	CO							
	NO_2							
RF_3	PM_{10}			5.509	3.697	23.33	0.91	96
	CO							

Note. MDNA = Mean Decrease in Node Accuracy; TINP = Total Increase in Node Purity; RMSE = Root Mean Square Error; MAE = Mean Absolute Error; MAPE = Mean Absolute Percentage Error; R^2 = Coefficient of determination.

To potentially clarify the reasons behind the observed outcomes of the feature importance analysis, a correlation-based network analysis was conducted (Figure 1). The Spearman's correlation coefficient was utilized for the network analysis due to the non-normal distribution of the data, specifically its skewed nature (the skewness parameter displays values from 1.305 for the NO_2 feature to 7.354 for the SO_2 feature). The results of the network analysis indicate that the $PM_{2.5}$, PM_{10}, and CO parameters exhibit a significant correlation. Specifically, the PM_{10} and $PM_{2.5}$ parameters exhibit a very strong correlation with a coefficient of 0.91, while the $PM_{2.5}$ and CO parameters exhibit a strong correlation with a coefficient of 0.71. In contrast, it can be observed that the parameters of SO_2 and NO_2 exhibit a limited correlation with $PM_{2.5}$, with coefficients of only 0.25 and 0.39, respectively.

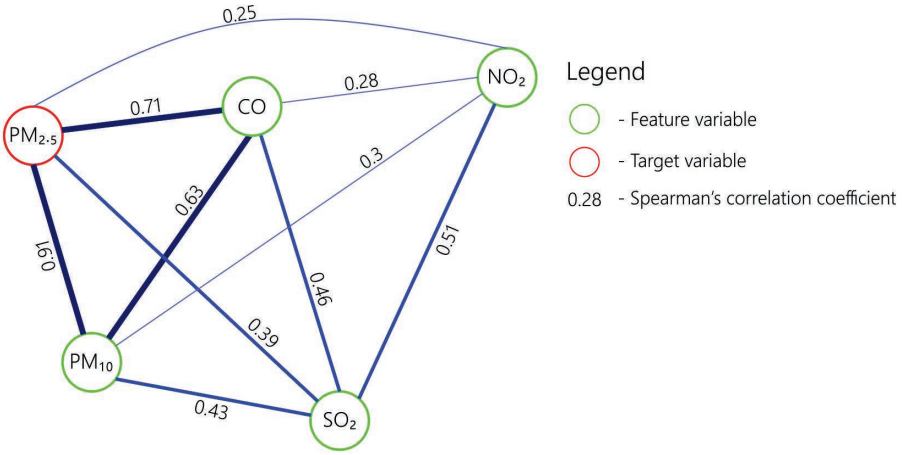

Figure 1. Modified network analysis utilizing Spearman's correlation coefficient for air quality data from the measuring station Mostar, Belgrade, Serbia (2019 to 2021).

It is noteworthy that the analysis was repeated utilizing supplementary data, including the month of the year, day of the month, and hour of measurement. The feature importance analysis, incorporating MDNA and TINP, revealed that PM_{10} and CO, consistent with the prior example, were the top two most significant features. The third most informative feature was identified as the month of the year. The features of SO_2 and NO_2 were found to be followed by the hour of measurement and the day of the week on which the measurement was taken, which were deemed to be the least informative features added. Subsequent research should incorporate supplementary data that delineates the time of measurement, specifically the month, as demonstrated in this instance. This information can potentially provide greater insight compared to the features of SO_2 and NO_2. The model incorporating supplementary data exhibited better results in terms of lower RMSE values of 4.929 $\mu g \cdot m^{-3}$, MAE values of 2.946 $\mu g \cdot m^{-3}$, and MAPE values of 20.11%. Additionally, this model demonstrated a higher R^2 score of 0.934.

4. Conclusion

The utilization of machine learning algorithms for air quality modelling and forecasting has been demonstrated to be a reliable, precise, and effective approach for predicting air quality data. The findings of this study demonstrate that effective modelling can be achieved through the displacement of redundant features, such as SO_2 and NO_2 in this case, resulting in a time reduction of approximately 40%. The process of feature selection plays a crucial role in enhancing the efficiency of RF modelling when dealing with extensive datasets that may encompass variables such as meteorological and transport data. Subsequent research should acquire additional features, including the previously mentioned meteorological and transportation information, and conduct a thorough analysis of feature selection.

References

Breiman, L. (2001). Random Forests. *Machine Learning, 45,* 5–32. http://dx.doi.org/10.1023/A:1010933404324

Ejohwomu, O. A., Shamsideen Oshodi, O., Oladokun, M., Bukoye, O. T., Emekwuru, N., Sotunbo, A., & Adenuga, O. (2022). Modelling and Forecasting Temporal $PM_{2.5}$ Concentration Using Ensemble Machine Learning Methods. *Buildings*, *12*, Article 46. https://doi.org/10.3390/buildings12010046

Environmental Protection Agency of the Republic of Serbia. *Air quality- Unverified hourly data in real time* [Data set]. Environmental Protection Agency of the Republic of Serbia. http://data.sepa.gov.rs/dataset/kvalitet-vazduha

JASP Team. (2023). JASP (Version 0.17.1) [Computer software]. https://jasp-stats.org/download/

Mahajan, M., Kumar, S., Pant, B., Tiwari, U.K. & Khan, R. (2021). *Feature selection and analysis in air quality data*. In 11th International Conference on Cloud Computing, Data Science & Engineering (pp. 280–285). Institute of Electrical and Electronics Engineers. https://doi.org/10.1109/Confluence51648.2021.9376882

Samal, K. K. R., Babu, K. S., Das, S. K., & Acharaya, A. (2019). Time series based air pollution forecasting using SARIMA and prophet model. In *Proceedings of the 2019 international conference on information technology and computer communications* (pp. 80–85). Association for Computing Machinery. https://doi.org/10.1145/3355402.3355417

Sethi, J. K., & Mittal, M. (2019). A new feature selection method based on machine learning technique for air quality dataset. *Journal of Statistics and Management Systems*, *22*(4), 697–705. https://doi.org/10.1080/09720510.2019.1609726

Shen, J., Valagolam, D., & McCalla, S. (2020). Prophet forecasting model: a machine learning approach to predict the concentration of air pollutants ($PM_{2.5}$, PM_{10}, O_3, NO_2, SO_2, CO) in Seoul, South Korea. *PeerJ*, *8*, Article e9961. https://doi.org/10.7717%2Fpeerj.9961

Statistical Office of the Republic of Serbia. (2011). *Statistical Yearbook of Serbia 2011*. Retrieved May 19, 2023 from https://publikacije.stat.gov.rs/G2011/PdfE/G20112004.pdf

Statistical Office of the Republic of Serbia. (2022). *Statistical Yearbook of the Republic of Serbia, 2022*. Retrieved May 19, 2023 from https://publikacije.stat.gov.rs/G2022/PdfE/G20222055.pdf

Ye, Z. (2019). Air pollutants prediction in Shenzhen based on ARIMA and Prophet method. *E3S Web of Conferences*, *136*, Article 05001. https://doi.org/10.1051/e3sconf/201913605001

Zhao, N., Liu, Y., Vanos, J. K., & Cao, G. (2018). Day-of-week and seasonal patterns of $PM_{2.5}$ concentrations over the United States: Time-series analyses using the Prophet procedure. *Atmospheric Environment*, *192*, 116–127. https://doi.org/10.1016/j.atmosenv.2018.08.050

Book of Abstracts and Contributed Papers
International Conference on Recent Trends in Geoscience Research and Applications 2023
Belgrade, Serbia & Virtual, October 23–27, 2023
Editors: Aleksandra Nina, Snežana Dragović, and Dejan Doljak

Contributed paper

CORRELATION BETWEEN PRECIPITATION, AIR TEMPERATURE AND DISCHARGE IN THE MLAVA RIVER BASIN (SERBIA)

Ana Milanović Pešić [1], Boško Milovanović [1], Milan Radovanović [1], Milovan Milivojević [1]*

[1]Geographical Institute "Jovan Cvijić" Serbian Academy of Sciences and Arts, Belgrade, Serbia ; e-mails: a.milanovic@gi.sanu.ac.rs; b.milovanovic@gi.sanu.ac.rs; m.radovanovic@gi.sanu.ac.rs; m.milivojevic@gi.sanu.ac.rs;

Abstract: This paper aims to present discharge, air temperatures and precipitation trends and their connection in the Mlava River, the right tributary of the Danube in Serbia. Data were used from hydrological and meteorological yearbooks for 11 meteorological stations and two hydrological stations for the period 1986–2010. Mann-Kendall test was applied to determine the statistical significance of the trend in air temperature, precipitation and discharges and Sen's slope estimation to assess the trend magnitude. In order to determine the relationship between the precipitation and air temperature on one side and the discharge on the other side, the Pearson correlation coefficient was used. Results have shown an increasing trend in air temperature and precipitation at annual and monthly levels. In addition, an increasing trend in the discharge of the Mlava River is registered in mostly months, as well as on an annual level. The exceptions are April, May, and June (at Žagubica station), as well as May, June, and July (at Gornjak station), when a decreasing trend in discharge is observed. Correlation coefficients between monthly and annual precipitation and discharge are high and sometimes statistically significant, compared with the correlation coefficients between monthly and air temperatures and discharge, which is mostly weak.

Keywords: discharge; air temperature; precipitation; trend; correlation coefficient

1. Introduction

Water resources are essential in all aspects of human activities and development. Therefore, determining their quantity and quality is very important and a subject of many global and local studies. For water quantity analyses, discharges and their changes are often used as a base component. Discharges depend directly on climatic elements, especially on air temperature and precipitation. Therefore, a large number of studies worldwide explored trends of air temperatures, precipitation and discharges, as well as their correlation (Dissanayaka & Rajapakse, 2019; Đorđević et al., 2020; Martić Bursać et al., 2022; Shrestha et al., 2021; Sing & Sharma, 2022; Xu et al., 2021). Many studies in Serbia also investigated discharge trends in rivers (Kovačević-Majkić & Urošev, 2014), as well as the correlation between precipitation and discharge trends (Dimkić, 2018; Milanović Pešić, 2015).

This study explored the trend analysis of average annual and monthly discharges at the Mlava River and the trend analysis of average annual and monthly air temperature and precipitation in its river basin. It was examined whether the changes in these hydrological

*Corresponding author, e-mail: a.milanovic@gi.sanu.ac.rs

and climatological elements exist, whether they are significant and on what level of confidence. In addition, the correlations between precipitation and air temperature on the one side and discharge on the other side were explored.

2. Study area

The study area covers the Mlava River Basin, located in the central part of Serbia (Figure 1). Mlava River is a right tributary of the Danube, 125.1 km long and covering 1,886 km^2 of area basin (Urošev et al., 2017). It springs from the source Žagubičko vrelo at 328 m a.s.l. and flows into the left branch of the Danube at 70 m a.s.l. (Urošev et al., 2017). Mlava River flows through a composite valley of several basins and gorges. The most significant is the Ribarsko-Gornjačka gorge, 28 km long and up to 320 m deep (Gavrilović & Dukić, 2014). The largest tributary is the Vitovnica River (48 km long, 304 km^2 basin area), followed by Tisnica Rivers (23.8 km long, 146 km^2 basin area). In addition, important tributaries are Busur River, Čokordin River, Do River and the small Krupajska River. Since 1979, the source of the Krupajska River has been under state protection as a nature reserve (Gavrilović & Dukić, 2014).

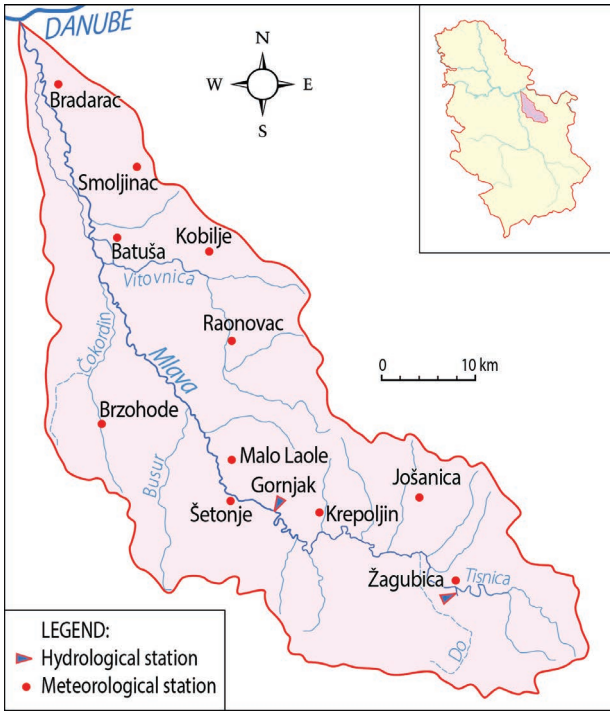

Figure 1. Map of the Mlava River Basin.

According to Köppen's climate classification, the area of the Mlava River Basin mostly belongs to the Cfb climate type, characterised by a moderately warm and humid climate (without a dry period) in which the highest average monthly temperature does not exceed 22.0 °C and at least four months have an average monthly air temperature above 10.0 °C. In

the lower course of the Mlava River, at the confluence with the Danube, there is a Cfa climate type, in which, compared to the previously mentioned climate type, the average monthly temperature of the warmest month is above 22.0 °C (Milovanović et al., 2017).

In 1961–2010, the average annual discharge at the upstream station Žagubica was 1.8 m^3/s, and at the downstream station Gornjak 6.71 m^3/s. The highest discharges are registered in April, 3.9 m^3/s (Žagubica station) and 14.4 m^3/s (Gornjak station), and the lowest in September, 0.76 m^3/s (Žagubica station) and 1.84 m^3/s (Gornjak station; Urošev et al., 2017). Therefore, the Mlava River belongs to rivers with a pluvial-nival regime of the moderate continental variety.

For this study, a river with a natural regime with no or little hydromorphological alteration and anthropogenic impact was selected, making it more appropriate for analysing the correlations between climate variables (air temperature and precipitation) and discharges.

3. Data and methodology

In the Mlava River Basin and its surroundings, average annual and average monthly air temperature from one climatological station (Žagubica) and average annual and average monthly precipitation from 11 precipitation stations were analysed. Also, average annual and average monthly discharge from two hydrological stations on the Mlava River (Žagubica and Gornjak) were analysed (Figure 1). All data were collected from the Meteorological and Hydrological Yearbooks of the Republic Hydrometeorological Service of Serbia (1986–2010a; 986–2010b) and analysed for the 1986–2010 period.

In this study, The Mann-Kendall test was applied to examine the statistical significance of the trend of precipitation, air temperature and discharge, and Sen's slope estimation for assessing the slope of the trend. According to Salmi et al. (2002) Sen's slope estimation can be calculated if there is a linear trend in a form:

$$f_t = Q_t + B \tag{1}$$

where Q is the slope and B is constant. To obtain slope Q in Equation 1, it is necessary to calculate the slope for all data with the Equation 2:

$$Q_i = \frac{x_j - x_k}{j - k} \tag{2}$$

with $j>k$. If there are 'n' values 'X_j' in a time series, Q is obtained as $N = n(n - 1) / 2$ slope estimation Q_i. Sen's slope estimate is the median of N values Q_i. N values of Q_i are ranked from small to large, with an estimated Sen's slope:

$$Q = Q_{\left[\frac{N+1}{2}\right]} \text{ if } N \text{ is odd} \tag{3}$$

or

$$Q = 0.5\left(Q_{\left(\frac{N}{2}\right)} + Q_{\left(\frac{N+2}{2}\right)}\right) \text{ if } N \text{ is even} \tag{4}$$

The Pearson correlation coefficient was used to determine the relationship between the precipitation or the air temperature on one side and the discharge of the Mlava River on the other side. This coefficient is defined by the Equation 5 (Snedecor & Cochran, 1989):

$$r = \frac{n(\sum xy) - (\sum x) \cdot (\sum y)}{\sqrt{[n\sum x^2 - (\sum x)^2][n\sum y^2 - (\sum y)^2]}} \quad (5)$$

where x and y are independent variables.

4. Results

According to data from the Žagubica climatological station, the average annual air temperature in the area of the Mlava River Basin amounts to 9.7°C. The coldest month is January (–1.1°C), and the warmest is July (19.8°C; Table 1).

Table 1. Average monthly and annual air temperature (°C) on the Žagubica climatological station for the period 1986–2010

I	II	III	IV	V	VI	VII	VIII	IX	X	XI	XII	Annual
–1.1	0.6	4.6	10.4	15.3	18.8	19.8	19.4	14.5	9.9	4.6	–0.1	9.7

According to the data from 11 precipitation stations, the average annual precipitation in the Mlava River Basin is 675.1 mm. The maximum precipitation occurs in May and June (from 65.0 mm to 76.3 mm), and the minimum from January to March (45.4 mm to 46.1 mm; Table 2).

Table 2. Average monthly and annual precipitation (mm) in the Mlava River Basin for the period 1986–2010

I	II	III	IV	V	VI	VII	VIII	IX	X	XI	XII	Annual
45.4	45.7	46.1	61.3	65.0	76.3	60.1	57.4	55.7	56.2	51.7	54.2	675.1

Obtained results from two hydrological stations on the Mlava River showed that the average annual discharge amounts from 1.76 to 6.50 m^3/s. Based on the annual discharge distribution, it can be concluded that the highest discharges are recorded in April and the lowest in September (Table 3).

Table 3. Average monthly and annual discharge (m^3/s) on the Mlava River for the period 1986–2010

Station	I	II	III	IV	V	VI	VII	VIII	IX	X	XI	XII	Annual
Žagubica	1.63	2.07	3.49	3.71	2.35	1.67	1.00	0.83	0.76	0.88	1.07	1.58	1.76
Gornjak	6.91	9.63	13.89	14.49	7.69	5.86	2.93	2.47	1.80	2.55	3.75	6.08	6.50

By analysing trends in air temperatures for the observed period, it can be concluded that there is a positive trend in almost all months and at the annual level (Table 4). The only exception is October, when no trend in the data is observed. The highest increase values are in May and June (0.1 °C/year) and the lowest in January and February, ranging from 0.013 °C/year to 0.038 °C/year. The trend is statistically significant in May and June (significance level 0.01) and at the annual level (significance level 0.05).

Table 4. Trends in annual and monthly average air temperature and precipitation in the Mlava River Basin for the period 1986–2010

Time series	Air temperature		Precipitation	
	Test Z	Sen's slope estimation (°C/year)	Test Z	Sen's slope estimation (mm/year)
I	0.37	0.013	1.66	1.513
II	0.49	0.038	1.56	1.258
III	1.10	0.092	0.21	0.102
IV	1.36	0.066	0.68	0.827
V	2.64**	0.100	0.12	0.112
VI	3.02**	0.100	0.02	0.018
VII	1.66	0.094	0.91	0.588
VIII	1.71	0.068	0.91	1.052
IX	0.33	0.027	0.72	0.508
X	0.05	0.000	1.33	1.352
XI	1.36	0.100	0.63	0.590
XII	1.35	0.078	0.96	0.490
Annual	2.55*	0.061	1.99*	7.494

Note. *Significant ($\alpha \leq 0.05$); **Significant ($\alpha \leq 0.01$).

Table 5. Trends in annual and monthly average discharge on the Mlava River for the period 1986–2010

Time series	Žagubica		Gornjak	
	Test Z	Sen's slope estimation (°C/year)	Test Z	Sen's slope estimation (mm/year)
I	2.71**	0.062	2.97**	0.330
II	1.10	0.026	1.78	0.339
III	0.12	0.008	0.75	0.181
IV	–0.86	-0.045	0.87	0.148
V	–2.17*	-0.068	–0.35	–0.032
VI	–0.89	-0.011	–0.44	–0.052
VII	1.19	0.010	–0.02	–0.003
VIII	1.80	0.015	1.03	0.018
IX	1.14	0.010	1.10	0.017
X	1.70	0.016	1.45	0.037
XI	3.41***	0.044	2.22*	0.149
XII	2.41*	0.059	2.71**	0.288
Annual	0.72	0.011	1.78	0.123

Note. *Significant ($\alpha \leq 0.05$); **Significant ($\alpha \leq 0.01$); ***Significant ($\alpha \leq 0.001$).

According to the obtained results in Table 4, there was an increase in the precipitation in all months and on an annual level. The highest increase is observed during January, February, August, and October (from 1.05 mm/year to 1.51 mm/year), while the smallest increase is during March, May and June (from 0.018 mm/year to 0.112 mm/year). There was a moderately significant increase of 7.94 mm/year at the annual level.

By analysing the trends in discharges on the Mlava River, differences can be observed between the months on both monitored stations (Table 5). At the Žagubica station, there is an increasing trend in discharge in mostly months, as well as on an annual level. The decreasing trend in discharge is observed during April, May and June. The highest and very significant increase in discharge occurs in November (0.044 m^3/s/year), followed by a significant increase during January (0.062 m^3/s/year) and a moderate significant increase in December (0.059 m^3/s/year). The lowest and statistically significant decrease (at the significance level of 0.05) in discharge was registered in May (–0.068 m^3/s/year). At Gornjak station, an increasing trend in discharge has been recorded in mostly months, as well as on an annual level. The exceptions are May, June and July when a decreasing trend in discharge is observed. The highest and statistically significant increase in discharge is in January (0.330 m^3/s/year), then in December (0.288 m^3/s/year) and in November (0.149 m^3/s/year). On both stations, the lowest increase in discharge occurred in September, August and October, and it is not statistically significant.

Table 6 shows the correlation coefficients between average monthly and annual precipitation and discharge at Mlava River. In this study was examined only correlations between discharge and precipitation observed in the same month or discharge with precipitation in the previous month (only those correlations are bolded in the table). Correlation coefficients between monthly and annual precipitation and discharge at Gornjak station are statistically significant, and the only exception is in October. The highest correlations are in May (r = 0.851) and July (r= 0.795), which means that about 72% (r^2 = 0.724) and about 63% (r^2 = 0.632) of the discharge variability in May and July can be explained by changes in the amount of precipitation in these months. It is interesting to emphasise that this station's discharges in February, March and July show a relatively high and statistically significant correlation with the precipitation in the preceding months (January, February and June). The correlation between discharge at the Žagubica station and the precipitation in the wider area of the Mlava River Basin is significantly lower, and only in some months, it shows statistical significance. As at the previous station, in this case, the highest correlation coefficient between precipitation and discharge is in May (r = 0.733), while discharge in March shows a higher (statistically significant) correlation with precipitation in February and then in March. A similar phenomenon occurs with the discharge in June and August, which shows a better correlation with the precipitation in May and June than with the precipitation in June and August (Table 6).

Table 6. Correlation coefficients between the discharge and precipitation in the Mlava River Basin

	I P	II P	III P	IV P	V P	VI P	VII P	VIII P	IX P	X P	XI P	XII P	Ann P
Gornjak													
I	.408*	.481*	–.371	.019	.022	–.142	.247	–.040	–.260	.259	–.121	.050	.123
II	.454*	.599**	–.169	.026	–.090	–.015	.070	–.140	–.360	–.085	–.110	.168	.004
III	.205	.667**	.438*	–.109	–.259	.200	.029	–.004	–.309	–.016	–.030	.303	.220
IV	.049	.268	.190	.455*	.202	–.115	.129	.200	.119	–.217	–.131	.448*	.364
V	.102	–.177	–.099	.271	.851**	.000	–.044	.139	–.026	–.219	.062	.111	.241
VI	–.252	–.260	.068	.323	.296	.579**	.115	.190	.373	–.121	.144	–.322	.404*
VII	–.052	.439*	–.253	.315	–.020	.427*	.795**	.029	–.077	.087	–.199	.273	.534**
VIII	–.351	–.047	–.189	.122	.019	–.126	.677**	.680**	–.200	.293	–.195	.077	.322
IX	–.300	–.138	.046	.502*	.225	.499*	.147	.154	.682**	–.088	.178	–.139	.562**
X	–.242	–.121	–.205	.380	.161	.076	.499*	.546**	.206	.380	.006	–.083	.558**
XI	.208	.265	–.032	–.288	.087	.249	.048	.220	.067	.462*	.698**	–.016	.563**
XII	.028	.479*	.013	.088	.049	–.050	.386	.374	.148	.230	.282	.633**	.702**
Ann	.205	.619**	.030	.301	.217	.177	.401*	.308	–.097	.060	.039	.401*	.688**
Žagubica													
I	.289	.293	–.358	–.103	–.043	–.208	.342	.072	–.197	.334	.050	.029	.144
II	.390	.348	.009	.037	–.323	.144	.112	–.050	–.299	–.054	.025	.008	.042
III	.091	.464*	.238	.180	–.193	.246	.202	.043	–.292	–.314	–.291	–.066	.047
IV	.020	.142	.264	.291	.062	–.108	.129	.256	–.214	–.326	–.371	.179	.039
V	.056	–.305	–.042	.174	.733**	.139	–.109	.048	–.144	–.208	.011	.036	.098
VI	–.165	–.295	.065	.152	.466*	.360	.016	.227	.120	–.074	.152	–.426*	.243
VII	.137	.392	–.139	–.010	–.062	.331	.519**	.109	–.163	.245	–.023	–.012	.412*
VIII	–.212	.063	–.267	.039	–.017	–.053	.636**	.491*	–.258	.174	–.292	.052	.192
IX	–.233	.037	–.222	.422*	.074	–.151	.561**	.523**	.233	–.095	–.323	.172	.334
X	–.190	–.147	–.398*	.237	.126	–.014	.549**	.494*	.141	.286	–.214	–.096	.340
XI	.270	.353	–.164	–.322	–.029	.041	.280	.167	–.059	.516**	.433*	.079	.453*
XII	–.140	.341	–.123	.051	.075	–.005	.284	.091	.235	.215	.141	.554**	.469*
Ann	.142	.382	–.025	.237	.164	.160	.494*	.328	–.304	–.094	–.223	.092	.373

Note. *Significant ($\alpha \leq 0.05$); **Significant ($\alpha \leq 0.01$).

In contrast to the significant correlations between precipitation and discharge, the connection between the air temperature at the Žagubica station and the discharge at the Gornjak and Žagubica stations is surprisingly weak (Table 7). The highest (negative and statistically significant) correlations are between discharge in May and air temperature in the same month. This phenomenon should be explored in more detail.

Table 7. Correlation coefficients between the discharge and air temperature in the Mlava River Basin

	I T	II T	III T	IV T	V T	VI T	VII T	VIII T	IX T	X T	XI T	XII T	Ann T
						Gornjak							
I	.126	–.147	–.019	.249	.235	.441*	.109	.220	.121	–.019	.421*	.092	.258
II	–.144	.102	.167	.424*	.089	.127	.218	.230	.222	.044	.455*	.274	.373
III	.056	–.203	.097	.429*	.243	–.106	.052	.063	.205	–.234	.008	.347	.129
IV	–.354	–.296	–.393	–.280	.125	–.043	.038	.005	–.003	–.157	.049	.234	–.153
V	–.205	.000	–.347	–.028	–.506**	–.136	.145	.017	.182	–.236	.140	–.035	–.067
VI	.049	.335	.395	–.016	–.193	–.308	.231	.146	.210	–.019	.010	–.478*	.175
VII	.240	–.158	.182	.160	–.028	–.292	.027	.143	.303	–.388	–.166	–.072	.039
VIII	.038	–.042	.106	–.490*	–.271	–.020	.007	–.081	.049	–.324	–.110	–.105	–.155
IX	.087	.168	.231	–.028	–.019	–.426*	.061	.082	–.002	.029	–.178	–.393	.007
X	.168	.183	.008	–.335	–.060	–.126	.025	.018	–.018	–.348	–.278	–.003	–.094
XI	.168	.228	.226	.267	.209	.240	.184	.169	.075	.006	.015	.073	.280
XII	.033	–.055	–.040	–.124	.270	.200	.036	.027	–.071	–.376	–.093	.357	–.019
Ann	–.059	–.089	.009	.150	.094	–.009	.206	.183	.246	–.347	.164	.230	.162
						Žagubica							
I	.171	–.219	–.062	.084	.145	.524**	.175	.185	.180	–.020	.234	.119	.216
II	.021	.329	.221	.276	.016	.135	.314	.257	.293	.272	.182	.223	.447*
III	.081	–.285	.103	.447*	–.028	–.459*	–.029	.007	.197	–.279	–.179	.095	–.032
IV	–.247	–.424*	–.385	–.245	–.021	–.169	–.159	–.242	–.035	–.301	–.195	.105	–.381
V	–.265	.045	–.250	–.067	–.537**	–.169	.136	–.021	.220	–.097	.186	–.057	–.038
VI	.027	.089	.261	–.021	–.463*	–.380	.237	.124	.251	–.128	–.004	–.391	.076
VII	.176	–.250	.271	.267	.008	–.227	.023	.123	.238	–.117	.057	–.211	.093
VIII	–.005	–.045	.163	–.250	–.148	.057	.010	–.028	.067	–.095	.128	–.263	–.033
IX	–.116	–.069	–.018	–.263	.075	–.048	–.038	–.072	–.089	–.199	.011	–.175	–.150
X	.188	.185	.060	–.175	.105	.147	.094	.082	.074	–.403*	–.027	–.185	.037
XI	.273	.062	.183	.269	.359	.500*	.198	.220	.157	–.083	.143	.176	.343
XII	.038	–.064	–.055	–.159	.410*	.464*	–.126	–.047	–.268	–.128	.067	.114	–.064
Ann	–.004	–.252	–.029	.137	–.076	–.103	.095	.045	.254	–.322	.032	.013	.005

Note. *Significant ($\alpha \leq 0.05$); **Significant ($\alpha \leq 0.01$).

5. Conclusion

According to the obtained results in this study, it can be concluded that in the Mlava River Basin, there is an increasing trend in air temperature at an annual level, as well as in all months (with the highest increase in May and June). A similar trend is also observed with precipitation, and there is an increase in the precipitation both on an annual and monthly level. There is a difference compared with the air temperature trend; namely, the lowest increase in precipitation is registered in March, May and June. It is important to highlight that the discharge at the Gornjak and Žagubica stations shows a decreasing trend during April, May, June and July, i.e. in the months when the increase in air temperature is the highest, and the increase in precipitation is the lowest in Mlava River Basin. In these months, the highest correlations were calculated between the air temperature and the precipitation on the one hand and the discharge of the Mlava River on the other. In addition, the discharges in these months also record high correlations with the precipitation in the

months preceding them. This phenomenon should be analyzed in more detail in further research, which would also include the analysis of the influence of other factors such as geological structure, terrain morphology, the influence of snow cover and its melting, and pedology on correlations of precipitation and discharges.

References

Gavrilović, Lj., & Dukić, D. (2014). *Reke Srbije* [Rivers of Serbia]. Zavod za udžbenike i nastavna sredstva.

Dimkić, D., (2018). Observed Climate and Hydrological Changes in Serbia—What Has Changed in the Last Ten Years. *Proceedings, 2*(11), Article 616. https://doi.org/10.3390/proceedings2110616

Dissanayaka, K. D. C. R., & Rajapakse, R. L. H. L. (2019). Long-term precipitation trends and climate extremes in the Kelani River basin, Sri Lanka, and their impact on the streamflow variability under climate change. *Paddy and Water Environment, 17,* 281–289. https://doi.org/10.1007/s10333-019-00721-6

Đorđević, B., Dašić, T., & Plavšić, J. (2020). Uticaj klimatskih promena na vodoprivredu Srbije i mere koje treba preduzimati u cilju zaštite od negativnih uticaja [Impact of climate change on Serbian water management and measures for protection against adverse impacts]. *Vodoprivreda, 52*(305–309), 39–68. https://www.vodoprivreda.net/wp-content/uploads/2020/12/3-Djordjevic-Dasic-Plavsic.pdf

Kovačević-Majkić, J., & Urošev, M. (2014). Trends of mean annual and seasonal discharges of rivers in Serbia. *Journal of the Geographical Institute "Jovan Cvijić" SASA, 64*(2), 143–160. https://doi.org/10.2298/IJGI1402143K

Martić Bursać, N., Radovanović, M., Radivojević, A., Ivanović, R., Stričević, Lj., Gocić, M., Golubović, N., & Bursać, B. (2022). Observed climate changes in the Toplica River valley — Trend analysis of temperature, precipitation and river discharge. *Quarterly Journal of the Hungarian Meteorological Service, 126*(3), 403–423. https://doi.org/10.28974/idojaras.2022.3.8

Republic Hydrometeorological Service of Serbia (1986–2010a). *Hidrološki godišnjaci - 1. Površinske vode* [Data set; Hydrological Yearbooks - 1. Surface waters]. https://www.hidmet.gov.rs/ciril/hidrologija/povrsinske_godisnjaci.php

Republic Hydrometeorological Service of Serbia. (1986–2010b). *Meteorološki godišnjak - klimatološki podaci* [Meteorological Yearbooks - climatological data; Data set]. https://www.hidmet.gov.rs/latin/meteorologija/klimatologija_godisnjaci.php

Milanović Pešić, A. (2015). Geographical aspects of natural disasters in Šumadija [Unpublished doctoral dissertation]. University of Belgrade, Faculty of Geography.

Milovanović, B., Ducić, V., Radovanović, M., & Milivojević, M. (2017). Climate regionalisation of Serbia according to Köppen climate classification. *Journal of the Geographical Institute "Jovan Cvijić" SASA, 67*(2), 103–114. https://doi.org/10.2298/IJGI1702103M

Salmi, T., Määttä, A., Anttila, P., Ruoho-Airola, T., & Amnell, T. (2002). *Detecting Trends of Annual Values of Atmospheric Pollutants by the Mann-Kendall Test and Sen's Slope Estimates - The Excel Template Application Makesense*. Finish Meteorological Institute

Snedecor, G. W., & Cochran, W. G. (1989). *Statistical Methods* (8th ed). Iowa State University Press

Singh, O., & Sharma, M.C. (2022). Variability and Trends in Temperature, Rainfall, and Discharge in a Western Himalayan Catchment. In S. Rani & R. Kumar (Eds.), *Climate Change*. *Springer Climate* (29–45). Springer. https://doi.org/10.1007/978-3-030-92782-0_2

Shrestha, R. R., Pesklevits, J., Yang, D., Peters, D. L., & Dibike, Y. B. (2021). Climatic controls on mean and extreme streamflow changes across the permafrost region of Canada. *Water, 13*(5), Article 626. https://doi.org/10.3390/w13050626

Urošev, M., Kovačević-Majkić, J., Štrbac, D., Milanović Pešić, A., Milijašević, D., Jakovljević, D., & Petrović, A. (2017). Vode Srbije [Water of Serbia]. In M. Radovanović (Ed.), *Geografija Srbije* [Geography of Serbia] (pp. 160–235). Geographical Institute "Jovan Cvijić" SASA.

Xu, Z. P., Li, Y. P., Huang, G. H., Wang, S. G., & Liu, Y. R. (2021). A multi-scenario ensemble streamflow forecast method for Amu Darya River Basin under considering climate and land-use changes. *Journal of Hydrology, 598,* Article 126276. https://doi.org/10.1016/j.jhydrol.2021.126276

GeosciRA23
Book of Abstracts and Contributed Papers
International Conference on Recent Trends in Geoscience Research and Applications 2023
Belgrade, Serbia & Virtual, October 23–27, 2023
Editors: Aleksandra Nina, Snežana Dragović, and Dejan Doljak

Contributed paper

CLIMATE TRENDS IN THE DURMITOR REGION, MONTENEGRO

Gordana Jovanovic[1]*

[1]University of Montenegro, Faculty of Science and Mathematics, Podgorica, Montenegro;
e-mail: gordanaj@ucg.ac.me

Abstract: The focus of this article is on climate variability in the Durmitor region, Montenegro, in the period 1991–2020. Data from three meteorological stations: Žabljak, Šavnik and Nikšić are used. For seasonal analysis the year is divided in two semi-annual periods, from November to April and from May to October. The influence of the North Atlantic Oscillation (NAO), measured by positive or negative NAO index, in these semi-annual periods is studied. It is shown that the changes in precipitation and temperature are much more pronounced in the period November–April than in the period May–October. This is primarily reflected in the increasing trend in the average precipitation and temperature in the whole Durmitor region for the period November–April. Precipitation is abundant mainly in the years with a negative NAO index and deficient in the years with a positive NAO index. The highest temperatures in the period from May to October are mostly in the years with a negative NAO index.

Keywords: climate change; North Atlantic Oscillation; Durmitor; Montenegro

1. Introduction

Climate change is generally believed to lead to an increase in climate variability and in the frequency and intensity of extreme events. In Europe, pronounced summer (June–August) warming of approximately 1.3 °C was recorded in the period 1986–2015 (García-Herrera et al., 2010; Rahmstorf & Coumou, 2011). Montenegro has also been exposed to climate change, especially at the end of the 20th and at the beginning of the 21st century (Knez et al., 2022). In this paper we study the climate change in the Durmitor region in the last 30 years. We analyze the climate variables such as the amount of precipitation and temperature in the two periods November-April and May-October. The recorded fluctuation of temperature and precipitation, especially from November to April motivated this research. Also, the mountain Durmitor is a national park in Montenegro and as such is the least susceptible to human influence. Therefore it is convenient for the study of the natural causes of the climate variability. One of them is the North Atlantic Oscillation (NAO), the leading climate factor in the North Hemisphere (Rousi et al., 2020). The NAO influence is measured by the NAO index (Hurrell & Deser, 2010). A relatively strong pressure gradient between the Azores high and the Icelandic low yields a positive NAO index (NAO^+) while a relatively weak gradient yields a negative NAO index (NAO^-). During NAO^+, we have warmer conditions in northern and central Europe and cooler conditions over the Mediterranean. This NAO^+ phase also leads to a decrease in the precipitation over the Mediterranean and Southern Europe (south of 45° N)

*Corresponding author, e-mail: gordanaj@ucg.ac.me

and an increase over Northern Europe. During NAO⁻ warm moist air enters the Mediterranean region and cold air enters northern Europe (Criado-Aldeanueva & Soto-Navarro, 2020). Montenegro is located on the border of these different influences and therefore it is scientifically justified to analyze the NAO effect on the climate variables especially in the northern part of Montenegro where the Durmitor Mountain is located.

2. Durmitor National Park, Montenegro

Montenegro is in the middle part of the temperate zone of the northern hemisphere with a latitude between 42°52′ N and 43°32′ N and longitude between 18°26′ E and 19°22′ E. Durmitor is a limestone massif located in the northwestern part of Montenegro and belonging to the Dinaric Alps or Dinarides. It is characterized by high peaks, abundant forests, and deep gorges. On September 6th 1952, the Assembly of the Republic of Montenegro proclaimed the mountain Durmitor as National Park. The nearby towns are Nikšić, Šavnik, and Žabljak, which is in the heart of the Durmitor region.

3. Methods and results

Climate variables for the period (1991–2020) in the Durmitor region are analyzed. Data from Nikšić, Šavnik, and Žabljak meteorological stations for aforementioned period were used. Žabljak is located in the middle of the National Park Durmitor but it is in the leeward position to the atmospheric advections from the southwest, which serves as the main sources of precipitation. That is why we consider the stations situated on the windward side, such as Šavnik and Nikšić.

In the following text, we will apply seasonal analysis and divide the year into two parts, from November to April and from May to October (Scafetta, 2021). We will analyze the amount of precipitation and average temperatures in these parts of the year to understand which part of the year has a greater potential to change climate variables.

3.1. Precipitation data for November–April

The amount of precipitation for Nikšić, Šavnik, and Žabljak for the season (November–April) in the period (1991–2020) is presented in Figure 1. The average amount of precipitation for this period in Nikšić, Šavnik, and Žabljak is 1261 mm, 1235 mm, and 885 mm, respectively.

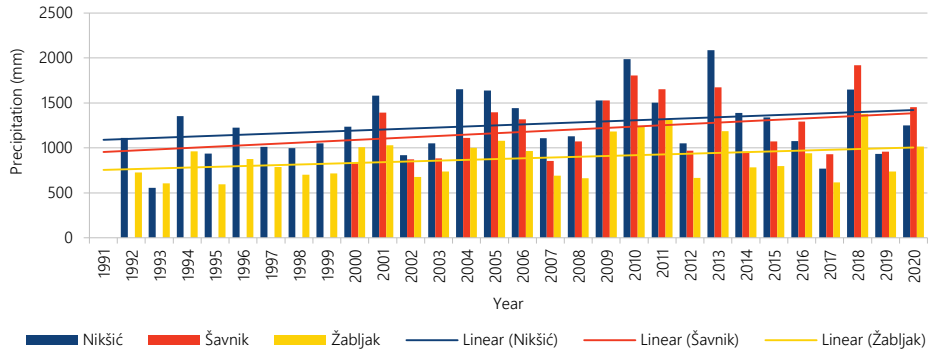

Figure 1. Precipitation from November to April for Nikšić, Šavnik, and Žabljak.

3.2. Precipitation data for May–October

The amount of precipitation for Nikšić, Šavnik, and Žabljak for the season (May-October) for the period (1991–2020) is presented in Figure 2. The average amount of precipitation in this part of the year for Nikšić, Šavnik, and Žabljak is 643 mm, 671 mm, and 627 mm, respectively.

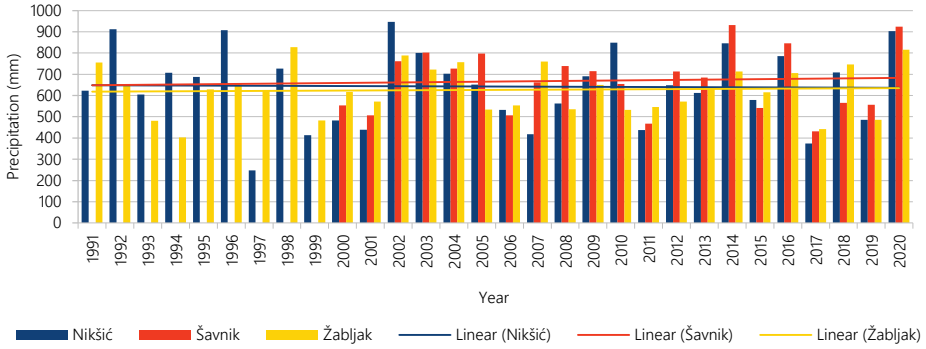

Figure 2. Precipitation from May to October for Nikšić, Šavnik, and Žabljak.

3.3. Temperature data for November–April

The average temperatures for Nikšić, Šavnik, and Žabljak for November–April in the period (1991–2020) are presented in Figure 3. In Nikšić the average temperature for this season is 5.34 °C, in Šavnik 3.34 °C, and in Žabljak, with the highest altitude among these cities, –0.16 °C.

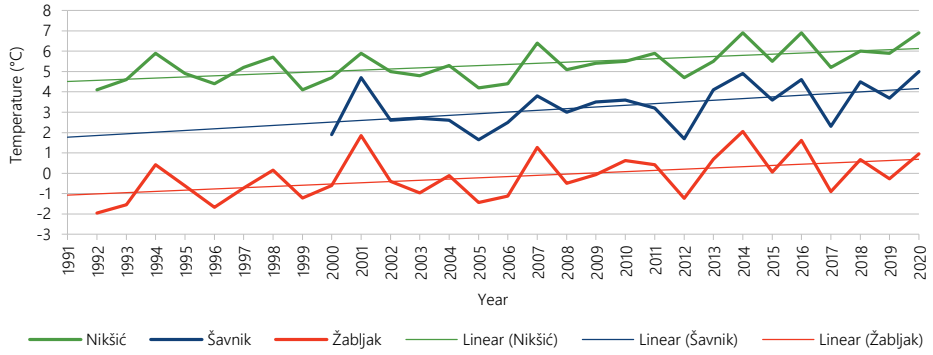

Figure 3. Average temperatures from November to April for Nikšić, Šavnik, and Žabljak.

3.4. Temperature data for May–October

Average temperatures for Nikšić, Šavnik, and Žabljak for May–October in the period 1991–2020 are presented in Figure 4. The average temperature for this part of the year in Nikšić is 17.8 °C, in Šavnik 15.8 °C, and in Žabljak 12.1 °C.

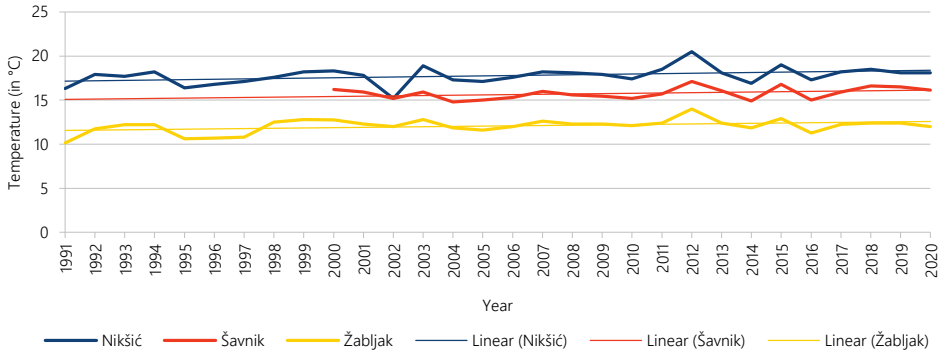

Figure 4. Average temperatures from May to October for Nikšić, Šavnik, and Žabljak.

4. Discussion

The average amount of precipitation for November-April in the period 1991–2020 is different in Nikšić and Šavnik which are on the windward side and Žabljak in the leeward position. Therefore, in this season the average amount of precipitation in Nikšić and Šavnik is about 40% higher than in Žabljak. The amount of precipitation from November to April shows a growing trend in the considered thirty-years period in all three cities (Figure 1). In general, in Montenegro the NAO has been found to influence amounts of precipitation, especially in winter. When NAO indices are negative (positive), the amount of precipitation is above (below) the average value (Burić, 2012). This was the case in 2010 and 2013, which were characterized by high amounts of precipitation in the Durmitor massif, with NAO indices –4.64 and –1.97, respectively. Years with a very low amount of precipitation, more than 25% below average, are: 1993, 1995, 2000, 2002, 2003, 2007, 2017, and 2019. These years, without exception, are characterized by positive NAO, i.e., 2.67, 3.96, 2.80, 0.76, 0.20, 2.79, 1.47, 2.09, respectively.

In the period from May to October, there are no big differences in average amounts of precipitation for Nikšić, Šavnik, and Žabljak. The average amount of precipitation in Nikšić is about 3% higher than in Žabljak, and in Šavnik it is 7% higher than in Žabljak. The NAO is not as correlated with precipitation in this part of the year as it was in the November to April period. Years with high amounts of precipitation are mostly with negative NAO: 1998 (–0.4), 2002 (–1.6), 2010 (–0.2), 2014 (–1.4), and 2020 (–0.29). The exceptions are the years 1992 (0.9) and 1996 (0.5). We suppose that the influence of strong El Niño in 1992 and moderate La Niña in 1996 could be the reason for this phenomenon. Namely, the combined effects of El Niño/La Niña and NAO are confirmed to be more profound than the effects they produce individually (Prabhu et al., 2017). In the case of a small amount of precipitation there are both positive and negative values of the NAO. Therefore, no conclusion can be made about the connection between the strong decrease in precipitation and the North Atlantic Oscillation. Notice that significant changes in the amount of precipitation refer to the period November–April, while in the period May–October these changes are much less pronounced (see trend lines in Figures 1 and 2).

Temperatures from November to April have extreme values mainly in years with a positive NAO: 1992 (3.28), 1999 (1.7), 2005 (0.12), 2007 (2.79), 2012 (3.17), 2014 (3.10), 2016

(0.98), 2018 (0.3), and 2020 (1.78). Only in 2001, there was a negative NAO of –1.9. In this year a strong La Niña influence was recorded (Scafetta et al., 2017).

Unlike the November–April period, the highest temperatures in the May–October are mostly in years with a negative NAO: 1999 (–1.3), 2003 (–1.1), 2012 (–1.2), 2015 (–1.4), and 2019 (–0.1). The only exception for 2018 is 2.1, and a possible reason for this is a moderate La Niña. The NAO does not have a decisive effect on the lowest temperatures in this period because there are years with positive and negative values of the NAO indices. Trend lines in Figures 3 and 4 show a constant increase in average temperatures in the Durmitor region. It is indicative that the temperature increase is significantly more pronounced in the winter part of the year (November–April) than in the summer part of the year (May–October). The higher temperatures in November–April could be the reason for the snow cover shift from December–January to January–February. This has been especially pronounced in the last few years, so the ski season in Žabljak starts later.

5. Conclusion

We found that climate changes in the Durmitor region are most pronounced in the period November–April than in the period May–October and are reflected in an increase in amount of precipitation and average temperatures in the Durmitor massif (Figures 1 and 3). The influence of the NAO, especially on the amount of precipitation in the period November–April is confirmed. Precipitation is abundant mainly in years with a negative NAO, while it is scarce in years with a positive NAO. It has been shown that extreme temperatures in the period November–April are mostly in years with a positive NAO. The situation may change due to the influence of the El Niño/La Niña phenomenon. In the period May–October the change in the climatic variables is less significant. A small increase in the amount of precipitation has been recorded in Šavnik, while in Nikšić and Žabljak it has an almost constant value for the period 1991–2020 (Figure 2). The highest temperatures in the May–October period are mostly in years with a negative NAO (Figure 4). Other climatic oscillations and patterns such as El Niño/La Niña have a significant influence on the lowest temperatures. This analysis could be a starting point for better forecasts and management of the resources and economic potential of Durmitor such as forests, water and tourism.

Acknowledgements

The research and writing of this work were carried out in the framework of the Montenegrin National Project “Physics of Ionized Gases and Ionized Radiation”.

References

Burić, M., Micev, B., & Mitrović, L. (2012). *Atlas klime Crne Gore* [Climate Atlas of Montenegro]. Crnogorska akademija nauka i umjetnosti.

Criado-Aldeanueva, F., & Soto-Navarro, J. (2020). Climatic Indices over the Mediterranean Sea: A Review. *Applied sciences, 10*(17), Article 5790. https://doi.org/10.3390/app10175790

García-Herrera, R., Díaz, J., Trigo, R. M., Luterbacher, J., & Fischer, E. M. (2010). A review of the European summer heatwave of 2003. *Critical Reviews in Environmental Science and Technology, 40*(4), 267–306. https://doi.org/10.1080/10643380802238137

Hurrell, J. W., & Deser, C. (2009). North Atlantic climate variability: The role of the North Atlantic Oscillation. *Journal of Marine Systems, 78*(1), 28–41. https://doi.org/10.1016/j.jmarsys.2008.11.026

Knez, S., Štrbac, S., & Podbrega, I. (2022). Climate change in the Western Balkans and EU Green Deal: status, mitigation and challenges. Energy, *Sustainability and Society*, *12*(1), Article 1. https://doi.org/10.1186/s13705-021-00328-y

Prabhu, A., Oh, J., Kim, I., Kripalani, R. H., Mitra, A. K., & Pandithurai, G. (2017). Summer monsoon rainfall variability over North East regions of India and its association with Eurasian snow, Atlantic Sea Surface temperature and Arctic Oscillation. *Climate Dynamics, 49*(7), 2545–2556. https://doi.org/10.1007/s00382-016-3445-4

Rahmstorf, S., & Coumou, D. (2011). Increase of extreme events in a warming world. *Proceedings of the National Academy of Sciences*, *108*(44), 17905–17909. https://doi.org/10.1073/pnas.1101766108

Rousi, E., Rust, H., Ulbrich, U., & Anagnostopoulou, K. (2020). Implications of Winter NAO Flavors on Present and Future European Climate. *Climate, 8*(1), Article 13. https://doi.org/10.3390/cli8010013

Scafetta, N., Mirandola, A., & Bianchini, A. (2017). Natural climate variability, part 2: Interpretation of the post 2000 temperature standstill. *International Journal of Heat and Technology, 35*(1), S18–S26. https://doi.org/10.18280/ijht.35Sp0103

Scafetta, N. (2021). Detection of non-climatic biases in land surface temperature records by comparing climatic data and their model simulations. *Climate Dynamics, 56*(14), 2959–2982. https://doi.org/10.1007/s00382-021-05626-x

PROGRAMME

Monday, 23 October

14:00 – 15:30 **Registration**

Chairs: Aleksandra Nina and Snežana Dragović

15:30 – 15:45 **Opening ceremony**

Chair: Bratislav Marinković

15:45 – 16:20 **Nigel John Mason** *Invited lecture*
COMPARATIVE PLANETOLOGY—WHAT DO WE LEARN ABOUT THE EARTH BY STUDYING OTHER PLANETS?

16:20 – 16:45 **Mirela Voiculescu, Cătălina Iticescu, Constantin Apetrei, Maxim Arseni, Mădălina Călmuc, Valentina Călmuc, Daniel Constantin, Adrian Roșu, Mihaela Timofti, Cătălina Țopa, Lucian P. Georgescu**
REXDAN—A NEW RESEARCH INFRASTRUCTURE WHOSE VESSEL WILL SOON SAIL ON DANUBE

16:45 – 18:45 **Welcome cocktail**

Tuesday, 24 October

Chair: Snežana Dragović

9:00 – 9:35 **Vladica Cvetković** *Invited lecture*
LITHOSPHERE GEODYNAMICS INFERRED FROM STUDY OF MANTLE XENOLITHS: THE EXAMPLE FROM SERBIA

9:35 – 10:00 **Ivan Lizaga, Borja Latorre, Montfort Bagalwa, Bossissi Nkuba, Kristof Van Oost, Pascal Boeckx**
UNVEILING CONFLICT HERITAGE: EXAMINING THE INFLUENCE OF HUMAN CONFLICTS ON LAND DEGRADATION AND LANDSCAPE MODIFICATION

10:00 – 10:25 **Nina Nikolova, Jelena Svetozarevic, Simeon Matev, Dimitar Krenchev, Rositsa Kenderova, Georgi Rachev**
RAINFALL EROSIVITY IN BULGARIA—SERBIA TRANSBORDER REGION

10:25 – 11:00 Coffee break

Chair: M. Y. Boudjada

11:00 – 11:35 **Rapoport Yuriy, Grimalsky Volodymyr, Petrishevskii Sergei, Grytsai Asen, Liashchuk Oleksandr, Krankowski Andrzej** *Invited lecture*
MODELLING WAVE STRUCTURES IN THE EARTH-ATMOSPHERE-IONOSPHERE AND RADIODIAGNOSTICS OF IONOSPHERIC SPACE WEATHER (ISW)

11:35 – 12:00 **Heba Salah Mohamed, Christine Amory-Mazaudier, Sampad Kumar Panda, Osama Mahmoud Shalabiea, Ayman Mohamed Mahrous**
DELAYED RESPONSE OF LOW LATITUDES TEC DURING THIRTY-SIX GEOMAGNETIC STORMS FROM 2014 TO 2017

12:00 – 12:25 **Tamal Basak, Sayak Chakraborty** *Invited progress report*
INVESTIGATING THE ALTITUDE PROFILE OF D-REGION IONOSPHERIC RESPONSE TIME DURING SOLAR FLARES

12:25 – 14:00 Lunch break

Chair: Maja Kuzmanoski

14:00 – 14:25 **Dharmendra Kumar Kamat, Som Kumar Sharma, Sourita Saha, Prashant Kumar, Kondapalli Niranjan Kumar**
INVESTIGATION OF THE ATMOSPHERIC CLOUDS AND BOUNDARY LAYER OVER THE WESTERN-INDIAN REGION

14:25 – 14:50 **Irina Mironova**
GEOMAGNETIC DISTURBANCE FORCING ON THE MIDDLE ATMOSPHERE

14:50 – 15:15 **Artem Padokhin, Elena Andreeva**
MULTI-GNSS GLOBAL AND LOCAL IONOSPHERIC MAPPING UTILIZING EXCLUSIVELY PHASE OBSERVATIONS

15:15 – 15:45 Coffee break

Chair: Irina Mironova

15:45 – 16:10 **Maja Kuzmanoski, Zorica Podraščanin, Ana Ćirišan, Zoran Mijić**
AEROSOL VERTICAL PROFILES AND ABL HEIGHTS CORRESPONDING TO DIFFERENT PM_{10} POLLUTION LEVELS IN BELGRADE, SERBIA

16:10 – 16:35 **Andrey Mironov, Vladimir Zubov, Eugene Rozanov**
STUDY OF POLAR OZONE ANNUAL CYCLE WITH CCM SOCOL-3

Wednesday, 25 October

Chair: Artem Padokhin

11:00 – 11:25 **Ivica Milevski, Slavoljub Dragicevic, Bojana Aleksova**
UAV-BAZED SURVEY OF THE NATURAL MONUMENT KUKLICA

11:25 – 11:50 **Klemen Medved, Božo Koler, Sofija Naod, Oleg Odalović**
MODELING OF VERTICAL GRAVITY GRADIENT FOR PURPOSES OF GRAVIMETRIC SURVEY

11:50 – 12:15 **Sumesh Gopinath, Chakkalayil Parameswaran Anil Kumar, Prince Prasad Revamma, Sherin Ann Abraham, Soosaleon Antony**
NON-EXTENSIVE TSALLIS ENTROPY ANALYSIS ON LONGTERM VARIATION OF JOULE HEATING AT HIGH LATITUDES

12:15 – 13:30 Lunch break

13:30 **Excursion**

Thursday, 26 October

Chair: Sergey Pulinets

9:00 – 9:35 **Pier Francesco Biagi** *Invited lecture*
A 50 YEARS RESEARCH ON EARTHQUAKE PRECURSORS: A PERSONAL EXPERIENCE

9:35 – 10:00 **Mohammed Y. Boudjada, Pier Francesco Biagi, Hans U. Eichelberger, Giovanni Nico, Patrick H. M. Galopeau, Maria Solovieva, Helmut Lammer, Bruno Besser, Manfred Stachel, Franz Giner**
INVESTIGATION OF VLF TRANSMITTER AMPLITUDE VARIABILITIES BEFORE THE M_W 7.8 TURKEY SYRIA EARTHQUAKES OF FEBRUARY 6, 2023

10:00 – 10:25 **Aleksandra Nina, Pier Francesco Biagi, Sergey Pulinets, Srđan Mitrović, Giovanni Nico, Luka Č. Popović**
NEW POTENTIAL EARTHQUAKE PRECURSOR: REDUCTION OF THE VLF SIGNAL NOISE

10:25 – 11:00 Coffee break

Chair: Pier Francesco Biagi

11:00 – 11:35 **Sergey Pulinets** *Invited lecture*
ENERGY TRANSFORMATION, RELEASE AND DISSIPATION DURING EARTHQUAKE PREPARATION PERIOD AS THE MANIFESTATION OF GEOSPHERE'S INTERACTION

11:35 – 12:00 **Giovanni Nico, Manilo Monaco, Pier Francesco Biagi, Anita Ermini, Aleksandra Nina**
ON THE DETECTION OF ANOMALIES IN TIME SERIES OF VLF SIGNALS RELATED TO SEISMIC ACTIVITY

12:00 – 12:10 **Meeting photo**

12:10 – 13:30 Lunch break

Chair: Giovanni Nico

13:30 – 13:55 **Hans U. Eichelberger, Mohammed Y. Boudjada, Konrad Schwingenschuh, Pier Francesco Biagi, Patrick H. M. Galopeau, Maria Solovieva, Christoph Schirninger, Bruno P. Besser, Manfred Stachel, Werner Magnes**
ANALYSES OF MAGNITUDE $M_W \geq 5.5$ EARTHQUAKES WITH SUB-IONOSPHERIC VLF/LF ELECTRIC FIELD MEASUREMENTS IN EUROPE

13:55 – 14:20 **Ljubcho Jovanov, Katerina Drogreshka, Jasmina Najdovska, Dragana Chernih**
HISTORICAL AND INSTRUMENTAL SEISMIC ACTIVITY OF THE SKOPJE EPICENTRAL AREA

14:20 – 15:30 **Posters**

20:00 – **Conference dinner**

Friday, 27 October

Chair: Hans Eichelberger

11:00 – 11:25	**Aleksandra Kolarski**	Invited progress report
	MODELING LOWER IONOSPHERIC RESPONSE TO LIGHTNING-INDUCED ELECTRON PRECIPITATION USING VLF RADIO SIGNAL RECORDINGS	
11:25 – 11:50	**Mario Batubara, Masa-yuki Yamamoto, Islam Hosni Hemdan Eldedsouki Hamama, Thomas Djamaluddin, Timbul Manik, Peberlin Parulian Sitompul, Musthofa Lathif, Poki Agung Budiantoro, Ibnu Fathrio, Ednofri, Sutan Takdir Ali Munawar, Alit Daryana, Parid Saparudin**	
	DEVELOPMENT OF A LOW-COST PORTABLE INFRASOUND AND ENVIRONMENTAL ATMOSPHERIC DATA MEASUREMENT FOR MONITORING GEOPHYSICAL PARAMETERS	
11:50 – 12:15	**Violeta Vasilić, Ljiljana Brajović, Dušan Petković, Dragan Blagojević**	
	TROPOSPHERIC REFRACTION AND ITS INFLUENCE THROUGH ZENITH TOTAL PATH DELAY AT DIFFERENT IGS STATIONS	
12:15 – 12:30	**Concluding remarks and closing of the Conference**	

LIST OF POSTERS

P1. **Dušan Petković, Sanja Grekulović, Miljana Todorović-Drakul, Oleg Odalović**
DETERMINATION OF IONOSPHERIC MODELS USING GLOBAL NAVIGATIONAL SATELLITE SYSTEMS AND BERNESE GNSS SOFTWARE

P2. **Olimpia Masci, Giovanni Nico, Giuseppina Prezioso**
GROUND-BASED RADAR INTERFEROMETRY: EXAMPLES OF APPLICATION TO THE MONITORING OF LANDSLIDES AND INFRASTRUCTURE

P3. **Aleksandra Nina, Vladimir Čadež, Luka Č. Popović**
IONOSPHERIC D-REGION DISTURBANCES INDUCED BY OUTER SPACE EVENTS

P4. **Ivana Smičiklas, Marija Egerić, Mihajlo Jović, Snežana Dragović**
CHANGES IN CONCENTRATION OF DTPA-EXTRACTABLE FORMS OF METALS IN RESPONSE TO SOIL TREATMENT WITH VARIABLE SEASHELL DOSES

P5. **Filip Arnaut, Aleksandra Kolarski**
FEATURE IMPORTANCE ANALYSIS IN RANDOM FOREST REGRESSION FOR AIR QUALITY FORECASTING IN BELGRADE, SERBIA

P6. **Gordana Jovanović**
CLIMATE TRENDS IN THE DURMITOR REGION, MONTENEGRO

P7. **Ana Milanović Pešić, Boško Milovanović, Milovan Milivojević, Milan Radovanović**
CORRELATION BETWEEN PRECIPITATION, AIR TEMPERATURE AND DISCHARGE IN THE MLAVA RIVER BASIN (SERBIA)

P8. **J. Arul Asir, H. Johnson Jeyakumar, C. P. Anil Kumar**
UNDERSTANDING THE EFFECTS OF ANTHROPOGENIC AEROSOLS AND CONTROL IN AIR QUALITY DURING COVID-19 LOCKDOWN PERIOD

P9. **Bratislav P. Marinković**
COVERAGE OF DATA RELEVANT FOR ATMOSPHERIC RESEARCH IN BEAM DATABASE

P10. **Mrđan Đokić, Miloš Manić, Milan Đorđević, Milena Gocić, Aleksandar Čupić, Mihajlo Jović, Ranko Dragović, Boško Gajić, Ivana Smičiklas, Snežana Dragović**
UTILIZATION OF REMOTE SENSING AND NUCLEAR TECHNIQUES FOR DETAILED MODELING AND QUANTITATIVE ASSESSMENT OF GULLY EROSION WITHIN THE FORESTED AREA OF THE MALČANSKA RIVER BASIN, EASTERN SERBIA

AUTHORS' INDEX

PARTICIPANTS

Sherin Ann Abraham, India
Filip Arnaut, Serbia
Arul Asir Jebakumar, India
Tamal Basak, India
Mario Batubara, Indonesia
Pier Francesco Biagi, Italy
Mohammed Boudjada, Austria
Ljiljana Brajović, Serbia
Vladica Cvetković, Serbia
Ranko Dragović, Serbia
Snežana Dragović, Serbia
Katerina Drogreshka, North Macedonia
Mrđan Đokić, Serbia
Milan Đordjević, Serbia
Hans Eichelberger, Austria
Sanja Grekulović, Serbia
Slavica Ilijević, Serbia
Ljubcho Jovanov, North Macedonia
Gordana Jovanović, Montenegro
Dharmendra Kamat, India
Aleksandra Kolarski, Serbia
Božo Koler, Slovenia
Maja Kuzmanoski, Serbia
Ivan Lizaga, Belgium
Bratislav Marinković, Serbia
Nigel Mason, UK
Klemen Medved, Slovenia
Ana Milanović Pešić, Serbia
Ivica Milevski, North Macedonia
Boško Milovanović, Serbia
Andrey Mironov, Russia
Irina Mironova, Russia
Heba Mohamed, Egypt
Jasmina Najdovska, North Macedonia
Giovanni Nico, Italy
Nina Nikolova, Bulgaria
Aleksandra Nina, Serbia
Oleg Odalović, Serbia
Artem Padokhin, Russia
Dušan Petković, Serbia
Luka Č. Popović, Serbia
Sergey Pulinets, Russia
Yuriy Rapoport, Poland
Ivana Smičiklas, Serbia
Miroslav Smolić, Croatia
Miljana Todorović Drakul, Serbia
Đorđe Trajković, Serbia
Dejan Vinković, Croatia
Mirela Voiculescu, Romania

CIP - Каталогизација у публикацији
Народна библиотека Србије, Београд

52-355.3(048)
533.92:537.228.5(048)
539.184.27(048)
550.38(048)

International Conference on Recent Trends in Geoscience Research and Applications 2023 (October 23–27, 2023, Belgrade, Serbia & virtual)
Book of abstracts and contributed papers / International Conference on Recent Trends in Geoscience Research and Applications 2023 (October 23–27, 2023, Belgrade, Serbia & virtual); edited by Aleksandra Nina, Snežana Dragović, and Dejan Doljak; [organizers Faculty of Civil Engineering, University of Belgrade and Institute of Physics Belgrade, University of Belgrade; Serbia]. - Belgrade : Faculty of Civil Engineering, University of Belgrade; Institute of Physics Belgrade, University of Belgrade; and Geographical Institute "Jovan Cvijić" SASA, 2023 (Beograd : Curent Print). – 120 str. : ilustr. ; 24 cm

Tiraž 50.

ISBN 978-86-7518-239-9
eISBN 978-86-7518-240-5

а) Астрофизика – Апстракти б) Плазма – Спектрална анализа – Апстракти в) Штарков ефекат – Апстракти г) Магнетизам земље – Апстракти

COBISS.SR-ID 123774729